**Doctoral Thesis**

# The Effect of pH on Electrocatalytic Oxidation of Small Organic Molecules on Platinum Studied by Surface-Enhanced Infrared Absorption Spectroscopy Coupled with Electrochemical Techniques

**JIYONG JOO**


博士学位論文（総合化学）
北海道大学

**2014**

# CONTENTS

**Table of Contents** ..... **i**

**Abstract** ..... **v**

**CHAPTER 1. INTRODUCTION** ..... **1**

1.1 Motivation and objectives ..... 1

1.1.1 Direct Liquid Fuel Cells (DLFCs) ..... 3

1.1.2 Electrocatalysis ..... 5

1.2 Earlier studies on electrocatalytic oxidation of small organic molecules ..... 8

1.2.1 Experimental studies ..... 8

1.2.2 Theoretical studies ..... 13

1.3 In situ characterization techniques at the electrochemical interface ..... 16

1.4 Principle of SEIRA ..... 20

1.4.1 General features of surface-enhanced infrared absorption (SEIRA) ..... 20

1.4.2 Electromagnetic Mechanism for SEIRA ..... 22

1.4.2.1 Surface selection rule ..... 24

1.5 Outline of the thesis ..... 27

References ..... 28

**CHAPTER 2. EXPERIMENTAL METHODS** ..... **31**

2.1 Chemicals and electrolyte solutions ..... 31

2.2 Electrochemical measurements ..... 31

2.2.1 Electrochemical instruments ..... 31

2.2.2 Conventional electrochemical measurements with a rotating disc ..... 31

2.3 Spectroelectrochemical measurements ..... 32

2.3.1 Spectroelectrochemical cell ..... 33

2.3.2 Preparation of the working electrode ..... 34

2.3.3 Reflection accessory ..... 35

2.4 Analysis of soluble reaction products by on-line HPLC (High Performance Liquid Chromatography ..... 36
References ..... 37

**CHAPTER 3. ELECTRO-OXIDATION OF CO ON Pt IN ALKALINE MEDIA ..... 39**

3.1 Introduction ..... 39
3.2 Experiments ..... 41
3.3 Results and discussion ..... 42
3.3.1 CO oxidation under potential sweep condition ..... 42
3.3.2 Origin of the preoxidation peak ..... 45
3.3.3 CO oxidation at the main oxidation ..... 48
3.3.4 Chronopotentiometry for Galvanostatic oxidation ..... 52
3.4 Conclusion ..... 56
References ..... 57

**CHAPTER 4. ELECTROCATALYTIC OXIDATION OF FORMIC ACID ON PLATINUM : IMPORTANCE OF ACID-BASE EQUILIBRIUM ..... 59**

4.1 Introduction ..... 59
4.2 Experiments ..... 62
4.3 Results and discussion ..... 64
4.3.1 Cyclic voltammetric studies ..... 64
4.3.2 SEIRAS studies ..... 67
4.3.3 Summary of spectroelectrochemical measurements : Pourbaix diagram ..... 75
4.4 The origin of the pH dependence of $HCOOH/HCOO^-$ oxidation ..... 79
4.4.1 Phenomenological explanation ..... 79
4.4.2 Kinetic model ..... 81
4.4.3 The kinetic modeling ..... 84
4.4.4 Validity of the parameters ..... 91

4.4.5 The role of bridge-bonded adsorbed formate in $HCOOH/HCOO^-$ oxidation ... 93
4.5 Effect of pH dependence on electrocatalytic proton-coupled electron transfer reactions : General consideration ... 94
4.6 Interpretation of multiple oxidation peaks in cyclic voltammograms ... 101
4.7 Conclusion and remarks ... 103
References ... 107

**CHAPTER 5. ELCTROOXIDATION OF METHANOL ON Pt ... 111**

5.1 Introduction ... 111
5.2 Experiments ... 113
5.2.1 Spectroelectrochemical measurements ... 113
5.3 Results and discussion ... 115
5.3.1 Cyclic voltammetry with a rotating Pt disc electrode (RDE) ... 115
5.3.2 Partially oxidized soluble byproducts ... 118
5.3.3 SEIRAS spectra ... 120
5.4 Conclusion ... 126
References ... 127

**CHAPTER 6. SUMMARY AND PROSPECT ... 129**

**List of Publications ... 137**

**Acknowledgements ... 139**

# 学 位 論 文 内 容 の 要 旨

博士の専攻分野の名称　博士（総合化学）　氏名　ジュー　ジヨン

## 学 位 論 文 題 名

The Effect of pH on Electrocatalytic Oxidation of Small Organic Molecules on Platinum Studied by Surface-Enhanced Infrared Absorption Spectroscopy Coupled with Electrochemical Techniques

（白金表面における小有機化合物の電極触媒酸化反応に及ぼす pH の影響に関する表面増強赤外吸収分光ならびに電気化学的手法による研究）

Recently, scientific and technological researches have focused on the development of clean, efficient power sources to diminish $CO_2$ emission coming from combustion of fuels and to avoid energy crisis. One of the most encouraging of these is fuel cells using small organic molecules such as formic acid and methanol. Despite extensive research, however, there still remain many technical difficulties, some of which come from our poor understanding of the mechanism of (electro)chemical reactions taking place in fuel cells. Under these circumstances, I have studied the electrocatalytic oxidation of formic acid and methanol on Pt electrodes at the molecular scale by using surface-enhanced infrared absorption spectroscopy in the ATR mode (ATR-SEIRAS) coupled with electrochemical techniques.

Owing to the technological importance, electrocatalytic oxiadtion of formic acid and methanol to $CO_2$ on Pt in acidic media has been studied intensively for more than four decades mostly by electrochemical techniques, from which a dual pathway mechanism has been proposed and this mechanism is now generally accepted. This mechanism consists of a main reaction pathway via an active intermediate and a pathway involving a poisoning species that is oxidized to $CO_2$ at high potentials. Carbon monoxide was identified as the poisoning species in the 1980s, while the intermediate in the non-CO pathway is still unclear. Recent SEIRAS studies found that a formate species is adsorbed on Pt electrodes with a bridge-bonded configuration during the oxidation of formic acid and methanol in acidic media and the bridge-bonded adsorbed formate ($HCOO_{ads}$) was proposed to be the reactive intermediate in the non-CO pathway. In formic acid oxidation, however, there exists a claim that the bridge-bonded adsorbed formate is a site-blocking spectator and that formic acid is directly oxidized via a weakly adsorbed molecular formic acid (HCOOH) precursor. To unveil the real reaction mechanism, formic acid is investigated intensively over a wide range of pH (0-12) in the present study, because the previously proposed two pathways was expected to be distinguished by examining the pH dependence of the reaction. By combining kinetic information obtained from electrochemical measurements and structural information of adsorbed species on the electrode obtained by SEIRAS, it is shown that the both previously proposed pathways are negligible, if any, and a new pathway in which formate ($HCOO^-$) is directly oxidized is

proposed. The validity of the pathway is confirmed by a mathematical kinetic modeling of the reaction. An additional important finding of the work is that the oxidation rate becomes maximal at a pH close to the $pK_a$ of formic acid. The significance of the present study goes beyond this relatively simple electrocatalytic system because the rule that the optimal reaction conditions are predicted by $pK_a$ of the molecule of interest is the general one applicable to other decoupled proton-electron transfer reactions, including the oxidation of methanol and formaldehyde.

The thesis is composed of 6 chapters. In Chapter 1, the motivation and importance of the present work are described together with brief summaries of preceding related work and the principle of SEIRAS. In Chapter 2, experimental details are described. Chapter 3 is devoted to oxidation of CO adsorbed on Pt, the poisoning species in the oxidation of other small organic molecules, where different oxidation behaviors in acidic and alkaline media are compared and discussed. In Chapter 4, the oxidation of formic acid/formate described before is discussed extensively. In Chapter 5, the pH dependence of methanol oxidation is discussed. On-line analysis of the electrolyte solution by HPCL shows that formaldehyde and formic acid are produced as byproducts. Through these experiments, it is shown that methanol is eventually oxidized to $CO_2$ in acidic and neutral media while the reaction is terminated at formate production in alkaline media. Finally, the work is summarized in Chapter 6.

Throughout the chapters, the importance of pH variation in electrocatalysis is emphasized.

# Chapter 1. Introduction

## 1.1 Motivation and objectives

An increased atmospheric concentration of $CO_2$ resulting from tremendous fossil fuel use is now generally believed to be the main reason of global warming [1-3]. Dramatic increase of $CO_2$ through human activities undoubtedly accelerates the global warming and climate change all over the world. Therefore, clean energy is very important for development of sustainable society by using environmentally friendly energy sources.

Recently, the research and development (R&D) of electrocatalysts for production and effective use of sustainable energy sources have gained strong interests due to the demand for the sustainable society. Especially, low temperature fuel cells, such as direct alcohol fuel cells (DAFCs) and direct formic acid fuel cells (DFAFCs) are prospected to be effective electric power generation devices thanks to their high-energy efficiencies: the direct conversion of chemical energy into electric energy is free from the limitation of the second law of thermodynamics. Also, liquids are much easier to handle and transport than gaseous hydrogen fuel. However, they have a lack of commercialization due to high price of Pt and Pt group metals (the active catalyst for fuel cells), as well as incomplete understanding of the reaction mechanism which is crucial for designing more efficient catalyst. Efforts to reduce the amount of loading of expensive catalysts through enhancing the performance of fuel cells have been considerably advanced in the last few decades [4]. Furthermore, trials to replace the precious metal catalysts to more abundant, cheap materials are going on. Nevertheless, the reaction mechanisms of the reactions taking place on electrocatalysis in fuel cells has not been understood so well despite intensive studies.

Under such circumstances, I have devoted my efforts to understand the reaction mechanisms and kinetics of electrooxidation of small C1 molecules, such as formic acid (HCOOH) and methanol ($CH_3OH$). Since acidic cation exchange polymers are used as the solid electrolyte membrane for most fuel cells, electrooxidation of these molecules has been studied in acidic media. Owing to the recent development of anion exchange membranes, a renewed interest in the oxidation in alkaline media is growing. However, studies in alkaline media are much less compared to those in acidic media. Interestingly, some molecules, such as methanol, are known to be oxidized more efficiently in alkaline media than in acid media, whereas other molecules, such as formic acid, is known to be inactive in alkaline media. From these well-known facts, I considered that deeper insights into reaction mechanism could be gained through systematically studying the pH dependence of the oxidation reactions of these molecules. Actually, in my study for the last three years I could unveil the reaction mechanism of formic acid oxidation on platinum very clearly by this approach and by using electrochemical techniques coupled to surface-enhanced infrared absorption spectroscopy (SEIRAS). Electrochemical measurements provide information on the kinetics of the reactions, while SEIRAS can characterize molecules adsorbed on the electrode in situ. Combining the information from two different techniques, the oxidation mechanisms of formic acid, methanol, formaldehyde, and CO (a poison formed from molecular fuels), are discussed at molecular scale. Before reporting my results, fundamental issues related to fuel cells, preceding studies, and in situ surface analytical techniques are briefly described for facilitating the understanding of readers.

### 1.1.1 Direct Liquid Fuel Cells (DLFCs)

Among sustainable energy sources, i.e., wind power, solar energy, geothermal energy, etc., fuel cells mostly rely on (electro) catalysts. As shown in Figure 1.1, the direct liquid fuel cell is composed of an anode, a cathode and a solid electrolyte membrane. Fuel is oxidized at the anode to $CO_2$, protons and electrons. The protons transported through the electrolyte membrane react with oxygen at the cathode to yield water, while the electrons flow from the anode to the cathode. Although $CO_2$ is emitted from the anode, the influence to the environment is less than in direct combustion of the fuels owing to the high energy conversion efficiency. The overall reaction taking place in the fuel cell, the standard Gibbs free energy, the cell potential, and equilibrium potential, and pKa for each fuel are summarized in Table 1.1. Among the fuels, ethanol has highest energy density, but the reaction is terminated at acetic acid and further oxidation to $CO_2$ is very difficult. The fuel that has next highest energy density is methanol (5 kWh/L), but it is toxic. In addition, crossover of methanol through the electrolyte membrane is a problem for DMFC. Thus, it reduces the conversion efficiency. Formaldehyde is also toxic and not suitable to use. Among the organic fuels formic acid is the most promising owing to high theoretical thermodynamic cell potential, fast oxidation kinetics, less toxic nature (can be used food additives) and less crossover through membrane although its energy density (2 kWh/L) is smaller than methanol. [5].

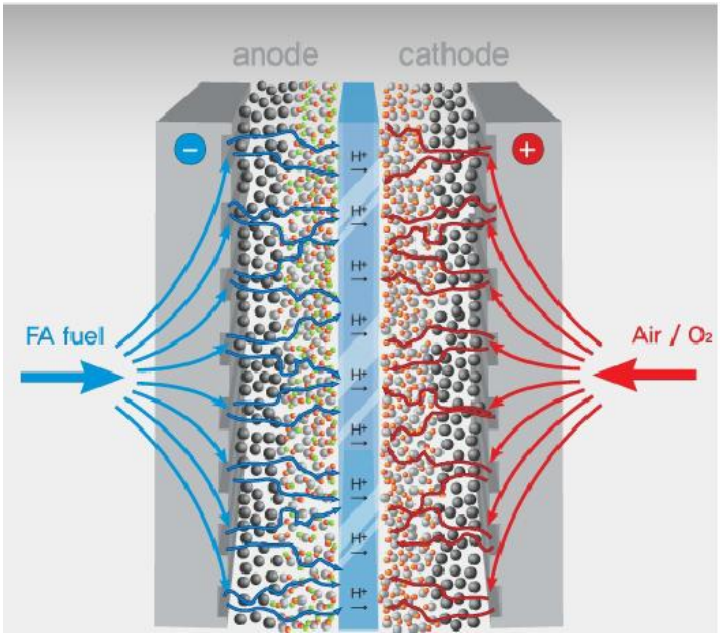


***Figure 1.1.*** (a) The schematic illustration of direct liquid fuel cells. Adopted from Electrochemical Reaction & Technology Laboratory at GIST [6].

***Table 1.1.*** The properties of fuels for DLFCs. Adopted from [5].

| **Fuel** | **Reaction** | **$\Delta G^o$/kcal mol$^{-1}$** | **$E^o$/mV** | **Potential vs. RHE/mV** | **pKa** |
|---|---|---|---|---|---|
| **Formic acid** | $HCOOH+1/2O_2 \rightarrow CO_2+H_2O$ | -68.2 | 1480 | -250 | 3.75 |
| **Methanol** | $CH_3OH+3/2O_2 \rightarrow CO_2+2H_2O$ | -166.77 | 1210 | 20 | 15.5 |
| **Formaldehyde** | $CH_2O+O_2 \rightarrow CO_2+H_2O$ | -124.7 | 1350 | -120 | 13.27 |
| **Ethanol** | $C_2H_5OH+3O_2 \rightarrow 2CO_2+3H_2O$ | -317.08 | 1145 | 85 | 15.9 |
| **Hydrogen** | $H_2+1/2O_2 \rightarrow H_2O$ | -56.69 | 1230 | 0 | _ |

As the solid electrolyte membrane, cation exchange polymers meet the needs of acceptable performance for DLFCs. Recently, electrocatalytic oxidation of small organic molecules in alkaline media has become to be received a renewed interest due to the recent advent of

alkaline anion exchange membrane for alkaline fuel cells (AFCs) [7-9] (See Figure 1.2). AFCs give some advantages over the fuel cells using cation exchange membranes, such as higher reaction kinetics at the electrodes and lower crossover rate than in acidic conditions, resulting in higher cell performance [10]. This high performance makes us to use a lower usage of a precious metal catalyst [11].

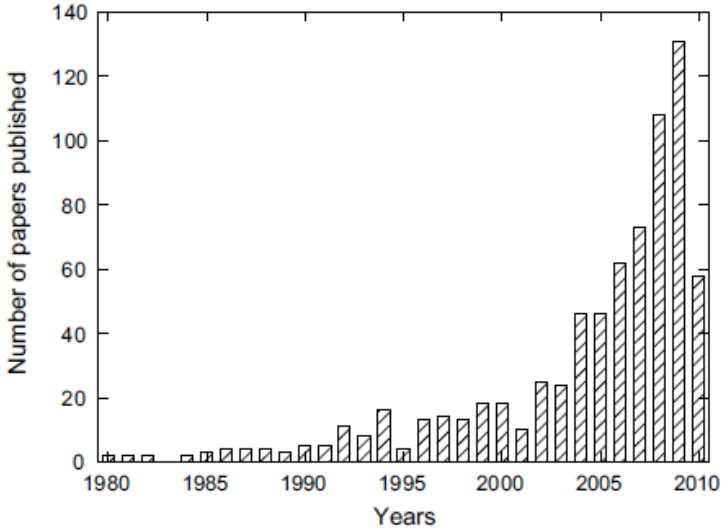


***Figure 1.2.*** Increase of the number of scientific papers related to AFCs published during the past thirty years. Adopted from [11].

## 1.1.2 Electrocatalysis

Platinum is known to have high electrocatalytic activity toward the oxidation of many C1 molecules (and also of $H_2$). However, Pt is very expensive due to its limited natural abundance, and hence its loading must be minimized for commercializing DLFCs. Several methods have been reported to lower the loading of Pt, such as spraying, electrodeposition, spreading, sputtering, painting, screen-printing, evaporation, and impregnation reduction [12].

A very serious problem common to all the organic molecules is the deactivation of the anode catalysts by the adsorption CO formed from the molecules (self-poisoning).

Associated with the accumulation of CO, the performance (current density) of fuel cells using Pt catalyst decreases with time as shown in Figure 1.3. Therefore, the development of *CO tolerant anode electrode* is a key issue for reducing Pt loading. A useful way to enhance CO tolerance is the alloying Pt with a second, or even a third metal (i.e., non-Pt metals).

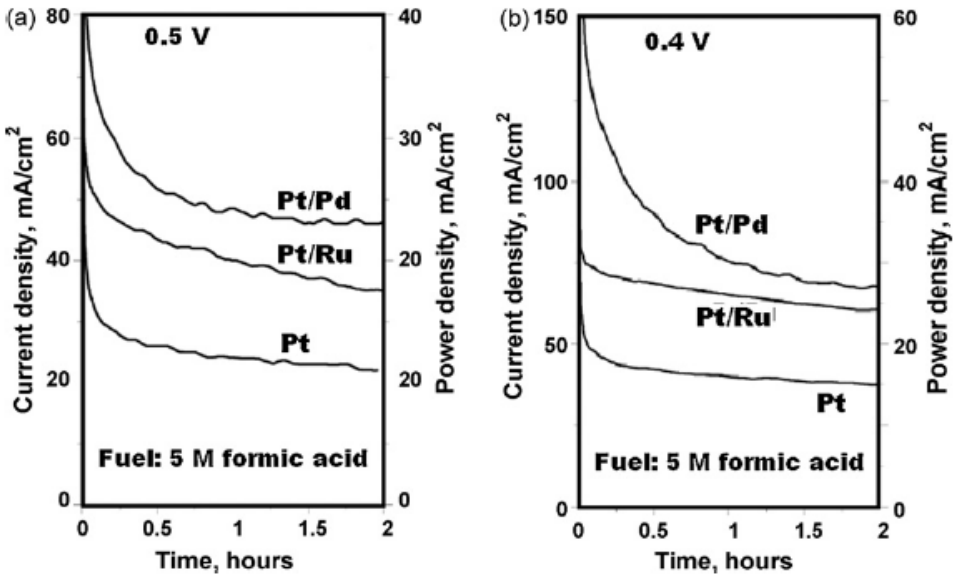


***Figure 1.3.*** Constant voltage tests on a DFAFC at cell potentials of (a) 0.5 V and (b) 0.4 V. Catalysts: platinum black, Pt/Ru, and Pt/Pd; fuel: 5 M formic acid at 0.2 ml/min; cell temperature was 30$^{o}$C. Adopted from [13]

Modifiers are believed to enhance CO tolerance and activity of Pt through : [14]

*(i) bifunctional mechanism,*

*(ii) third-body effect,*

*(iii) electronic effect*

Bifunctional mechanism assumes that the second alloying element has high affinity to oxygen and adsorbs oxygen-containing species (most likely OH). CO adsorbed on Pt reacts with the oxygen containing species adsorbed on neighboring second metal atoms to yield $CO_2$. Third-body effect assumes that more than one surface sites are required for CO formation

(ensemble effect) and that CO formation is inhibited by blocking neighboring sites by the second alloying element [15]. Electronic effect assume that d-band of Pt is modified to reduce reactant-substrate interactions, which changes a molecular orientation of the reactant molecule adsorbed on the surface by perturbing the electric field at the surface.

Effective second alloying elements are summarized in Table 1.2. Among precious metals in Group I, $Pt_{0.5}Ru_{0.5}$ exhibits highest performance for oxidation of many alcohols, particularly methanol, which has been explained in terms of bifunctional mechanism. Pt/Pd alloys also have high catalytic activity especially toward formic acid oxidation. However, Pd is unstable for extended periods of time in acidic solutions due to dissolution [5]. Ir and Au are active toward formic acid oxidation presumably due to third-body effect.

Although Pt alloys with precious metals, categorized in to Group I, has high catalytic activities, the natural abundances of these metals are small and hence they are all expensive. To overcome the cost problem, Pt alloys with cheaper non-precious metals and post-transition metals also has been examined. In this case, durability is key issues [5]. Uhm et al. [16] showed that Bi is the most attractive modifier for formic acid oxidation due to high tolerance to CO poisoning, high electrocatalytic activity and long durability over a wider range of potential.

***Table 1.2.*** Classification of secondary metals paired with Pt or Pd for formic acid fuel cell anode catalysts. Adopted from [5].

| | Elements | Remarks |
|---|---|---|
| **Group I** | Au, Ir, Pd, Pt, Ru | Precious metals |
| **Group II** | Cr, Cu, Fe, Mo, Nb, V | Non-precious transition metals |
| **Group III** | Bi, Pb, Sb, Sn | Post-transition metals |

Pt is widely believed to be the best choice for acidic solution, but other metals exhibit high performance in base. Au has been used in a number of studies [17-19]. It is inactive in acid but it show better activity than Pt or Pt/Pd alloys in basic solutions, without poisoning [19].

## 1.2 Earlier studies on electrocatalytic oxidation of small organic molecules

### 1.2.1 Experimental studies

In the earlier studies before 2002, electro-oxidation of formaldehyde [20-22], formic acid [22-25] and methanol [26-34] to $CO_2$ was studied by using conventional electrochemical methods, mostly by cyclic voltammetry. Through a tremendous number of researches by many researchers, dual pathway mechanism shown in Figure 1.4. became to be accepted widely.[References: Capon and Parsons] This mechanism composed of a main pathway *via* a reactive intermediate and a pathway involving a catalytic poison formed from the fuel molecules that is oxidized to $CO_2$ at high potentials. Several species such as –COH or CHO, and COOH, were assumed to be reactive intermediates for the direct pathway [35].

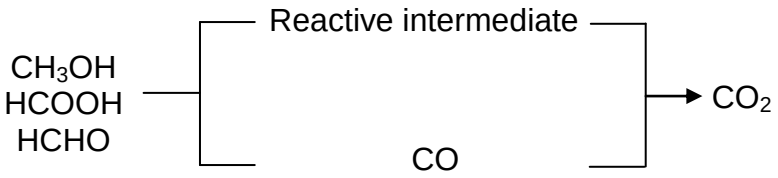


***Figure 1.4.*** Dual-path mechanism for oxidation of mechanol, fomic acid and formaldehyde at a Pt electrode.

Conventional electrochemical methods actually provide a myriad of kinetics and mechanistic information for heterogeneous redox processes and are inevitable, but it is desirable to supplement this with the molecular structural information that can now be provided by several *in situ* surface analytical techniques. Of the techniques available, infrared spectroscopy is well suited for this task since the spectral data can yield valuable information on the identity as well as reactivity of the interfacial species. This is especially true when examining multistep reactions involving adsorbed intermediate. By using infrared reflection absorption spectroscopy (IRAS, Figure 1.5a), Beden et al. [Beden, Lamy, Kunimatsu, and Bewick] showed that the poisoning species in methanol oxidation is CO. Kunimatsu et al. found that the poisoning species in formic acid oxidation is also CO. In these studies, no other species were detected. On the other hand, by using surface-enhanced infrared spectroscopy in attenuated total reflection mode (ATR-SEIRAS, figure 1.5b), Miki et al. observed for the first time that a formate species is additionally adsorbing on the electrode surface in a bridge-bonded configuration under reaction conditions. Chen et al. [JACS] and Samjeské et al. observed that the bridge-bonded formate is adsorbing on Pt electrodes also in oxidation of methanol and formaldehyde, respectively, indicating that bridge-bonded adsorbed formate is a key species for understanding the reaction mechanisms of small organic molecules as well as adsorbed CO. Since then, an effort was devoted to study the role

of bridge-bonded adsorbed for formic acid oxidation, the simplest electrocatalytic oxidation among small organic molecules.

On the basis of systematic time-resolved ATR-SEIRAS analysis of the oxidation dynamics in acidic media, Samjeské *et al.* [36, 37] suggested that adsorbed formate ($HCOO_{ads}$) is a reactive intermediate in the main pathway of formic acid oxidation and its decomposition to $CO_2$ is the rate-determining step (*rds*), as shown in Figure 1.6a, where the adsorbed formate is in equilibrium with HCOOH in the bulk solution [36].

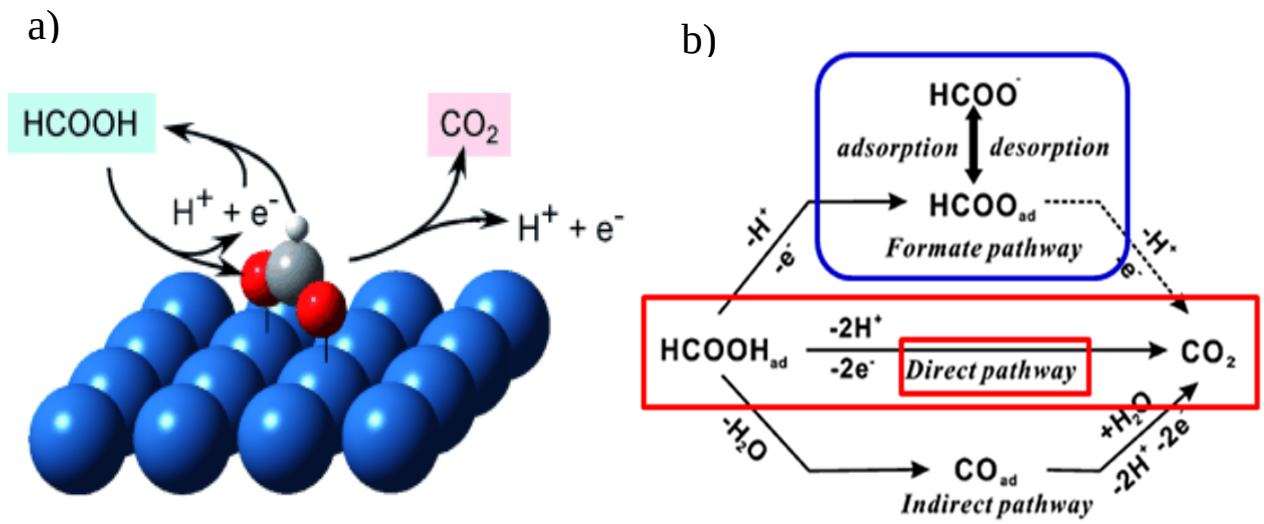


***Figure 1.6.*** Schematic description of the (a) bridge bonded formate reaction [36] (b) triple pathway reaction mechanism for formic acid oxidation on Pt [38]. White, red, grey and blue spheres represent hydrogen, oxygen, carbon and platinum atoms, respectively.

The bridge bonded formate pathway is based on the following experimental results: (i) the oxidation current increases (decreases) when the band intensity of bridge-bonded formate increases (decreases) [37], (ii) when the electrolyte solution containing $H^{13}COOH$ was exchanged to $H^{12}COOH$ containing solution, $H^{13}COO_{ads}$ is replaced to $H^{12}COO_{ads}$ within 1 s. The oxidation current calculated from the rate of the displacement is in good agreement with the observation [37], and (iii) it is well established that formic acid is oxidized to $CO_2$ in gas

phase reaction via bridge-bonded adsorbed formate and its kinetics is represented by

$$HCOOH + 2* \underset{k_1}{\overset{k_{-1}}{\leftrightarrows}} HCOO_{ads} + H^+ + e^- \xrightarrow[rds]{k_2} CO_2 + 2H^+ + 2e^- + 2* \quad (1.1)$$

$$i_{formate} \propto k_2\, \theta_{formate} \cdot \theta_{vacant} \quad (1.2)$$

where the asterisk represents a free site on the Pt surface and $k_n$ (n=1,-1, and 2) is the rate constant of each step. $\theta_{formate}$ and $\theta_{vacant}$ are the coverages of formate and vacant sites, respectively. This model is convenient to explain the oscillatory behaviors in formic acid oxidation [39-41].

On the centrally, Chen *et al.* [38, 42] claimed that bridge-bonded adsorbed formate is a site-blocking spectator rather than the intermediate, which led them to propose the triple pathway reaction mechanism as shown in figure 1.6(b) in which most oxidation current is carried by the direct oxidation of HCOOH *via* weakly adsorbed molecular HCOOH ($HCOOH_{ads}$)

$$HCOOH + p* \rightarrow HCOOH_{ads} \xrightarrow{rds} CO_2 + 2H^+ + 2e^- + p* \quad (1.3)$$

The experimental techniques used in these studies were the same and the results were essentially identical. The two different reaction mechanisms proposed stem from the different interpretations of the non-linear relationship between the band intensity of bridge-bonded formate ($\theta_{formate}$; approximately proportional to coverage) and oxidation current ($j$) (See Figure 1.7). Chen *et al.* [38] assumed that the oxidation current in formate pathway is proportional to the coverage of adsorbed formate ($\theta_{formate}$). They estimated the contribution of this pathway to the total oxidation current to be 25 % at most (15% at most for DCOOH oxidation) by assuming the oxidation current carried by the bridge-bonded adsorbed formate

is proportional to its coverage.

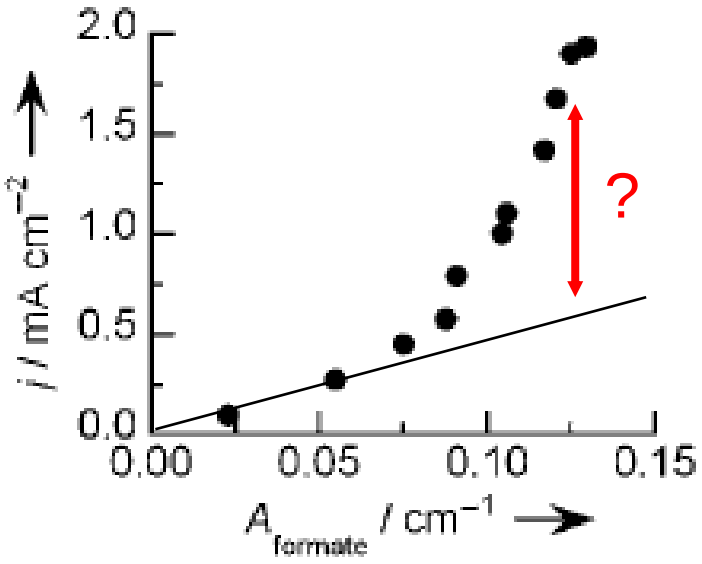


***Figure 1.7.*** Nonlinear relationship between oxidation current *j* and the band intensity of bridge-bonded adsorbed formate $A_{formate}$. $A_{formate}$ is the average of 10 spectra around t=0.5 s. Adopted from [36].

$$i_{formate} \propto k_2 \, \theta_{formate} \tag{1.4}$$

Chen et al. also found that the oxidation rate of HCOOH is twice as fast as that of DCOOH, indicating that the C-H (C-D) scissoring is the rate determining of formic acid oxidation. They ascribed the rate-determining step to the C-H bond scissoring of HCOOH, but same discussion is possible also to the C-H bond scissoring of adsorbed bridge-bonded formate.

It is important issue whether adsorbed formate is a reaction intermediate or a site-blocking spectator in the electrooxidation of HCOOH. Because adsorbed formate on Pt is commonly observed during the oxidation of all these small organic molecules (e.g., methanol, formaldehyde, etc). If adsorbed formate were a site blocking spectator, the catalyst should be designed to suppress its adsorption for better performance of DLFCs [36].

In an alkaline media, John *et al.* [43] investigated the electro-oxidation of formate

($HCOO^-$) on poly crystalline Pt by cyclic voltammetry, differential electrochemical mass spectrometry (DEMS). From the results, they suggest a dual pathway mechanism for $HCOO^-$ oxidation, analogous to HCOOH oxidation in acid. On the other hand, Jiang et al. [44] argued a triple-path mechanism :,(i) the direct path involving the formate oxidation to $CO_2$, (ii) an indirect path involving the formation of surface CO and its further oxidation to $CO_2$, and (iii) an independent third path via the oxidation of adsorbed formate ($HCOO_{ads}$) at higher potentials. They insisted that the adsorption of formate anions on Pt results in the formation of different precursor adsorbates with different reactivity. In conclusion, mechanistic study still remains unclear.

### 1.2.2 Theoretical studies

Neurock *et al* [45] theoretically studied the mechanism of electrochemical oxidation of formic acid on Pt by first principles simulation. The result at the applied potential of 0.5 V (vs. NHE) is shown in Figure 1.8. The results show that bridge-bonded formate is easily formed from formic acid, but the activation barrier for the subsequent breaking of the C-H bond of formate to form $CO_2$ is rather high (1.1 eV), i.e., bridge-bonded adsorbed formate is stable. On the other hand, although the activation barrier of HCOOH to COOH, a possible adsorbed intermediate, is 0.47 V, it is unstable and easily decomposed to $CO_2$. From the result, they concluded that the direct HCOOH oxidation pathway proposed by Chen et al. is more likely than the bridge-bonded adsorbed formate pathway proposed by Samjeské et al. Wang and Liu [46] also reached a similar conclusion as shown Figure 1.9. However, they suggested that, although bridge-bonded formate is stable, it facilitates the approach of HCOOH to the electrode surface with a CH-down orientation and lowers the activation energy of HCOOH oxidation, i.e., bridge-bonded formate acts as a catalyst for HCOOH oxidation.

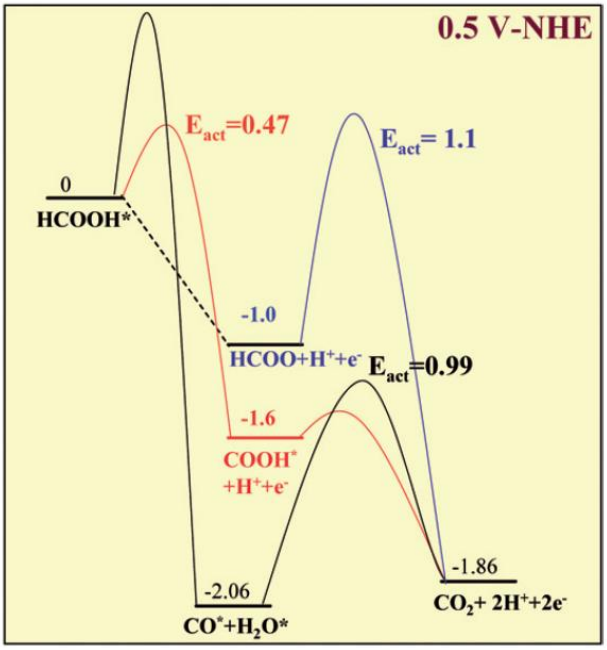


***Figure 1.8.*** DFT-calculated potential energy surface for the direct, indirect, and formate paths for the oxidation of formic acid over Pt(111) to $CO_2$ held at a constant potential of 0.5 V. Adopted from [45].

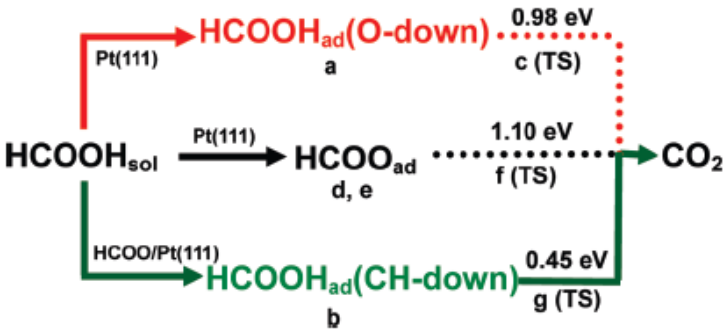


***Figure 1.9.*** Triple pathways for formic acid ($HCOOH_{sol}$) oxidation leading to $CO_2$ at Pt/$H_2O$ interface. The data are the calculated barriers. Adopted from [46].

On the other hand, Gao *et al.* [47] predicted that the both pathways are possible but the bridge-bonded formate pathway is slightly more favorable than the direct HCOOH

oxidation pathway over the entire potential range calculated as shown in Figure 1.10. Nevertheless, the difference in the activation energies of the two pathways is only ~0.1 eV, and hence it is difficult to draw definite conclusion on the predominant pathway under electrochemical condition.

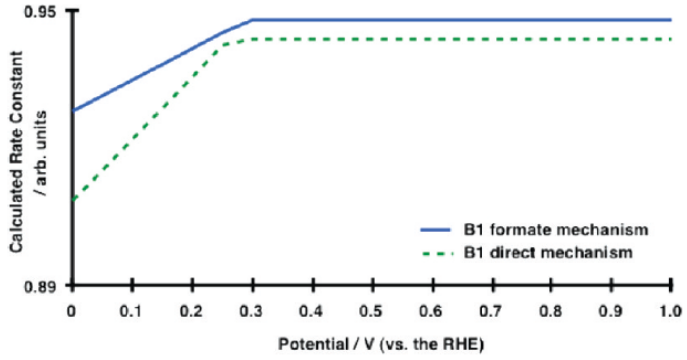


***Figure 1.10.*** Comparison of potential-dependent rate constant as calculated from canonical transition-state theory. While the formate mechanism always has a larger calculated single rate constant than the direct pathway, both mechanisms appear to converge at potentials > 0.2V, implying that both mechanisms should be operational. At potential <0.2 V, the formate pathway would ideally predominate on a Pt(111) terrace. Adopted from [47].

Furthermore, the reactivity of methanol on Pd is studied with DFT method [48, 49]. It has been found that methanol molecule cannot be activated in neutral and acid but be activated outstandingly in alkaline solution.

## 1.3 In situ characterization techniques at the electrochemical interface

Conventional electrochemical techniques, such as cyclic voltammetry and potential step chronoamperometry, are of course very powerful and inevitable in studying electrocatalytic reactions. However, it is difficult to elucidate reaction mechanisms at molecular and atomic scales only from macroscopic information obtained from such electrochemical measurements. [50]

Before mid 1980's, there had been only few *in situ* methods available for studying the electrochemical interface. Nowadays, many powerful *in situ* techniques are available, as summarized in the following:

(1) surface vibrational spectroscopy: infrared reflection spectroscopy (IRAS), surface-enhanced infrared absorption spectroscopy (SEIRAS), surface-enhanced Raman spectroscopy (SERS), and sum frequency generation (SFG)

(2) scanning probe microscope (SPM): scanning tunneling microscope (STM) and atomic force microscope (AFM)

(3) X-ray diffraction (XRD) and surface X-ray scattering (SXS)

SPM, XRD and SXS are very powerful for analyzing the structures of the electrode surface, two dimensional arrangements of adsorbed molecules, and electrode/electrolyte interface. Unfortunately, however, they do not have enough molecular specificity to identify unknown adsorbed species. In addition, it takes long time for these measurements (from a few tens seconds for SPM to several hours for X-ray based measurements).

Of the techniques available, vibrational spectroscopy is well suited for analyzing reactions at the electrochemical interface since the spectral data can yield valuable information on the identity as well as reactivity of the interfacial species. This is especially

true when examining multistep reactions involving adsorbed intermediate. Raman spectroscopy was first introduced to the studies of electrochemical interface. Owing to the surface-enhanced Raman scattering (SERS) effect in which Raman cross section of adsorbed molecules is extraordinary enhanced, it is a very promising. Nevertheless, its use is limited to coinage metals such as Ag and Au in practice. Although SERS has been observed also on transition metals including Pt and Pd, the enhancement is not so significant as on coinage metals.

Next introduced was infrared reflection absorption spectroscopy (IRAS).[Iwasita & Nart] In this measurement, infrared radiation is shed on the electrode through an infrared transparent window (mostly $CaF_2$) and the electrolyte solution, and the reflected beam is detected, as shown in Figure 1.5a. Since the aqueous solution strongly absorbs the infrared radiation, the thickness of the solution sandwiched between the working electrode and the window must be thin enough (a few micrometer). An advantage of IRAS is that well defined single crystals can be used as working electrodes, as well as polycrystalline [51, 52]. Thanks to the development of Fourier transform infrared (FT-IR) spectrometers, IRAS has enough sensitivity to detect submonolayers on metal surfaces and has been used widely in surface science studies in vacuum and gas phase. However, complete subtraction of the background signal of the solution is difficult even if the thin layer is used and the interference from the solution hampers the detection of weakly IR absorbing molecules. Furthermore, this technique has several other serious problems when it is applied for dynamic studies, which arises from the use of thin solution layer. One is the slow response of the thin layer cell with respect to the externally applied potential modulations due to the large solution resistance [51-54]. The other is the limited mass transport between the thin solution layer and the reservoir, which makes monitoring of the reactions difficult, because the reactant molecules in the thin layer are exhausted quickly and the reaction products are accumulated during the

spectral measurements. This is the reason why IRAS failed to detect bridge-bonded adsorbed formate in the oxidation of methanol and formic acid.[Senzaki et al]

ATR-SEIRAS is free from such problems of IRAS. In this measurement, infrared radiation is introduced from the backside though an IR transparent (Si or Ge) prism and the beam reflected from the thin working electrode is detected. Since the IR radiation does not path though the solution, the solution is not necessary to be thin as in IRAS, and so the interference from the solution is much smaller. In addition, IR absorption of molecules adsorbed on the electrode is significantly enhanced. As a result, reactions at the electrode surface can be monitored at a high time resolution (typically ms to s) without interference from the solution.

SFG is a rather new technique that has high surface sensitivity and selectivity. In this measurement, a visible beam with a frequency of $\omega_{vis}$ and an IR beam with a frequency of $\omega_{IR}$ are overlapped at the surface, which yields a photon with the sum frequency of $\omega_{vis} + \omega_{IR}$. When $\omega_{IR}$ is equal to a vibrational level of the molecule, the SFG signal is resonantly enhanced [55, 56]. SFG does not occur in homogenous media with symmetry of inversion under electric dipole approximation and is active only at the surface or interface where symmetry of inversion is broken [55, 56]. This is an important character of SFG, but it has the same problem as IRAS that the solution layer must be thin enough to reduce the absorption of IR photons by the solution. In addition, SFG system is quite expensive and the interpretation of SFG spectra is still not easy. Due to these reasons, SFG is less popular than IR in the studies of electrocatalysis.

In addition to the abovementioned surface analytical tools, differential electrochemical mass spectrometry (DEMS) and high performance liquid chromatography (HLPC) are used to analyze volatile and soluble reaction products, respectively, in conjunction with electrochemical techniques.

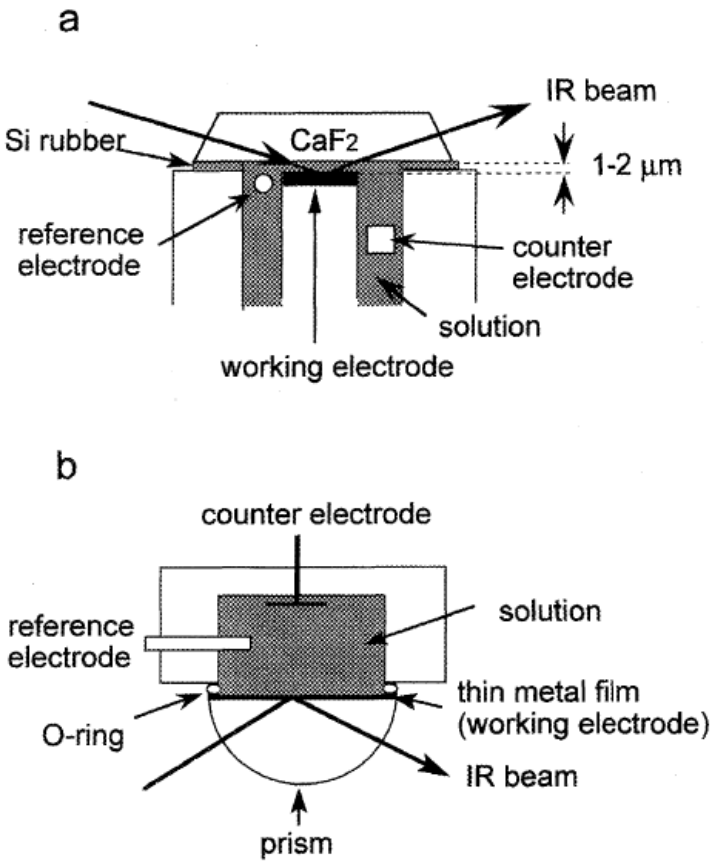


***Figure 1.5.*** Electrochemical cells and optical arrangements used for *in situ* characterization of electrode/electrolyte interfaces with IRAS and ATR-SEIRAS techniques (a and b, respectively). Adopted from [57].

Each technique has advantages and drawbacks, but so far ATR-SEIRAS is most successfully used in the studies of electrocatalysis owing its advantages:

- *Less interference from the solution background*
- *Simple surface selection rule*
- *Fast response of cell*
- *Free mass transport*
- *High signal sensitivity*

## 1.4 Principle of SEIRA

### 1.4.1 General features of surface-enhanced infrared absorption (SEIRA)

Surface-enhanced infrared absorption (SEIRA) is a phenomenon in which infrared absorption of molecules adsorbed on metal surfaces is greatly enhanced [58, 59]. This phenomenon was observed for the first time by Hartstein et al. [60] and further confirmed by Hatta et al.[Hatta, Ohshima, and Suetaka] SEIRA has following general features:

(1) The effect is significant on nano particles and rough surfaces on the order of nanometers. AFM images of typical SEIRA-active surfaces [61] are shown in Figure 1.11. Figure 1.11a is of a thin Au film chemically deposited on Si, while Figure 1.11b is of a thin film vacuum evaporated on Si. The vacuum evaporated film is composed of metal islands of an average dimension of 70 nm and exhibited a pale color arising from the excitation of collective electron resonance (or plasmon) characteristic to nanoparticles. On the other hand, the surface of the chemically deposited film is shiny and exhibits gold color characteristic to massive Au, but the AFM image shows that its surface is rough with average dimension of about 300 nm hand height less than 20 nm. Such nanostructures are known to play an important role in SEIRA.

(2) The SEIRA effect is extreme for the first adsorbed layer and fades away with increasing the distance from the surface.

(3) Molecular vibrations that have oscillating dipole components normal to the surface are selectively enhanced, and hence SEIRA spectra are generally simpler than those of the original molecules.

The aforementioned nature is similar to that of surface-enhanced Raman scattering (SERS) in which Raman scattering of molecules adsorbed on metal nanoparitcles and rough

metal surfaces is significantly enhanced. However, there is a significant difference in the kind of metals available for SEIRA and SERS. SERS is essentially limited to free electron metals, especially to coinage metals such as Ag, Au, and Cu, while any metals are available for SEIRAS including Pt and Pt-group metals as well as coinage metals.[[62], Miyake et al., Chem. Phys Lett. And PCCP, [63]]. Therefore, SEIRA spectroscopy (SEIRAS) is more useful than SERS for analyzing the mechanism and kinetics of electrocatalytic reactions.[[63, 37],Samjeske,Miyake et al. PCCP]. In addition, the short ranged signal enhancement facilitates *in situ* examination of the electrode surface without significant interference from the bulk solution with high time resolutions ranging from *ps* to *ms* [Ataka et al.(heptylviologen),Yamakata, Uchida, Kubota, Osawa, J. Phys. Chem. B].

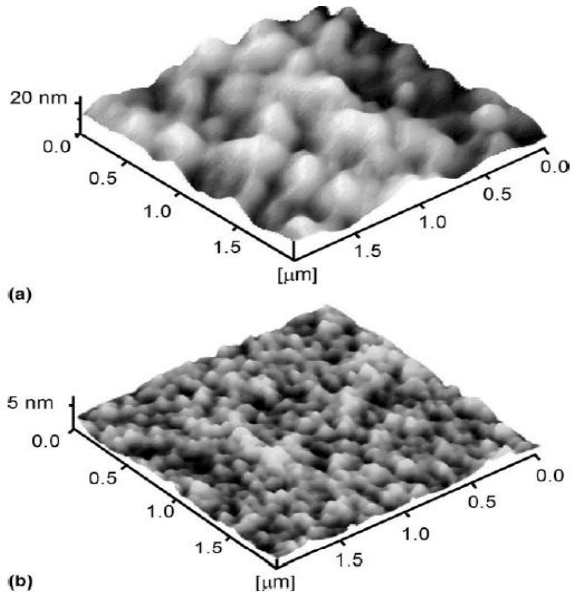


***Figure 1.11.*** AFM images of chemically deposited (a) and vacuum evaporated (b) Au films on Si (2 x 2 $\mu m^2$). Adopted from [4].

### 1.4.2 Electromagnetic Mechanism for SEIRA

It is well established that a strong electric field is generated around metal nanoparticles and on rough metal surfaces by incident photons through the excitation of surface plasmon (i.e., polarization). Such an electromagnetic mechanism is one of the major origins of SERS. In analogy, the same mechanism is expected to contribute also to SEIRA. We will model a thin island film, the most typical SEIRA-active substrate, by an array of rotating ellipsoids, as shown in Figure 1.12. Rough metal films also may be modeled similarly. The enhanced electric field that excites adsorbed molecules is perpendicular to the surface at any points of the surface of nanoparticles and decays in proportion to $1/r^3$, where r is the distance from the surface. This model is convenient to explain the surface selection rule (as described in more detail later) and the short-ranged enhancement.

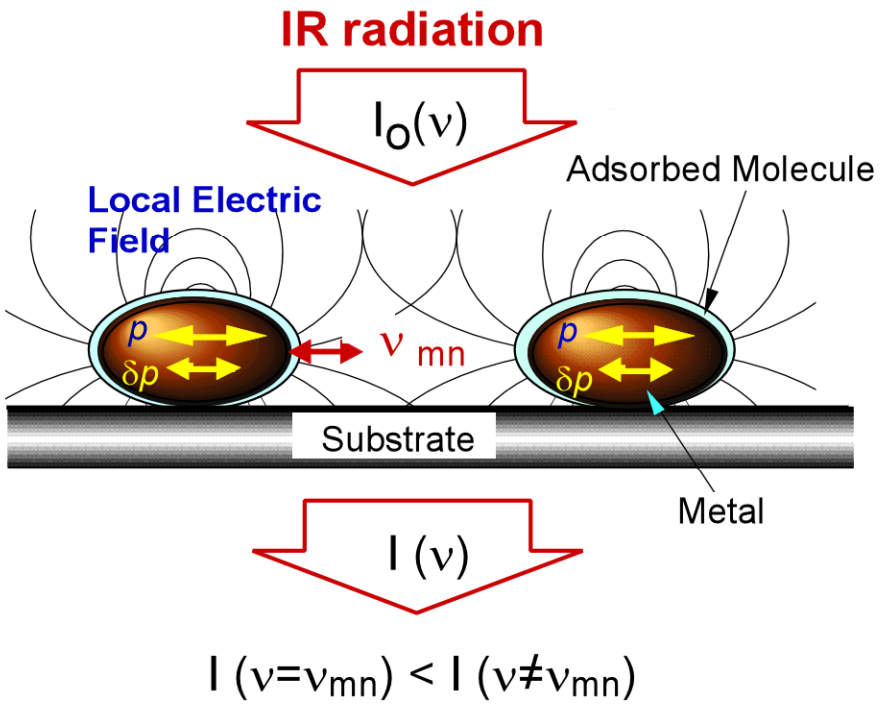


***Figure 1.12.*** Schematic representation of the electromagnetic mechanism of SEIRA on metal island films. Incident photon filed $I_o$ polarizes the metal islands and the dipole $p$ generates an

enhanced local electric field around the islands, which excites molecular vibration $\nu_{mn}$. The molecular vibration induces an additional dipole $\delta p$ in the metal islands and perturbs the optical properties of the metal island film. Adopted from [53].

The oscillating dipole moment of the adsorbed molecule ($d\mu$) can perturb the polarization induced in nanoparticles ($p$), which changes the absorbance or reflectance of the nanoparticle array. The perturbation is more significant at molecular vibrational frequencies than other frequencies. Therefore, the molecular vibrations are expected to be observable through measuring the absorbance or reflectance of the metal island film. Osawa et al. confirmed this mechanism by a simple electromagnetic simulation as follow.

The metal particles are much smaller than the wavelength of IR radiation (2.5–25 μm), and hence the nanoparticle array can be further simplified to a uniform film composed of the metal, adsorbed molecules and medium surrounding, as shown in Figure 1.13.

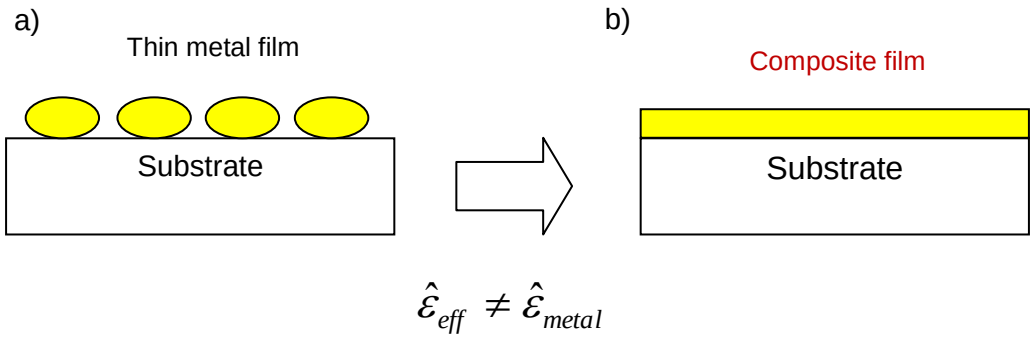


***Figure 1.13.*** (a) Structure of an evaporated thin metal film, which can be approximated by a uniform composite film of the metal, adsorbed molecules and host media (b). Adopted from [64].

The effective (or averaged) dielectric function of the modeled composite film, $\varepsilon_{eff}$, can be estimated by an effective medium theory. A simulated result using the Bruggeman effective medium theory is shown in Figure 2.4. The solid spectra are of nanoparticles with different aspect ratios ($\eta$ = a/b, where where a and b are the radius along the major and minor

axes of the ellipsoid, respectively), while dashed spectra is of normal spectra without the metal, which clearly demonstrates that SEIRA actually occurs via the above-mentioned electromagnetic mechanism and the enhancement is greatly affected the shape of the nanoparticle.

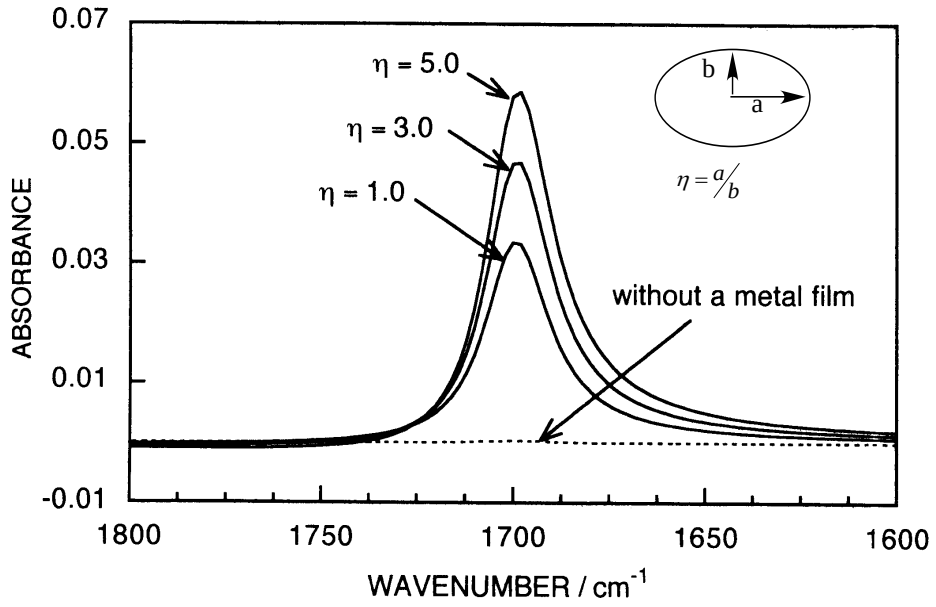


***Figure 1.14.*** SEIRA spectra of a model molecule adsorbed on Ag island films simulated by using the Bruggeman effective-medium models. The mass thickness of the Ag film is 8 nm. The dashed trace is the spectrum of a molecular layer on the substrate ($CaF_2$) without a metal film. $\eta$ represents the aspect ratio of the metal ellipsoid. Adopted from [51].

### 1.4.2.1 Surface selection rule

SEIRA-active substrates are either nanoparticles or rough surface, and hence the orientation of adsorbed molecules is random on average. Nevertheless, only vibrations having dipole transition moments along the surface normal is observable. The surface selection rule in SEIRAS that is identical to that in IRAS on flat surfaces. The experimental fact can be understand if we assume that the local electric field around the nanoparticles is normal to

local surface at any point. This is what predicted by the electromagnetic model discussed above. In this model, absorbance A is given as

$$A \propto \left| d\vec{\mu}/dQ \cdot \vec{E} \right|^2 = \left| d\vec{\mu}/dQ \right|^2 \cdot \left| \vec{E} \right|^2 \cdot \cos^2\theta \propto \cos^2\theta$$

where $d\vec{\mu}/dQ$ is the oscillating dipole moment of a vibration, $\vec{E}$ is the local electric field (normal to the surface), and $\theta$ is the angle between them (Figure 1.15). By using this equation, $\theta$, i.e., the tilting angle of the dynamic dipole moment or molecular orientation, can be determined.

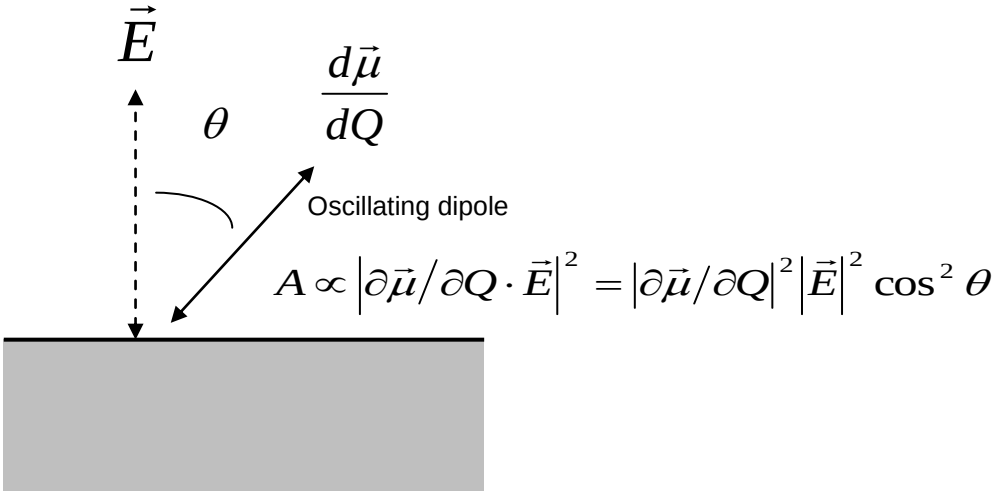


***Figure 1.15.*** A schematic illustration of absorbance (A). See further details in the text.

The surface selection rule can be explained also by the image dipole model shown in Figure 1.16. Positive (negative) charge on the surface induces negative (positive) image charge in the metal (Figure 1.16a). Thereby, the perpendicular component is doubled, whereas the parallel component is canceled by its image dipole [65]. Therefore, only molecular vibrational motion giving rise to a dynamic dipole moment perpendicular to the substrate will be detected in the vibrational spectrum [51, 57, 64, 65]. In this case also,

absorbance is proportional to $\cos^2\theta$.

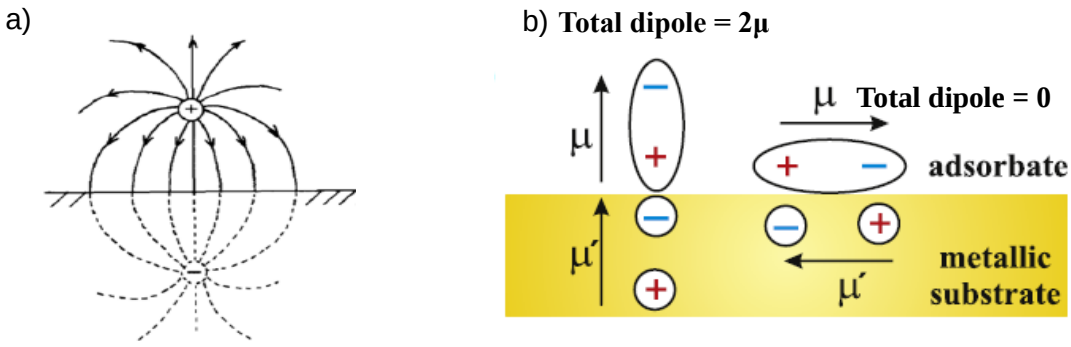


***Figure 1.16.*** Qualitative explanation of the orientation selection rule for dipole surface scattering: (a) the lines of force and the electrical image resulting from a positive charge over the surface of a conductor (the metal surface is the upper line above the hatched area). (b) the image dipole within the substrate compensates the effect of the adsorbed dipole for paralleled orientation but enhances the effect of dipoles with a normal orientation. Adopted from [65].

Figure 1.17 illustrates how surface selection rule is applied to the adsorbed molecules on the surface. Formate exhibit two characteristic IR bands ascribed to symmetric and asymmetric O-C-O stretching modes, which yield dynamic dipole moment along and normal to the C-H bond. Recalling that the intensity of a band is proportional to $\cos^2\theta$, if formate is adsorbed through two oxygen atoms as shown in this figure, the stretching O-C-O mode is IR active and the asymmetric O-C-O mode is IR inactive. The C-O stretching mode of adsorbed CO is also IR active. The surface selection rule is used to analyze the geometry of adsorbed species from chapter 3 to chapter 5.

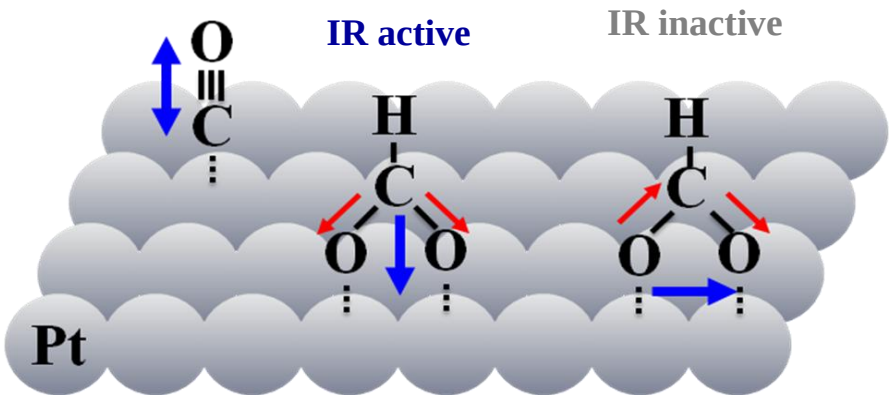


***Figure 1.17.*** The cartoon showing surface selection rule on the metal substrate.

## 1.5 Outline of the thesis

The present thesis is composed of six chapters including Chapter 1 devoted to Introduction and describes principle of SEIRAS.Experimental method is introduced in Chapter 2. Detailed experimental conditions for the *in situ* ATR-SEIRAS coupled to electrochemistry are also given. It begins with the relatively simple CO oxidation (Chapter 3), and move on to HCOOH (Chapter 4) and $CH_3OH$ oxidation (Chapter 5), sequentially. In Chapter 3, CO oxidation on Pt in alkaline media is studied and compared with that in acidic media that has been studied extensively. The systematic study for HCOOH oxidation over the wide range of pH (0-12) is the main subject of Chapter 4. We will show that the bridge-bonded formate pathway actually works, and moreover the formate ion, $HCOO^-$, is the major reactant over the whole pH range examined, even in acid. Therein, the pH dependence is explained by simple kinetic modeling. From the results, oxidation current shows a maximum at a pH close to the pKa of HCOOH. Then, in chapter 5, $CH_3OH$ oxidation is carried out to reinforce the importance of pH variation in catalytic proton-coupled electron transfer reactions by supported Chapter 4. Finally, a summary and prospect is given in Chapter 6.

# References

[1] I.P.O.C. Change, Agenda, 6 (2007).

[2] J.G. Charney, A. Arakawa, D.J. Baker, B. Bolin, R.E. Dickinson, R.M. Goody, C.E. Leith, H.M. Stommel, C.I. Wunsch, in, Washington, DC: National Academy of Sciences Press, 1979.

[3] J.T. Houghton, Y. Ding, D.J. Griggs, M. Noguer, P.J. van der LINDEN, X. Dai, K. Maskell, C. Johnson, Climate change 2001: the scientific basis, Cambridge University Press Cambridge, 2001.

[4] P. Costamagna, S. Srinivasan, J. Power Sources, 102 (2001) 242-252.

[5] S. Uhm, H.J. Lee, J. Lee, Phys. Chem. Chem. Phys.**,,** 11 (2009) 9326-9336.

[6] http://env1.gist.ac.kr/ertl/new/.

[7] A.M. Bartrom, J.L. Haan, J. Power Sources, 214 (2012) 68-74.

[8] J. Jiang, A. Wieckowski, Electrochem. Commun., 18 (2012) 41-43.

[9] E.H. Yu, X. Wang, U. Krewer, L. Li, K. Scott, Energy Environ. Sci., 5 (2012) 5668-5680.

[10] Y.-J. Wang, J. Qiao, R. Baker, J. Zhang, Chem. Soc. Rev., 42 (2013) 5768-5787.

[11] G. Merle, M. Wessling, K. Nijmeijer, J. Membrane Sci., 377 (2011) 1-35.

[12] W. Zheng, A. Suominen, A. Tuominen, Energy Procedia, 28 (2012) 78-87.

[13] C. Rice, S. Ha, R.I. Masel, A. Wieckowski, J. Power Sources, 115 (2003) 229-235.

[14] J. Lipkowski, Electrocatalysis, John Wiley & Sons, pp. 75-153, (1998).

[15] W. Schmickler, Interfacial Electrochemistry, Oxford University Press, USA, 1996.

[16] S. Uhm, H.J. Lee, Y. Kwon, J. Lee, Angew. Chem. Int. Ed., 120 (2008) 10317-10320.

[17] Y. Kwon, S.C.S. Lai, P. Rodriguez, M.T.M. Koper, J. Am. Chem. Soc., 133 (2011) 6914-6917.

[18] M. Enyo, J. Appl. Electrochem., 15 (1985) 907-911.

[19] R. Parsons, T. VanderNoot, J. Electroanal. Chem., 257 (1988) 9-45.

[20] A. Miki, S. Ye, T. Senzaki, M. Osawa, J Electroanal. Chem., 563 (2004) 23-31.

[21] E.A. Batista, T. Iwasita, Langmuir, 22 (2006) 7912-7916.

[22] R.P. Buck, L.R. Griffith, J. Electrochem. Soc., 109 (1962) 1005-1013.

[23] A. Capon, R. Parsons, J. Electroanal. Chem., 44 (1973) 1-7.

[24] A. Capon, R. Parsons, J. Electroanal. Chem., 45 (1973) 205-231.

[25] H. Kita, T. Katagiri, K. Kunimatsu, J. Electroanal. Chem., 220 (1987) 125-138.

[26] V.S. Bagotzky, Vassilye.Yb, Electrochim. Acta, 12 (1967) 1323-1343.

[27] E.A. Batista, G.R.P. Malpass, A.J. Motheo, T. Iwasita, Electrochem. Commun., 5 (2003) 843-846.

[28] E.A. Batista, G.R.P. Malpass, A.J. Motheo, T. Iwasita, J. Electroanal. Chem., 571 (2004) 273-282.

[29] Y.X. Chen, A. Miki, S. Ye, H. Sakai, M. Osawa, J. Am. Chem. Soc., 125 (2003) 3680-3681.

[30] K. Franaszczuk, E. Herrero, P. Zelenay, A. Wieckowski, J. Wang, R.I. Masel, J. Phys. Chem., 96 (1992) 8509-8516.

[31] T.H.M. Housmans, M.T.M. Koper, J. Phys. Chem. B, 107 (2003) 8557-8567.

[32] T. Iwasita, Electrochim. Acta, 47 (2002) 3663-3674.

[33] Z. Jusys, R.J. Behm, J. Phys. Chem B, 105 (2001) 10874-10883.

[34] S. Wasmus, A. Kuver, J. Electroanal. Chem., 461 (1999) 14-31.

[35] S.G. Sun, J. Clavilier, A. Bewick, J. Electroanal. Chem., 240 (1988) 147-159.

[36] M. Osawa, K. Komatsu, G. Samjeske, T. Uchida, T. Ikeshoji, A. Cuesta, C. Gutierrez, Angew. Chem. Int. Ed., 50 (2011) 1159-1163.

[37] G. Samjeske, A. Miki, S. Ye, M. Osawa, J. Phys. Chem. B, 110 (2006) 16559-16566.

[38] Y.X. Chen, M. Heinen, Z. Jusys, R.J. Behm, Langmuir, 22 (2006) 10399-10408.

[39] Y. Mukouyama, M. Kikuchi, G. Samjeske, M. Osawa, H. Okamoto, J. Phys. Chem. B, 110 (2006) 11912-11917.

[40] G. Samjeske, A. Miki, S. Ye, A. Yamakata, Y. Mukouyama, H. Okamoto, M. Osawa, J. Phys. Chem. B, 109 (2005) 23509-23516.

[41] G. Samjeske, M. Osawa, Angew. Chem. Int. Ed., 44 (2005) 5694-5698.

[42] Y.X. Chen, M. Heinen, Z. Jusys, R.J. Behm, Angew. Chem. Int. Ed., 45 (2006) 981-985.

[43] J. John, H.S. Wang, E.D. Rus, H.D. Abruna, J. Phys. Chem. C, 116 (2012) 5810-5820.

[44] J. Jiang, J. Scott, A. Wieckowski, Electrochim. Acta, 104 (2013) 124-133.

[45] M. Neurock, M. Janik, A. Wieckowski, Faraday Discuss., 140 (2008) 363-378.

[46] H.F. Wang, Z.P. Liu, J. Phys. Chem. C, 113 (2009) 17502-17508.

[47] W. Gao, J.A. Keith, J. Anton, T. Jacob, J. Am. Chem. Soc., 132 (2010) 18377-18385.

[48] X.Q. Qi, Z.D. Wei, L.L. Li, L. Li, M.B. Ji, Y. Zhang, M.R. Xia, X.L. Ma, J. Mol. Struct., 980 (2010) 208-213.

[49] J. Yang, Y.H. Zhou, H.B. Su, S.P. Jiang, J. Electroanal. Chem., 662 (2011) 251-256.

[50] S. Ye, T. Kondo, N. Hoshi, J. Inukai, S. Yoshimoto, M. Osawa, K. Itaya, ChemInform, 41 (2010).

[51] M. Osawa, Surface-Enhanced Infrared Absorption, in: S. Kawata (Ed.) Near-Field Optics and Surface Plasmon Polaritons, Springer Berlin Heidelberg, 2001, pp. 163-187.
[52] Y.G. Yan, Q.X. Li, S.J. Huo, M. Ma, W.B. Cai, M. Osawa, J. Phys. Chem. B, 109 (2005) 7900-7906.
[53] M. Osawa, Surface-Enhanced Infrared Absorption Spectroscopy, in: Handbook of Vibrational Spectroscopy, John Wiley & Sons, Ltd, 2006.
[54] M. Osawa, In-situ Surface-Enhanced Infrared Spectroscopy of the Electrode/Solution Interface, in: Advances in Electrochemical Science and Engineering, Wiley-VCH Verlag GmbH, 2008, pp. 269-314.
[55] S. Ye, M. Osawa, Chem. Lett., 38 (2009) 386-391.
[56] A.J. Bard, Electrochemical methods: Fundamentals and Applications, 2nd ed. John Wiley & Sons, Inc (2001).
[57] M. Osawa, Bull. Chem. Soc. Jpn., 70 (1997) 2861-2880.
[58] M. Osawa, W. Suetaka, Surf. Sci., 186 (1987) 583-600.
[59] M. Osawa, M. Kuramitsu, A. Hatta, W. Suetaka, Surf. Sci., 175 (1986) L787-L793.
[60] A. Hartstein, J.R. Kirtley, J.C. Tsang, Phys. Rev. Lett., 45 (1980) 201-204.
[61] H. Miyake, S. Ye, M. Osawa, Electrochem. Commun., 4 (2002) 973-977.
[62] H. Miyake, E. Hosono, M. Osawa, T. Okada, Chem. Phys. Lett., 428 (2006) 451-456.
[63] H. Miyake, T. Okada, G. Samjeske, M. Osawa, Phys. Chem. Chem. Phys., 10 (2008) 3662-3669.
[64] M. Osawa, K. Ataka, K. Yoshii, T. Yotsuyanagi, J. Electron Spectrosc., 64-5 (1993) 371-379.
[65] P. Tegeder, J. Phys.: Condens. Mat., 24 (2012).

# Chapter 2. Experimental methods

## 2.1 Chemicals and electrolyte solutions

Chemicals were analytical grade ones purchased by Wako Pure Chemicals and used as received without further purification. All solutions were prepared using water purified with a Millipore Milli-Q Advantage A10 system (18 MΩ cm). Details of chemicals and supporting electrolyte solution will be described in experimental section of the forthcoming chapters. The solutions were deaerated by bubbling with ultra-pure Ar before each experiment.

## 2.2 Electrochemical measurements

### 2.2.1 Electrochemical instruments

A potentiostat/galvanostat (EG&G PAR model 263A) interfaced to a PC was used to control the electrode potential, and to record cyclic voltammograms (CV) and chronopotentiograms under galvanostatic conditions. The cell resistance was measured by current interruption method [1] and used to compensate ohmic drop in cyclic voltammetry by using M270 software package (Princeton Applied Research).

### 2.2.2 Conventional electrochemical measurements with a rotating disc

Conventional electrochemical measurements were performed with a Pt rotating disc electrode sheathed in Teflon rod (5 mm in diameter, Hokuto Denko). The electrode surface was mirror finished with 0.5 μm alumina slurry and sonicated in Milli-Q water. The electrode surface was further cleaned in the test electrolyte solution before each experiment by cycling the electrode potential between hydrogen evolution and surface oxidation regions until a steady CV was obtained. The electrochemical cell used was a three-electrode design with an

Ag/AgCl (KCl saturated) reference electrode and a Pt mesh counter electrode. The working electrode was rotated at 0-2000 rpm with a Hokuto Denko HR-301 system. A picture of the rotating disc electrode system is represented in Figure 2.1.

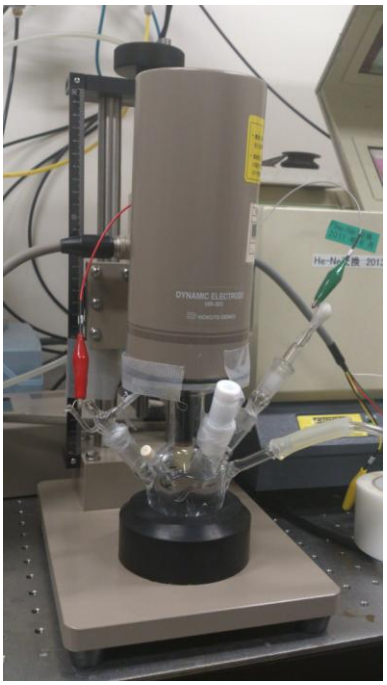

***Figure 2.1.*** Rotating electrode system.

## 2.3 Spectroelectrochemical measurements

SEIRA spectra of the working electrode surface was collected sequentially with a time resolution of 0.39 or 2 s (a time required for accumulating 5 or 25 interferometer scans, respectively) simultaneously with electrochemical measurements (cyclic voltammetry or chronopotentiometry under galvanostatic conditions) with the ATR configuration (Figure 1.5b). A Bio-Rad 60A/896 or 575C Fourier transform infrared (FT-IR) spectrometer equipped with an HgCdTe (MCT) detector was used in recording spectra. Spectral resolution used was 4 $cm^{-1}$. The reference spectrum, $R_{ref}$. was collected in advance at a suitable potential in the pure electrolyte solution and then the target molecule (methanol, formic acid, or formaldehyde) was added to the solution to a desired concentration (typically, 20 mM). All

spectra are shown in absorbance units defined as $A = -\log(R_s/R_f)$, where $R_s$ represents the sample spectrum collected after adding the target molecule.

### 2.3.1 Spectroelectrochemical cell

The electroelectrochemical cell with a three-electrode design made of either glass or Kel-F was used in the SEIRAS measurements. The glass spectroelectrochemical cell used in the most experiments is schematically shown in Figure 2.2. A Luggin capillary placed close to the working electrode was used to minimize ohmic drop. The Pt-coated Si prism (the working electrode, vide infra) was attached to the bottom flange of the cell by sandwiching an O-ring (Kalrez® ) and an Au ring. The Au ring was used to make electric contact with the potentiostat /galvanostat. In the study of methanol oxidation, the flow cell made of Kel-F (See Figure 2.3) was used for washed away the partially oxidized products (formaldehyde and formic acid) formed during the reaction.

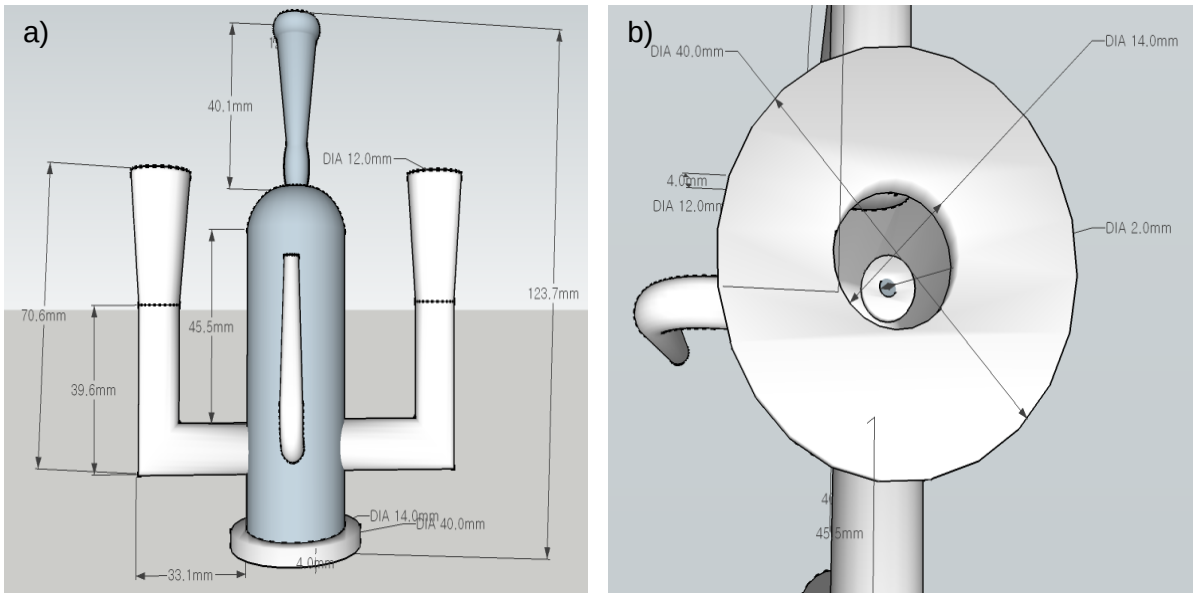


***Figure 2.2.*** Schematic drawing of the experimental setup for electrochemical reaction cell.

(a) front view and (b) bottom view.

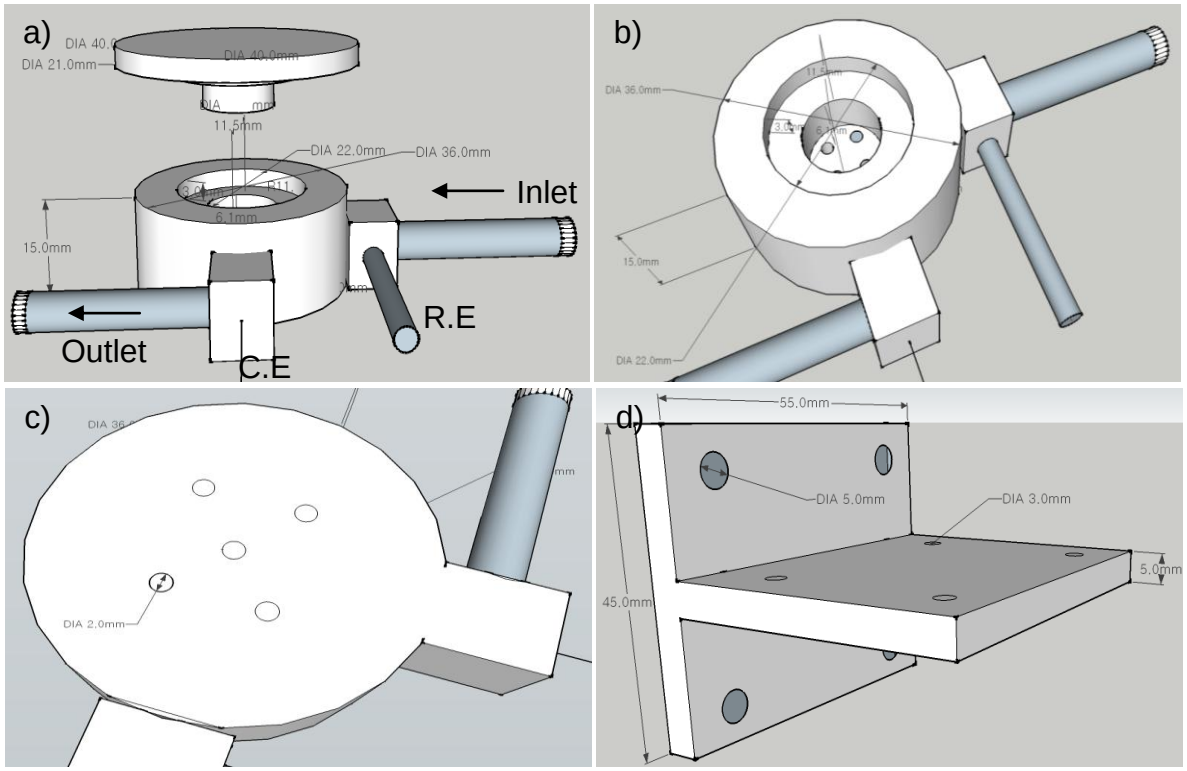


***Figure 2.3.*** Schematic drawing of a flow cell made of Kel-F : (a) front view (b) top view (c) bottom view, and (d) flow cell holder.

## 2.3.2 Preparation of the working electrode

A thin Pt film (~50 nm thick) was chemically deposited on the reflecting plane of a Si triangle prism (Pier Optics, Tatebayashi) following the recipe developed by Miki et al. [2] Briefly, after removing surface oxide and terminating the surface with H by contacting the reflection plane to 40% $NH_4F$ for 1.5 min., Pd was deposited on the Si substrate surface by contacting with 1 wt% HF containing 1 mM $PdCl_2$ for 5 min to make nucleation sites and to improve the adhesion of the Pt film to the substrate. After rinsing with Milli-Q water, Pt was deposited subsequently on the Pd layer by dropping a commercially available plating bath

(LECTROLESS PT100, Electroplating Engineering of Japan) at 60 ℃ for a desired period of time (typically 3-5 min), as shown in Figure 2.4.

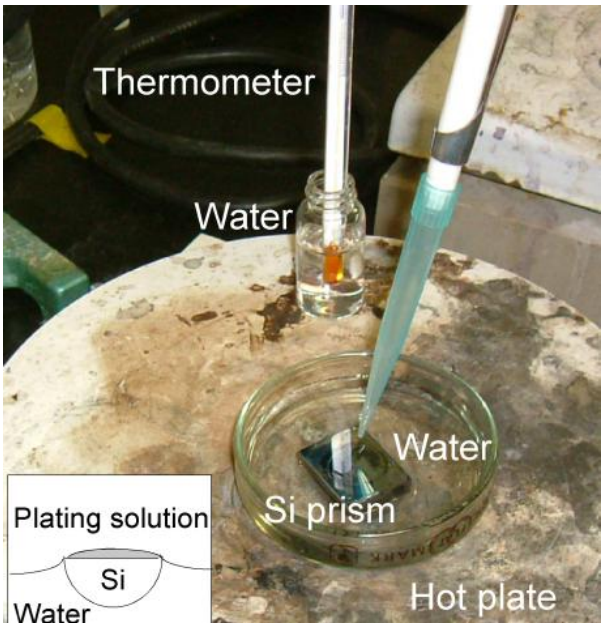


***Figure 2.4.*** Chemical deposition of a thin Pt film on Si on a hot plate. The temperature of the prism is kept at 60℃ by immersing water bath.

### 2.3.3 Reflection accessory

The reflection accessory used for ATR-SEIRAS measurements, which were set in the sample compartment of the FT-IR spectrometer, is shown in Figure 2.5. A flat Au mirror prepared by vacuum evaporating on the both sides of a glass plate (for microscopic observation) is placed at the focusing point by rotating 45° with respect to the incident beam. The IR radiation reflected from the flat mirror (2) is flipped up and focused again at the sample position with a concave mirror (3). The reflected beam (4) is flipped back and focused at the backside of the center flat mirror by another concave mirror (5), and introduced to the detector in the FT-IR spectrometer.

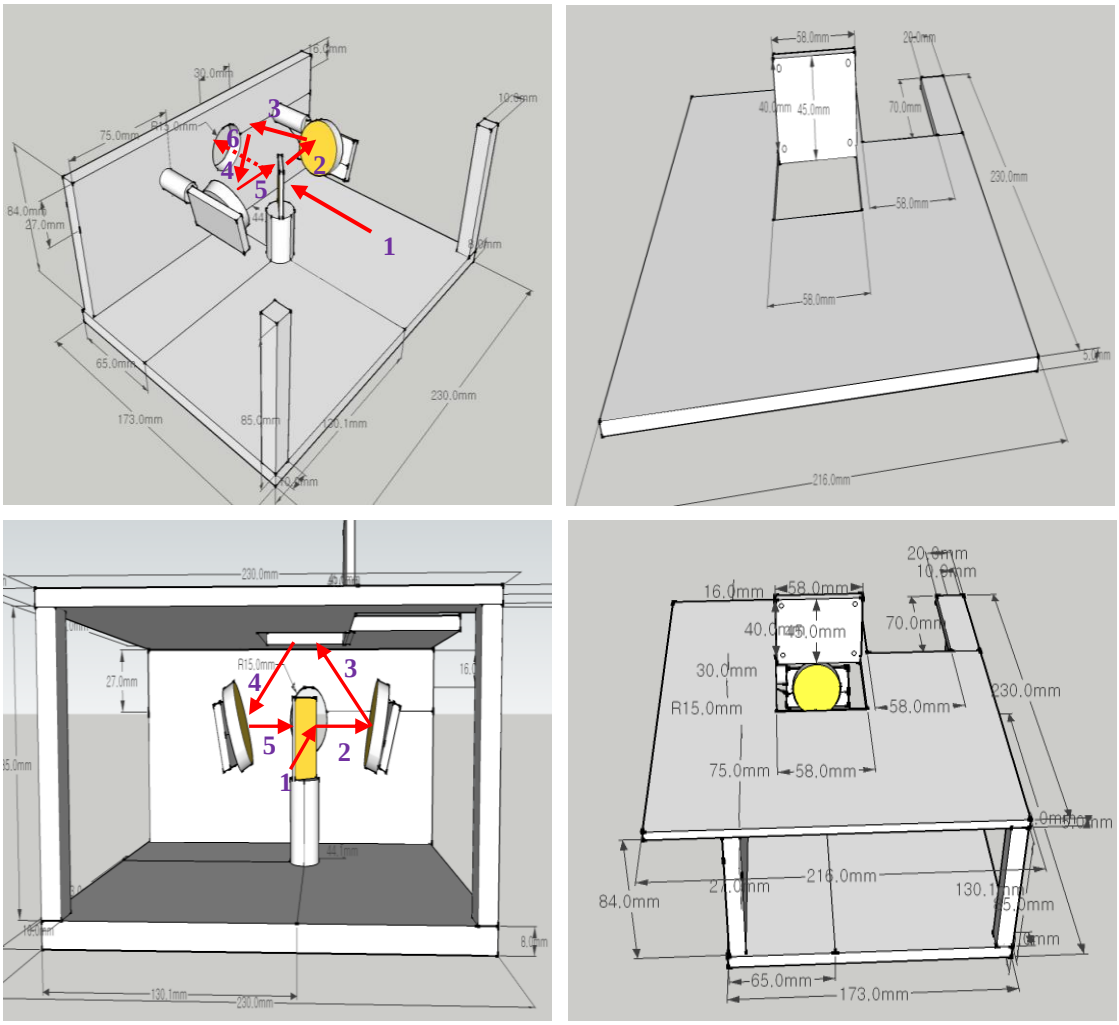


***Figure 2.5.*** Schematic of the homemade single reflection accessory.

## 2.4. Analysis of soluble reaction products by on-line HPLC (High Performance Liquid Chromatography)

For monitoring soluble reaction products during voltammetry, the on-line HPCL equipment combined with an electrochemical cell shown in Figure 2.6 was used. The reaction products were collected with a small Teflon tip (0.38 mm inner diameter) positioned close (~10 μm) to the center of the electrode surface, which was connected to a PEEK capillary with inner/outer diameters of 0.13/1.59 mm to enable rapid sample collection during voltammetry [3]. The collected samples during voltammetry were analyzed by high-

performance liquid chromatography (Prominence HPLC, Shimadzu) by injecting 30 μL of sample into the column. The column used was an Aminex HPX 87-H (Bio-Rad) and diluted 0.5 mM sulfuric acid was used as the eluent. The temperature of the column was maintained at 85$^{o}$C in a column oven (CTO-20A), and the separated compounds were detected with a refractive index detector (RID-10A) [3].

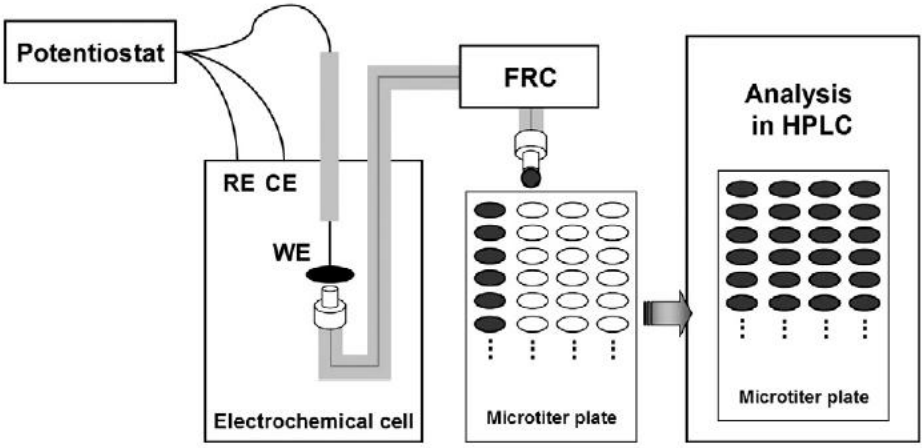


***Figure 2.6.*** Schematic diagram of the on-line sample collection with fraction collector (FRC) equipped with micro-sized sample collecting tip for rapid sample collection close to the electrode surface during voltammetry, with subsequent analysis of sample fractions in a HPLC system. WE: working electrode, RE: reference electrode, and CE: counter electrode. Adopted from [4].

# References

[1] A.J.a.L.R.F. Bard, Electrochemical methods: Fundamentals and Applications, 2nd ed. (2001).

[2] A. Miki, S. Ye, M. Osawa, Chemical communications, (2002) 1500-1501.

[3] Y. Kwon, M.T.M. Koper, Analytical chemistry, 82 (2010) 5420-5424.

[4] A. Santasalo-Aarnio, Y. Kwon, E. Ahlberg, K. Kontturi, T. Kallio, M.T.M. Koper, Electrochem Commun, 13 (2011) 466-469.

# Chapter 3. Electro-oxidation of CO on Pt in alkaline media

## 3.1 Introduction

Electro-catalytic oxidation of small organic molecules on Pt has been studied extensively in acidic media owing to its relevance to fuel cells. Intrinsically, CO is formed on the surface by dehydration or dehydrogenation of the molecules. It is well known that CO poisons the catalyst and significantly dissipates its catalytic activity [1, 2]. In recent years, the advent of alkaline anion exchange membrane (AAEMs) has resulted in renewed interest in alkaline fuel cells [3]. Therefore, the study of CO oxidation in alkaline media is very crucial. But, its study has been restricted compared to that in acidic media [4-10] due to the formation of carbonate [7].

It is widely accepted that the active OH species, supplied from the reaction $H_2O + * \leftrightarrow OH_{ads} + H^+ + e^-$, adsorb at low-coordination "defect" sites preferentially over terrace sites and react with adsorbed CO according to $CO_{ads} + OH_{ads} \rightarrow CO_2 + H^+ + e^- + 2*$ [4]. The increase in the apparent rate constant with increase of defect sites, such as step and kinks, implies the preferential oxidation at defect [11]. Furthermore, it is also generally believed that CO is fast oxidized on the terrace, by terrace-adsorbed OH, in a characteristic mean-field-type Langmuir-Hinshelwood transient at sufficiently high final potentials by means of potential step chronoamperometry [5] and extensive Kinetic Monte Carlo (KMC) simulations [12, 13]. The good fit of the mean-field model strongly suggests that CO diffusion on the terrace is very fast, as in acidic media [4, 14]. While, it has remained unclear whether every combination of $CO_{ads}$ and $OH_{ads}$ near a step is equally reactive or a differential reactivity exists. Like this, vague conclusion makes the need for further investigation.

There still exists another question pertaining to the small preoxidation peak preceding the main CO oxidation. The origin of the preoxidation peak has been discussed extensively. According to the representative explanations for origin of prepeak in a previous work, preoxidation is regarded as a preferential oxidation at or near defect sites [15], kinetically unstable state [16], preferential oxidation of bridge-bonded CO [17] and oxidation by a potential induced rearrangement of CO [18]. Considering the last explanation only, The CO adlayer has a structure of p(2x2)-3CO ($\theta_{CO}$=0.75) and is quickly converted into $\left(\sqrt{19}\times\sqrt{19}\right)R23.4^{o}-13CO$ ($\theta_{CO}$=0.684) structure together with the appearance of the prepeak [19]. Yoshimi *et al.* [18] proposed that the change in the structure of the CO adlayer creates the vacant sites for the adsorption of water and facilitates CO oxidation at the prepeak. However, an alternative interpretation that the partial oxidation resulting in the rearrangement of adsorbed CO also would be possible [20]. Taking the whole circumstance into consideration, we realized the need of examination in how and why CO is partially oxidized at such a low potential.

Another important issue is both the reaction kinetics and CO's mobility on the Pt surface. It is well known that the surface mobility of CO in alkaline media is 3 or 4 order much lower than that in acid media. Herrero *et al.* [8] estimated $CO_{ads}$ surface diffusion on Pt to be *ca.* $2.7\times10^{-20}$ $m^2$ $s^{-1}$. Meanwhile, those obtained in acid media are found for nanoparticles a value around $1.5\times10^{-16}$~$3.36\times10^{-17}$ $m^2\,s^{-1}$ estimated by NMR. When it comes to much lower CO mobility in alkaline media, Koper *et al.* [4] explained that $CO_{ads}$ mobility is closely related with the adsorption of the CO oxidation product in alkaline media. On the other hand, Herrero *et al.* [8] suggest that it can be conclude that the low mobility is a consequence of the low absolute potential at which the adsorption and oxidation processes occur. The reason for the obvious low CO mobility and the faster CO oxidation in alkaline solution compared to acidic media are also not clear.

In the present study, we employed Surface-Enhanced Infrared Absorption Spectroscopy (SEIRAS) coupled to cyclic voltammetry (CV) or chronoamperometry to investigate the kinetic and dynamics of CO oxidation on a polycrystalline Pt electrode in alkaline media at molecular level.

## 3.2 Experiments

Experimental details of ATR-SEIRAS were described elsewhere [21]. A Pt thin film chemically deposited on the total reflecting plane of Si triangle prism was used as the working electrode in the spectroelectrochemical measurements. A Bio-Rad transform infrared spectrometer FTS-60A896 equipped with a MCT detector and a homemade single reflection accessory (incident angle of $60^o$) was used in recording SEIRA spectra at a spectral resolution of 4 $cm^{-1}$ and time resolution of 0.5s. Spectra are shown in absorbance units defined as $-\log(I/I_o)$, where I and $I_o$ represent spectra of the CO-covered and CO-free surfaces, respectively.[20]

The electrochemical cell was a glass one with a Pt mesh counter electrode and a Ag/AgCl electrode. However, all potentials in this manuscript are quoted vs. the reversible hydrogen electrode (RHE). The Pt-coated Si prism was attached to the cell by sandwiching an O-ring.

The electrolyte solution was prepared from Milli-Q water (>18 MΩ) and NaOH (Suprapur, Merck). After deoxygenating of the solution with Ar, the electrode surface between surface oxidation and hydrogen adsorption regions was cleaned by cycling until a stable CV was obtained. After a reference spectrum of the clean surface at 0.18 V was taken, the solution was bubbled with CO gas at 0.18 V for 3 min to establish a CO adlayer on the Pt surface, and finally CO dissolved in the solution was purged by Ar bubbling. Electrochemical measurements were carried out with a potentiostat/galvanostat (EG&G PAR model 263A).

## 3.3 Results and discussion

### 3.3.1 CO oxidation under potential sweep condition

Figure 3.1 presents the series of time resolved SEIRA spectra of CO on a Pt. The time resolution measured was 0.5s (i.e., 25 mV intervals). The sharply strong band at 2104-1965 $cm^{-1}$ and weak band at 1899-1681 $cm^{-1}$ are assigned to the CO stretching modes of linearly bonded CO at atop site ($CO_L$) and bridge-bonded CO ($CO_B$), respectively. The frequency of both $CO_L$ and $CO_B$ is much lower than those measured in acid media [20, 22]. Couto *et al.* [23] and García *et al.* [24] suggested that CO stretching frequency would decrease with increasing pH as a result of increased back donation caused by a more negative electrode potential or more positive Pt Fermi level (i.e., 59 mV per unit pH). After all, these bands disappear at around 0.78 V due to the oxidative stripping of adsorbed CO. Simultaneously, the band at 3614 $cm^{-1}$, assigned to the OH stretching mode of water on top of the CO adlayer, disappears and the negative going peak at 3410 and 1615 $cm^{-1}$ are the OH stretching and $H_2O$ bending modes, respectively. These peaks correspond to the water that was expelled from the surface by the adsorption of CO. No other peaks from the spectra are detected else. Oxidation product is easily converted into carbonate taking into account strong alkaline solution. However, we couldn’t probe the adsorption of any carbonate at the expected frequency [25]. Since SEIRAS probes only the interface, carbonate in the bulk solution cannot be able to be detected and it is also difficult to be observed in the environment of being dissolved a tiny amount of products.

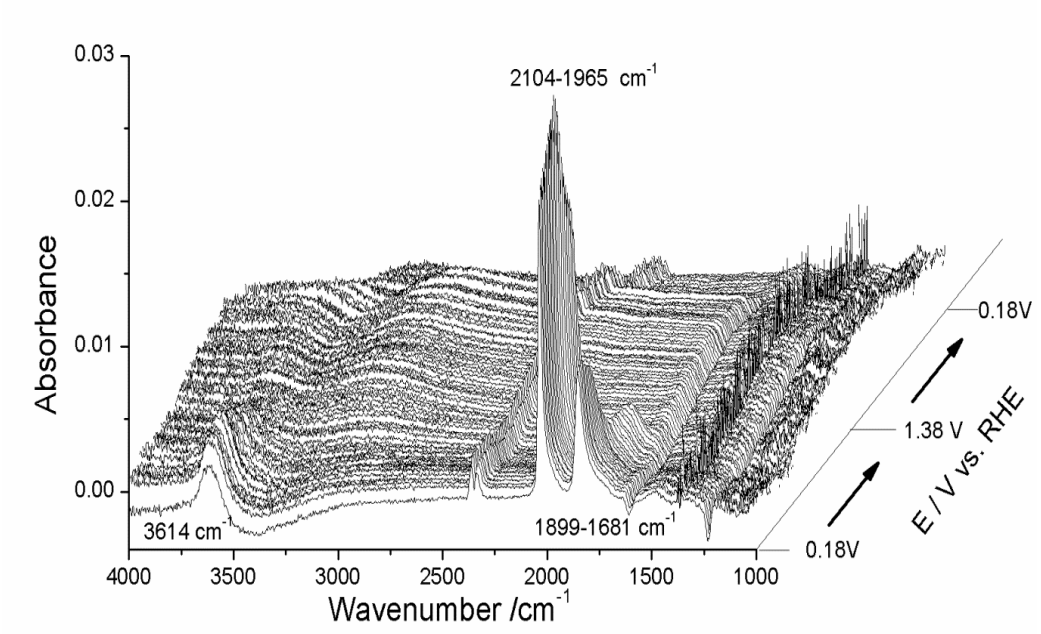


***Figure 3.1.*** Series of time resolved SEIRAS spectra of CO on a Pt surface electrode in 0.1 M NaOH. Scan rate is 50 mV $s^{-1}$.

For the sake of comparison of the IR spectra together with the CV, the integrated band intensities of $CO_L$, $CO_B$ and of the vibrational frequency of $CO_L$ are shown in figure 3.2(a)-(c). The band intensity of $CO_L$ is almost maintained up to 0.38 V and is slightly increased in the preoxidation region (labeled Region I) in spite of the partial oxidation, followed by a fast decease from E>0.58 V (labeled Region II and III). On the other hand, the band intensity of $CO_B$ decreases from 0.18V (especially, at 0.38-0.58 V) and >0.68 V. Comparison with the CV shows that the main CO oxidation peak at 0.63 V and at 0.71 V are obviously drawn from the oxidation of $CO_L$ and $CO_B$, respectively. The origin of the prepeak will be discussed in the next section, in detail.

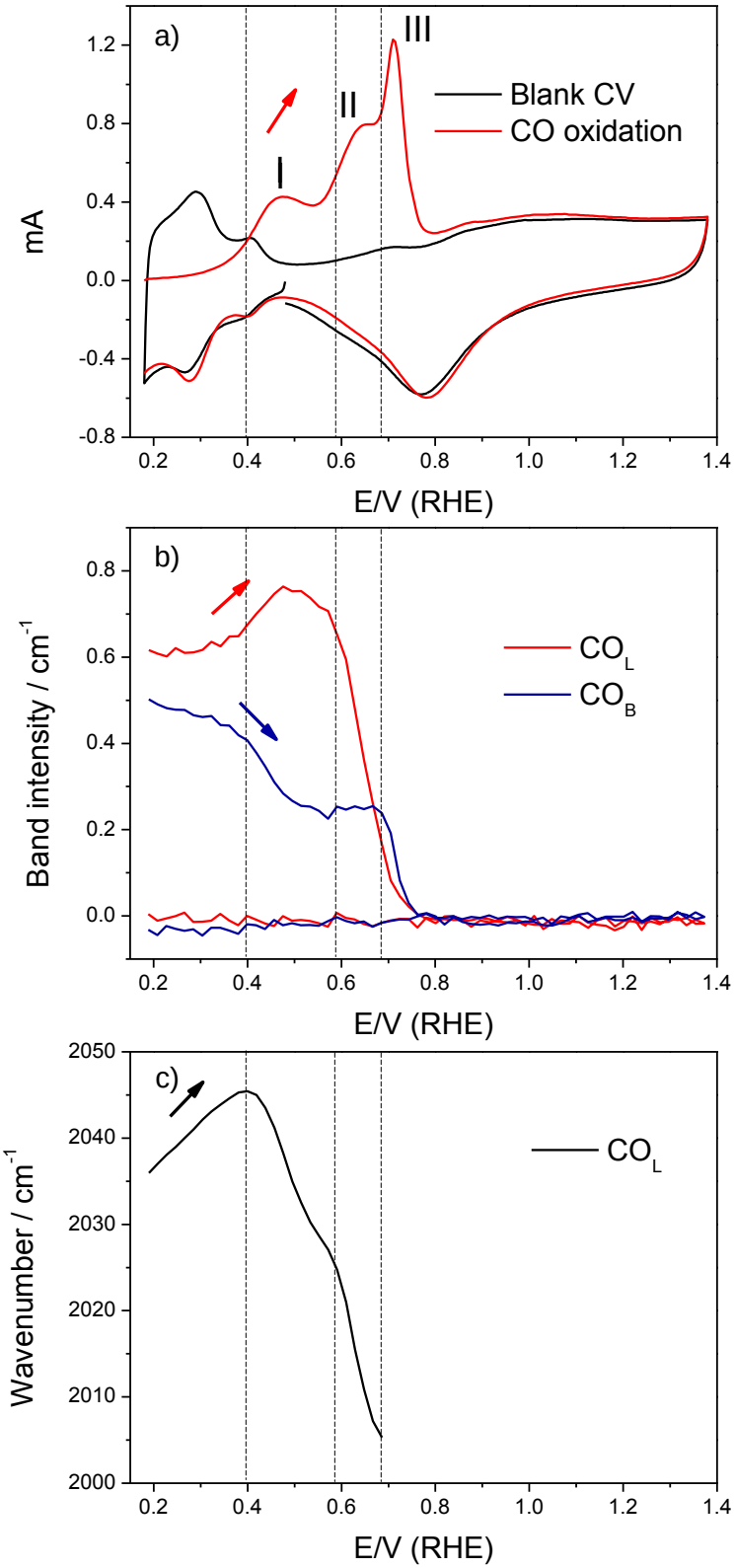


***Figure 3.2.*** (a) Cyclic voltammetry of electrooxidation of CO. (b) Potential dependence of the integrated band intensity of $CO_L$ (red), $CO_B$ (blue), and (c) vibration frequency of $CO_L$ . Scan rate is 50 mV $s^{-1}$.

Figure 3.2 (c) is a plot of the vibrational frequency of $CO_L$ against the applied potential. The vibration frequency of $CO_B$ is also potential dependent but not reflected in the figure because the band center is ambiguous due to the broad and asymmetric shape of this band. As is well known, the vibrational frequency of $CO_L$ is blue-shifted as the potential is made to more positive ($H_{upd}$ region). The potential-dependent shift of the vibrational frequency is explained in the aspect of the electric field effect at the interface (so called the vibrational stark tuning effect) or/and the change in the back-donation of electrons from the metal to $2\pi^*$ orbital of adsorbed CO [26]. At the beginning of preoxidation, the frequency of $CO_L$ is soon red shifted associated with rapid CO oxidation. It is ascribed to the reduction of the dipole-dipole interaction among $CO_L$ molecules. Interactions between CO molecules and the surface (electronic interactions with the surface) also can shift the vibrational frequency, but this effect is smaller than the dipole coupling [27].

### 3.3.2 Origin of the preoxidation peak

Typically, most of platinum surface is always observed a prepeak preceding the main oxidation. When the prepeak for the different stepped and kinked surface is compared, the difference in the charge and shape of the prepeak can be considered negligible, that is, the prepeak shows no dependence on the nature and density of step and kink sites [8]. Its presence also depends on the adsorption potential with difference of acidic [28, 29] and alkaline media [23, 30]. And, the prepeak is always absent when the CO coverage has not reached a saturation value. In acidic media, Cuesta *et al.* [31] proposed the model for $CO_{ads}$ oxidation, in which oxidation is limited by slow diffusion of CO to the active sites in prepeak region. Of late, Wang *et al.* [13] shows that preoxidation is attributed to the oxidation of a compressed layer of CO in which the oxidation nucleates on the neighboring low-coordination defects by diffusion of adsorbed CO towards there. In addition, Kunimatsu *et al*.

[17] also argued the prepeak is explained to be a preferential oxidation of $CO_B$ on the basis of the decline of the $CO_B$ band intensity. On the other hand, Samjeské *et al.* [20] shows it is more likely that shift of bridge-boned CO ($CO_B$) to atop sites ($CO_L$) invokes the partial oxidation of CO at atop sites, which results in the preoxidation peak.

In contrast to acid media, however, there are a relatively lack of information concerning the origin of a preoxidation in alkaline media. It is well known that the absolute potential at which the adlayer has been made is much more negative than that in acid media [8]. It could be formed a different adlayer depending on the pHs. Actually, it has been practiced that CO adlayer formed in NaOH media on a Pt (111) electrode is transferred to a sulfuric acid solution and it is oxidized, the prepeak appears at lower potentials and is measured a higher charge than that of when the CO adlayer has been formed in sulfuric acid solutions [10]. This result suggests that its intrinsic feature of the adlayer is the origin of the presence of the prepeak in the oxidation process, and this property obviously depends on the electrode potential. Besides, Herrero *et al.* [8] argued that prepeak can be linked to a significant number of defects in the borders of the different domains results from low mobility of CO adlayers in alkaline media. Because, if the mobility is low, the coalescence of the different translational and rotational domains formed in the initial stages of the CO adsorption process is complicated [8]. In conclusion, they insisted that a significant number of defects trigger large prepeak in the stripping voltammograms. Accordingly, it is highly required to scrutinize the reaction on the surface by means of *in situ* IR technique coupled to electrochemical modulation. We investigated CO oxidation in the same way, as reported in ref. 20.

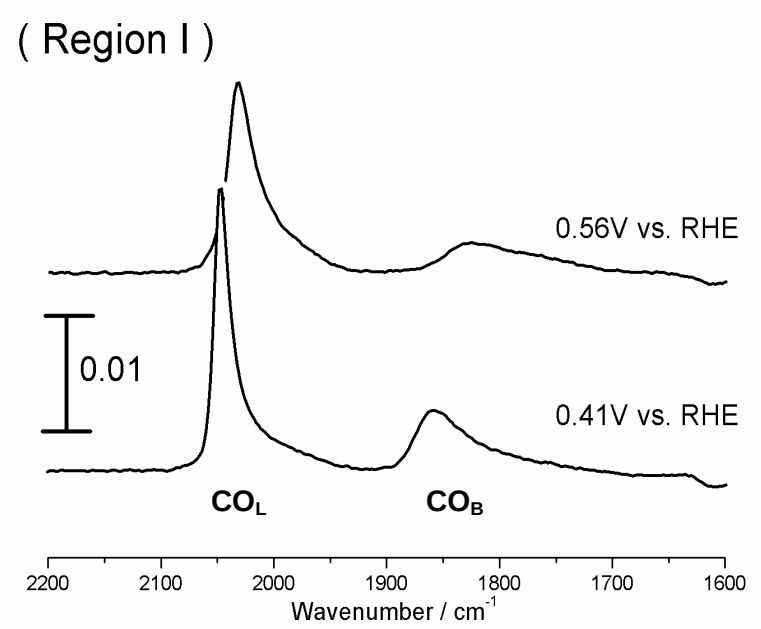


***Figure 3.3.*** Change in spectra features before and after peak I in figure 3.2.

Figure 3.3 shows adsorption bands of $CO_L$ and $CO_B$ are asymmetric. Since, the surfaces always contain step edges and other defects. Therefore, main absorption and shoulder of $CO_L$ band located in lower frequency are related to the $CO_{ads}$ in CO domain (probably on terraces) and CO at edges of CO domain, respectively [32]. And hence, low frequency tail is assigned to CO at or near steps on which dipole-dipole interaction is weaker. By comparing of two adsorption bands of figure 3.3, full width at half maximum (FWHM) of $CO_L$ indicated in 18 $cm^{-1}$ at 0.41V was increased up to 30 $cm^{-1}$ at 0.56V. From the documents reported earlier, broadening shape of spectrum is explained that CO is distributed homogeneously over the surface by repulsive intermolecular interaction [20]. This result definitely implies that highly packed CO adlayer is relaxed to a more stable, less compressed one over the surface by the partial oxidation at the prepeak region (labeled region I). In order to clarify the potential dependent behavior of preoxidation, we go back into region I of figure 3.2(b). The integrated intensity of linear CO ($CO_L$) coverage rises as same as coverage of descending $CO_B$. On the basis of CO oxidation result in acid media by Samjeské *et al.* [20],

the potential step result from 0.05 to 0.6V (RHE) is composed of two processes. An initial very fast process was involved in decreasing the intensity of the $CO_B$ band. The latter slow process is distinctly the oxidation of $CO_L$ which is found from the gradual red shift of the vibration. And then, desorption of $CO_B$ generates vacant sites, which enables the adsorption of OH or water and it can eventually result in the oxidation of $CO_L$. From our results, even though the integrated band intensity of $CO_L$ is increased, vibration of frequency is rapidly decreased as a result of reduction of dipole-dipole interaction (See figure 3.2(c)). And hence, the partial oxidation of $CO_L$ is more facilitated by forming more open structure. Since the stabilization of the CO adlayer inhibits CO oxidation, the partial CO oxidation can give a rising to a peak curve in the cyclic voltammetry walking in step with trajectory of $CO_L$ band intensity. Therefore, we safely conclude that preoxidation of CO in alkaline media is in very good agreement with findings by Samjeské *et al.* [20] examined in acid media.

### 3.3.3 CO oxidation at the main oxidation

A single main peak appears in the main oxidation region in acid media. As shown in figure 3.2 (a), however, a single main peak splits into two regions (II & III) in alkaline media. According to cyclic voltammetry, peak II and III appeared in accordance with different potentials. Gisbert *et al.* [7] also showed that CO oxidation sensitively depends on both the structure of Pt and a potential. They assigned the four CO oxidation peaks obtained at the poly-oriented Pt electrode to four different active sites on the surface in alkaline media, i.e., (kink-type) defects, (111), (110) and (100) sites. From those results, peaks II and III have been ascribed to the oxidation of CO on (110) terrace and (100) terrace, respectively. To facilitate the simple understanding, we integrate bands of both $CO_L$ and $CO_B$ in these regions as shown in figure 3.2(b). First, in the region II, most of $CO_L$ is quickly oxidized while $CO_B$

is not oxidized. And then, remaining $CO_B$ is oxidized in the region III, selectively. It indicates that $CO_L$ is dominant on (110) and $CO_B$ is dominant on (100).

As is well known, $CO_{ads}$ mobility in alkaline media is much lower than that of acid media. The koper group [5, 24] reported that $CO_{ads}$ diffusion on platinum in alkaline solution is slower than in acid solution and the anion effects of CO surface mobility were also investigated. That $CO_{ads}$'s mobility on rhodium in sulfuric acid solution is considerably suppressed when compared to perchloric acid solution [33]. It may be summarized in the following. The reason why main peak spilt into two peaks is that lowering the $CO_{ads}$ mobility suppresses the CO oxidation toward active sites in alkaline media. Garcia *et al.* [4] already reported that even though the origin for much lower mobility of CO in alkaline media than in acidic media has not yet been fully clarified, this behavior would be related to the coadsorption of the CO oxidation product. (i.e., carbonate). Furthermore, Garcia *et al.* [5, 6] and Gisbert *et al.* [7] concluded that blocking effect produced by carbonate which adsorbs close to defect sites would explain the multiple CO oxidation peaks observed during the CO stripping voltammetry. As mentioned earlier, we couldn't observe any carbonate at expected frequency under very careful inspection (See figure 3.1). We would like to say that adsorbed carbonate could not affect the $CO_{ads}$'s mobility itself, but it may depend on the other influence. Interestingly, Herrero *et al.* [8] shows two peaks are already well resolved at pH where main product of CO oxidation is still $CO_2$, and the amount of carbonate in solution can be regarded negligible. Thus, the origin of the low mobility of CO cannot simply be explained by carbonate adsorption.

Oxidation of CO begins in a similar potential window in the RHE scale, which means CO oxidation moves towards negative potential as the pH increases with respect to the absolute scale (SHE). Thus, the diminished mobility of CO can be described because the process in alkaline media is occurring at lower absolute potentials than that in acid media.

The negative charge or more positive Pt Fermi level in the electrode causes an increase in the back donation between the Pt-CO bond, which in turn results in stronger binding Pt-CO bond [8]. And, it will reflect somewhat in the kinetic of CO oxidation [8]. The stronger Pt-CO bond could lead to slow mobility of CO on the surface, resulting in a different behavior of the adlayer in alkaline media comparing to the acid media. Besides, Garcia *et al.* [24] already suggested that at very negative potentials vs. NHE, such as in alkaline solution, larger binding energy difference exist between hollow, bridge and atop sites. Thus, CO surface diffusion will be decreased. Its increasing binding energy of Pt-CO also affects frequencies to be more reduced in alkaline media than in acidic media. We also believe that low mobility of CO on surface to active site in alkaline media is primary involved in electronic consideration regardless of carbonate adsorption, if any.

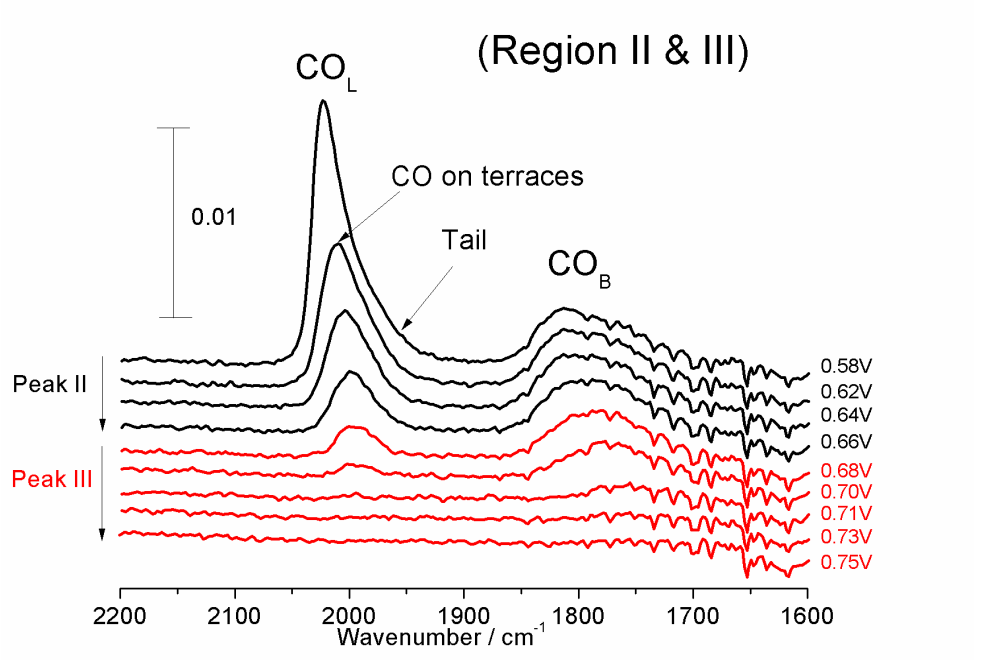


***Figure 3.4.*** Time-resolved IR spectra of the Pt electrode collected during CO stripping in peak II: (0.58-0.66V) and Peak III : (0.68 -0.76 V) regions.

To obtain further insights into the reaction on the surface, ATR-SEIRAS was e-

mployed. Figure 3.4 shows a selected time-resolved IR spectra of the Pt electrode during CO stripping both peak II : (0.58-0.66V) and Peak III : (0.68-0.76V) regions. From the region II, low frequency tail completely disappears and $CO_L$ band on terrace remains. And, asymmetric shape of $CO_L$ is suddenly reformed to symmetric shape, which means a selective CO oxidation at steps first. At the beginning of 0.58 V, CO oxidation reactions are facilitated as a result of enhancing the $CO_{ads}$ surface diffusion. With further increase of the potential, the $CO_L$ vibration shifts to lower frequencies accompanied by noticeable broadening and weakening. It is worth nothing that this band becomes symmetric in main oxidation region. As previously mentioned, the symmetric broad shape is indicative of homogeneous dispersion of $CO_L$ over the surface, and the red shift also indicates the increase of intermolecular spacing, which signals fast surface diffusion of CO. Since oxidation occurs efficiently at steps, terrace CO may be oxidized after diffusing to steps. In conclusion, at the main oxidation peak, CO is oxidized by Langmuir-Hinshelwood type one owing to the faster diffusion of CO resulting from well mixture between $CO_{ads}$ and $OH_{ads}$ species. We will deeply discuss the kinetic analysis of CO oxidation in next section on the basis of galvanostatic oxidation.

### 3.3.4 Chronopotentiometry for Galvanostatic oxidation

The method of galvanostatic oxidation has an advantageous to adjust the reaction rate, which is willing to allow the minimal potential for oxidation of the adsorbate and a much faster resolution of the catalytic natures of a surface [34]. Analogy with cyclic voltammetry result of figure 3.2, we can be able to divide into three parts of reaction regions. As can be seen from figure 3.5, in the region I, small potential plateau corresponds to the prepeak. After the oxidation of region I, the potential shortly follows region II and III at which it implies that reaction mechanism is different from region I (i.e., main oxidation). On the basis of integrated both $CO_L$ and $CO_B$ peaks as shown in figure 3.5(b), $CO_L$ is initially oxidized with the partial shift of $CO_B$ to atop site conversion (Refer to part of *origin of preoxidation peak*). And then, $CO_L$ is selectively oxidized first in the region II. Finally, remaining $CO_B$ is fully oxidized before surface oxidation (Region III).

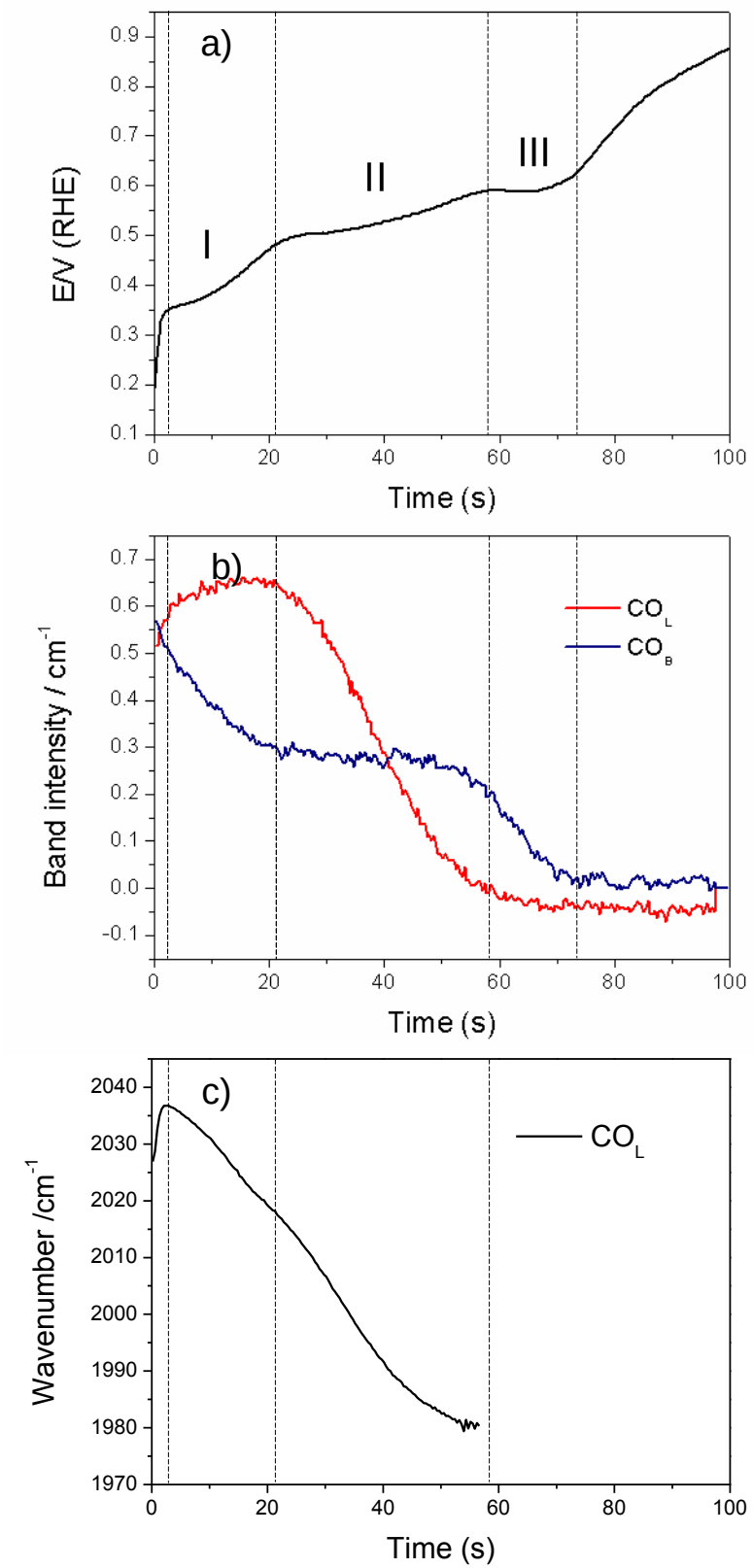


***Figure 3.5.*** (a) Potential transient under galvanostatic condition. (b) The integrated band intensities of $CO_L$ (red), $CO_B$ (blue), and (c) vibrational frequency of $CO_L$ (black).

A series of steps under galvanostatic oxidation are convincingly simulated by kinetic model that is suggested by Massong *et al.* [34]. Equations from (3.1) to (3.3) correspond to a region I of figure 3.5. The current is given by

$$r = \frac{i}{nF\Gamma_{\max}} = \frac{d\theta}{dt} = k_{ox}(E) \cdot \theta \tag{3.1}$$

$$k_{ox}(E) = k^{o} \cdot \exp\left(\frac{\alpha nFE}{RT}\right) \tag{3.2}$$

When the current $i$ and the rate $r$ are kept constant, $\theta$ is proportional to $1/k_{ox}$. Since $k_{ox}$ is exponentially dependent on the potential $E$, $E$ itself proportional to $ln\ \theta$. Since $\theta$ is changing linearly with time, the potential increases monotonously with time [34] :

$$\frac{\alpha \mathrm{nFE}}{\mathrm{RT}} = \ln\frac{r}{\theta} - \ln k^{o} = -\ln\theta + \ln\frac{r}{k^{o}} \tag{3.3}$$

In the case of equation (3.4) and (3.5), however, it corresponds to region II and III of figure 3.5. It is well explained by a *Langmuir-Hinshelwood mechanism* [34].

$$r = \frac{i}{nF\Gamma_{\max}} = \frac{d\theta}{dt} = k_{ox}(E) \cdot \theta \cdot (1-\theta) \tag{3.4}$$

and can be rearranged as below.

$$\frac{\alpha \mathrm{nFE}}{\mathrm{RT}} = -\ln\left[\theta \cdot (1-\theta)\right] + \ln\frac{r}{k^{o}} \tag{3.5}$$

with decreasing coverage, the potential therefore decrease to reach a minimum at $\theta = 0.5$ [34].

Furthermore, above described equations are transformed into kinetic model of

potentiostatic oxidation which is suggested by koper's group [4, 5]. The fitting equation is by

$$\frac{i(t)}{nF\Gamma_{\max}} = k_{ox}(E)\cdot e^{-k_{ox}t} \tag{3.6}$$

$$j(t) = Ak_s \exp\left(-k_s t\right) + \frac{BCk_t \exp\left(-k_t t\right))}{\left[1 + C\exp\left(-k_t t\right)\right]^2} \tag{3.7}$$

where $k_s$ and $k_t$ are the rate constant for CO oxidation at the step and terrace, respectively, and A, B, and C are constants depending only on the initial conditions [4]. The first term on the right-hand side of equation of 3.7 for the current transient has lately been derived for a one-dimensional instantaneous nucleation and growth mechanism for CO oxidation [4, 5, 12]. The second term is the well-known mean-field expression for CO oxidation [4, 5]. This fitting is quite acceptable with experimental results. The results predict that the main peak is primarily due to terrace-adsorbed CO being oxidized in the step, following the well-known competitive adsorption mechanism, rather than to oxidation on the terrace itself. Moreover, Koper *et al.* [35] suggested that it was concluded that mixing of CO on terrace is good, implying rapid diffusion and CO and OH are well mixed.

In the present study, we proof that galvanostatic and potentiostatic experiments are essentially consistent with each other. And the mobility of $CO_{ads}$ plays a significant role in $CO_{ads}$ electrooxidation kinetics.

## 3.4 . Conclusion

Electro oxidation of CO on a polycrystalline Pt electrode was scrutinized by ATR-SEIRAS at the preoxidation and main oxidation peaks. We showed that the origin of the prepeak is the partial oxidation of linear CO ($CO_L$) invoked by site conversion of bridged bonded CO ($CO_B$) into linear CO ($CO_L$). We unveiled that the oxidation of $CO_L$ brings about the appearance of a prepeak as a result of surface diffusion by which the initially formed highly compressed metastable CO adlayer is relaxed to a more open structures to reduce dipole dipole interaction. At the main oxidation peak, $CO_L$ and $CO_B$ are oxidized at different potentials. We found that $CO_L$ and $CO_B$ are likely to be the dominant adsorbates on (110) and (100), respectively. And CO at near step are oxidized faster than CO at terraces. CO is also oxidized by a ***Langmuir-Hinshelwood mechanism*** with fast surface diffusion. The fast CO diffusion towards active defect sites and subsequent oxidation was manifested itself by broadening and red shift of the terrace CO band. Finally, the origin of low mobility of $CO_{ads}$ on surface in alkaline media can be mainly explained by electronic effect owing to a lowering absolute potential regardless of carbonate adsorption, if any.

# References

[1] Y.X. Chen, A. Miki, S. Ye, H. Sakai, M. Osawa, J. Am, Chem. Soc., 125 (2003) 3680-3681.

[2] G. Samjeske, A. Miki, S. Ye, M. Osawa, J. Phys. Chem. B, 110 (2006) 16559-16566.

[3] G. Merle, M. Wessling, K. Nijmeijer, J. Membrane Sci., 377 (2011) 1-35.

[4] G. Garcia, M.T.M. Koper, J. Am. Chem. Soc., 131 (2009) 5384-5385.

[5] G. Garcia, M.T.M. Koper, Phys. Chem. Chem. Phys., 11 (2009) 11437-11446.

[6] G. Garcia, P. Rodriguez, V. Rosca, M.T.M. Koper, Langmuir, 25 (2009) 13661-13666.

[7] R. Gisbert, G. Garcia, M.T.M. Koper, Electrochim. Acta, 56 (2011) 2443-2449.

[8] E. Herrero, Q.S. Chen, J. Hernandez, S.G. Sun, J.M. Feliu, Phys. Chem. Chem. Phys., 13 (2011) 16762-16771.

[9] P. Rodriguez, G. Garcia, E. Herrero, J.M. Feliu, M.T.M. Koper, Electrocatalysis, 2 (2011) 242-253.

[10] J.S. Spendelow, J.D. Goodpaster, P.J.A. Kenis, A. Wieckowski, J. Phys. Chem. B, 110 (2006) 9545-9555.

[11] N.P. Lebedeva, M.T.M. Koper, J.M. Feliu, R.A. van Santen, Electrochem. Commun., 2 (2000) 487-490.

[12] T.H.M. Housmans, C.G.M. Hermse, M.T.M. Koper, J. Electroanal. Chem., 607 (2007) 69-82.

[13] H. Wang, Z. Jusys, R.J. Behm, H.D. Abruña, J. Phys. Chem. C, 116 (2012) 11040-11053.

[14] N.P. Lebedeva, M.T.M. Koper, J.M. Feliu, R.A. van Santen, J. Phys. Chem. B, 106 (2002) 12938-12947.

[15] A. Lopez-Cudero, A. Cuesta, C. Gutierrez, J. Electroanal. Chem., 579 (2005) 1-12.

[16] H. Kita, H. Naohara, T. Nakato, S. Taguchi, A. Aramata, J. Electroanal. Chem., 386 (1995) 197-206.

[17] K. Kunimatsu, T. Sato, H. Uchida, M. Watanabe, Electrochim. Acta, 53 (2008) 6104-6110.

[18] K. Yoshimi, M.B. Song, M. Ito, Surf. Sci., 368 (1996) 389-395.

[19] N.M. Markovic, P.N. Ross, Surf. Sci. Rep., 45 (2002) 121-229.

[20] G. Samjeske, K. Komatsu, M. Osawa, J. Phys. Chem. C, 113 (2009) 10222-10228.

[21] M. Osawa, Bull. Chem. Soc. Jpn., 70 (1997) 2861-2880.

[22] Y.G. Yan, Y.Y. Yang, B. Peng, S. Malkhandi, A. Bund, U. Stimming, W.B. Cai, J. Phys. Chem. C, 115 (2011) 16378-16388.

[23] A. Couto, A. Rincon, M.C. Perez, C. Gutierrez, Electrochim. Acta, 46 (2001) 1285-1296.

[24] G. Garcia, M.T.M. Koper, Phys. Chem. Chem. Phys., 10 (2008) 3802-3811.

[25] A. Berna, A. Rodes, J.M. Feliu, F. Illas, A. Gil, A. Clotet, J.M. Ricart, J. Phys. Chem. B, 108 (2004) 17928-17939.

[26] S. Holloway, J.K. Norskov, J. Electroanal. Chem., 161 (1984) 193-198.

[27] F.M. Hoffmann, Surf. Sci. Rep., 3 (1983) 107-192.

[28] K. Kunimatsu, H. Seki, W.G. Golden, J.G. Gordon, M.R. Philpott, Langmuir, 2 (1986) 464-468.

[29] K. Kunimatsu, W.G. Golden, H. Seki, M.R. Philpott, Langmuir, 1 (1985) 245-250.

[30] J.A. Caram, C. Gutierrez, J. Electroanal. Chem., 305 (1991) 275-288.

[31] A. Cuesta, Electrocatalysis, 1 (2010) 7-18.

[32] F.M. Hoffmann, Surf. Sci. Rep., 3 (1983) 107-192.

[33] T.H.M. Housmans, M.T.M. Koper, Electrochem. Commun., 7 (2005) 581-588.

[34] H. Massong, S. Tillmann, T. Langkau, E.A.A. El Meguid, H. Baltruschat, Electrochim. Acta, 44 (1998) 1379-1388.

[35] M.T.M. Koper, N.P. Lebedeva, C.G.M. Hermse, Faraday Discuss., 121 (2002) 301-311.

# Chapter 4. Electrocatalytic oxidation of formic acid on platinum: Importance of acid-base equilibrium

## 4.1 Introduction

Electrooxidation of formic acid (HCOOH) to $CO_2$, the reaction taking place at the anode of direct formic acid fuel cells (DFAFCs), is one of the most fundamental model electrocatalytic reactions and has been investigated intensively over the last four decades mostly in acidic meida [1-3]. It is generally accepted that HCOOH is oxidized *via* a dual pathway mechanism[1] : a main reaction pathway *via* adsorbed intermediate(s) and a pathway *via* a poisoning species that is oxidized to $CO_2$ at high potentials. CO was identified to be the poisoning species in 1980s by using infrared reflection absorption spectroscopy (IRAS) [4, 5], While the main pathway, non-CO pathway, is still matter of strong debate. No other adsorbed species had been detected until Miki et al. [6] observed the adsorption of a formate species that is bonded to the surface *via* two oxygen atoms (bridge-bonded formate) by employing surface-enhanced infrared absorption spectroscopy in the attenuated total reflection mode (ATR-SEIRAS)[7,8]. Through systematic ATR-SEIRAS studies combined to electrochemical measurements, Samjeské et al. [9-12] and Cuesta et al. [13, 14] proposed the bridge-bonded formate being an intermediate in the non-CO pathway (termed hereafter as *bridge-bonded formate pathway*) and its decomposition to $CO_2$ is the rate-determining step. On the other hand, Chen et al. [15-17] claimed that bridge-bonded formate is a site-blocking spectator and HCOOH is directly oxidized to $CO_2$ *via* a weakly adsorbed molecular HCOOH precursor (termed as *direct HCOOH pathway*). The experimental techniques used in these studies were the same and the results were essentially identical. The two different reaction mechanisms

proposed stem from the different interpretations of the non-linear relationship between the band intensity of bridge-bonded formate (approximately proportional to coverage) and the oxidation current. Recently, Grozovski et al. [18] reported that the oxidation current is proportional to the coverage of adsorbed formate determined by fast cyclic voltammetry and concluded that adsorbed formate is the intermediate in HCOOH oxidation. There are similar disagreements also in theoretical studies of the reaction. Neurock et al. [19] and Wang and Liu [20] predicted that bridge-bonded formate is stable and HCOOH is oxidized *via* adsorbed COOH or directly, respectively, while Gao et al. [21] predicted that the both pathways are possible but the bridge-bonded formate pathway is slightly more favorable.

In recent years, electrocatalytic oxidation of small organic molecules in alkaline media has received a renewed interest due to the recent advent of alkaline anion exchange membranes for alkaline fuel cells. HCOOH is relatively weak acid with pKa of 3.75 and mostly exists as formate ($HCOO^-$) in neutral and alkaline media. However, studies of $HCOO^-$ oxidation in neutral and alkaline media are very limited. Buck and Griffith [22], Bagotsky and Vassiliyev [23], Beden et al. [24], Kita et al.[25], Haan and Masel [26] have shown that the oxidation current increases as the pH of the solution is increased from 1 to 4 or 5. As an example, the result reported by Kita et al. [25] is shown in Figure 4.1. However, $HCOO^-$ oxidation is well known to be very slow in alkaline solutions. Very recently, John et al. [27] extensively studied $HCOO^-$ oxidation in strong alkaline solution (pH −14) and proposed that $HCOO^-$ is oxidized to $CO_2$ *via* a dual pathway mechanism similar to that for HCOOH oxidation in acidic media [13, 14], in which a strongly adsorbed precursor is involved for both direct $HCOO^-$ oxidation and indirect oxidation *via* adsorbed CO.

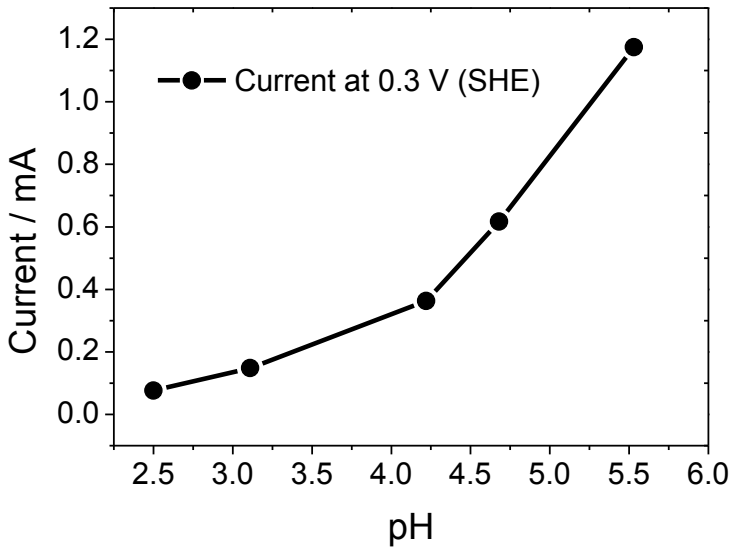


***Figure 4.1.*** Dependence of pH on the current at 0.3 V (vs. SHE) on the Pt electrode (0.34 $cm^2$) in the presence 10 mM HCOONa. Adopted from [25].

They ascribed the low activity of $HCOO^-$ in strong alkaline media to the high stability of the precursor and also inhibition of its adsorption by adsorbed OH. Adsorption of CO on Pt in alkaline media has been confirmed by an IRAS study by Christensen et al. [28], while the precursor in $HCOO^-$ oxidation has not been identified yet. To our best knowledge, no systematic mechanistic studies of HCOOH/$HCOO^-$ oxidation over a wide range of pH have been reported in the literature.

The aim of the present manuscript is to extend our understanding of the oxidation of HCOOH/$HCOO^-$ over the entire range of pH (0-14) and to clarify the real reaction mechanism through an in-depth analysis of the reaction using ATR-SEIRAS coupled to cyclic voltammetry [7, 29]. The systematic study over the wide range of pH shed considerable light on the HCOOH and $HCOO^-$ oxidation. It will be shown that the bridge-bonded formate pathway actually works, and that $HCOO^-$ is more reactive than HCOOH and the dominant reactant even in acid media. A simple mechanistic model that well explains the HCOOH/$HCOO^-$ oxidation over the entire pH range will be presented.

The significance of the present study goes beyond this relatively simple electrocatalytic system because many electrocatalytic reactions are strongly pH dependent and the pH dependence must be related to the decoupling of proton and electron transfer at some stage in the reaction mechanism [30-32]. Recently, such an effect was shown to be important for predicting the optimal pH for electrooxidation of alcohols on gold electrode [33]. We will show that the experimental results presented here serve as a generic example highlighting the importance of pH variation in catalytic proton-coupled electron transfer reactions.

## 4.2 Experimental

All solutions were made using 18 MΩcm Milli-Q water. In most experiments, 0.2 M phosphate buffer solutions with pHs between 1.5 and 12, prepared from $H_3PO_4$, $NaH_2PO_4$, $Na_2HPO_4$, and/or $Na_3PO_4$ were used as the electrolyte. In some experiments, 1 M $H_3PO_4$ and 0.1-1 M $HClO_4$ were also used to extend the pH range to less than 1. As the $HCOOH/HCOO^-$ source, HCOONa was added to the electrolyte solutions to be a desired concentration (either 20 or 50 mM). The change of pH caused by the addition of HCOONa was negligible. Thus prepared solutions were deaerated with Ar before each experiment. All chemicals were analytical grade purchased from Wako Pure Chemicals (Tokyo) and used as received.

Cyclic voltammetry was performed with a standard three-electrode glass cell and a potentiostat/galvanostat (EG&G PAR, model 263A). A rotating mirror finished Pt disc electrode (5 mm in diameter) was used as the working electrode. Pt gauze and a Ag/AgCl (sat'd KCl) electrode served as the counter and reference electrode, respectively. The Ag/AgCl reference electrode was separated from the working electrode *via* a Luggin capillary. However, all potentials refer the standard hydrogen electrode (SHE), unless otherwise noted. The electrode surface was cleaned in the supporting electrolyte solution without

$HCOOH/HCOO^-$ by repeating potential scans between surface oxidation and hydrogen adsorption potential regions until a stable CV was obtained.

Experimental details of ATR-SEIRAS were described in chapter 3 and elsewhere [29, 34, 35]. A three electrode spectroelectrochemial cell similar to that shown in Figure 4.2 was used. A Pt thin film deposited on the total reflecting plane of a Si triangle prism (Pier Optics, Tatebayashi, Japan) by a chemical deposition technique [6], was used as the working electrode in the spectroelectrochemical measurements. The counter and reference electrodes were same as above. A Bio-Rad Fourier transform infrared spectrometer FTS-60A/896 equipped with a MCT detector and a homemade single reflection accessary (incident angle of 60°) was used in recording SEIRA spectra at a spectral resolution of 4 $cm^{-1}$. Spectra were sequentially acquired at every 2 s interval (time required for co-adding 10 interferograms) simultaneously with CVs at 20 mV $s^{-1}$. Accordingly, a spectrum is an average of 40 mV interval. A single beam spectrum collected in advance in the pure supporting electrolyte was used as the reference for calculating the sample spectra. All spectra are shown in the absorbance unit. All experiments were carried out at room temperature.

## 4.3 Results and discussion

### 4.3.1 Cyclic voltammetric studies

The oxidation of $HCOOH/HCOO^-$ yields protons ($HCOOH \rightarrow CO_2 + 2H^+ + 2e^-$, $HCOO^- \rightarrow CO_2 + H^+ + 2e^-$) and can change the pH at the interface, which results in a considerable change in the ratio of HCOOH and $HCOO^-$ concentrations, especially in the pH range around pKa. To avoid such an effect, phosphate buffer solutions (pH 1.5-12) were used as the electrolyte. Additionally, a rotating disk electrode was used aiming at further minimizing the possible change of local pH, which is also useful to avoid the accumulation of $CO_2$ (which exists as $HCO_3^-$ and $CO_3^{2-}$ in neutral and alkaline solutions, respectively) [36].

Typical cyclic voltammograms (CVs) of 50 mM HCOONa in buffer solutions with different pH values recorded at 50 mV $s^{-1}$ are shown in Figure 4.2a. The electrode was rotated at 1000 rpm in the experiment, but no significant effects of the rotation (0-1000 rpm) were observed on the CVs at this concentration, indicating that the change in local pH is negligible in the buffer solutions used and that $HCOOH/HCOO^-$ oxidation is kinetically controlled.

As can be found from the Figure 4.2a, voltammetric features are sensitive to pH and one or two oxidation peaks are observed on the both positive- and negative-going scans. The observed peaks are denoted by p1, p2, p3, and p4 in the order of their appearances for the positive- and following reverse negative-going scans. Since the peaks negatively shift with pH at a rate of −60 mV $pH^{-1}$ (Figure 4.2c), each peak locates at the same potential with respect to the reversible hydrogen electrode (RHE).

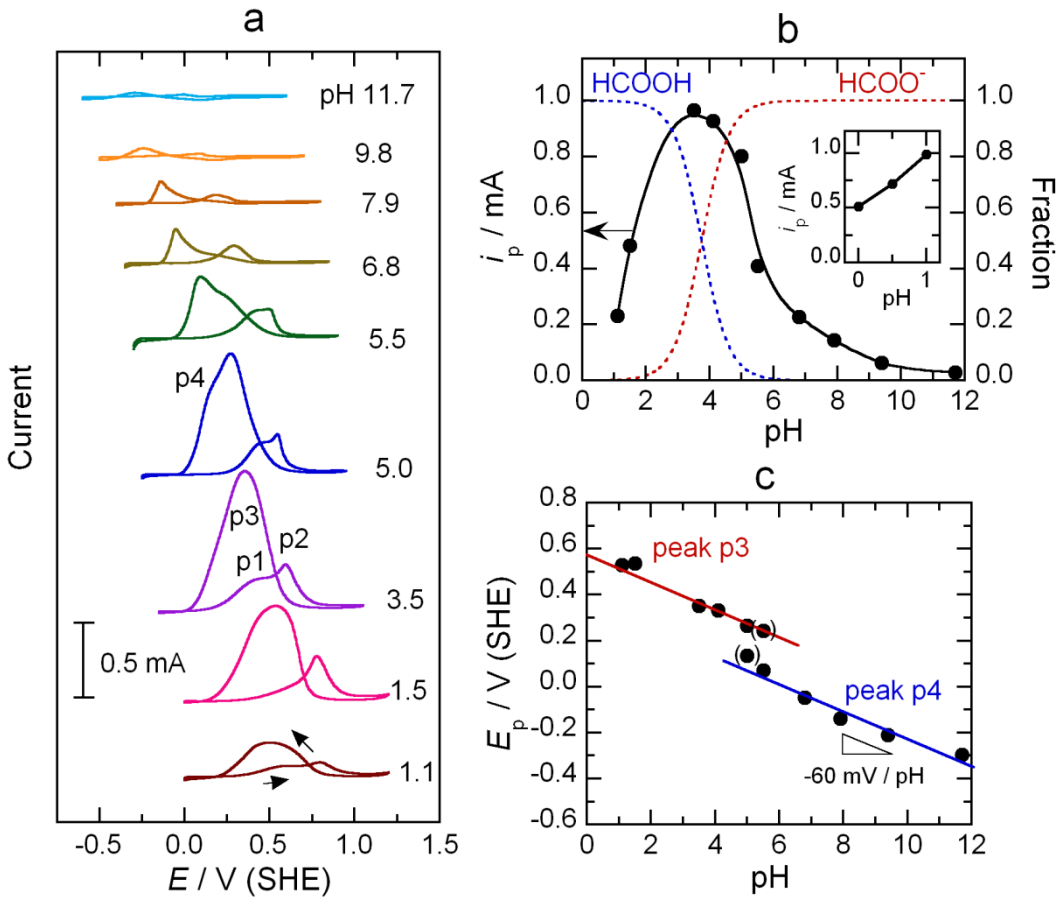


***Figure 4.2.*** (a) Cyclic voltammograms for 50 mM HCOOH/$HCOO^-$ in 0.2 M phosphate buffer solutions with different pH values shown in the figure (1 M $H_3PO_4$ for pH 1.1) recorded at 50 mV $s^{-1}$ by using a rotating Pt disk electrode (1000 rpm). (b) Dependence of pH on the peak current ($i_p$) on the negative-going scan. Inset shows $i_p$ at pH 0-1 measured with $HClO_4$ as the supporting electrolyte. Blue and red dashed traces represent the fraction of HCOOH and $HCOO^-$ in the solution. Solid curves are only for eye guidance (c) Dependence of pH on the peak potential $E_p$ for peak p3 and peak p4. Data points shown by parenthesis are the potentials of shoulders.

In acidic solutions (pH 1.1-5.5), two oxidation peaks p1 and p2 are observed on the positive-going scan, and a larger peak p3 appears on the negative-going scan after the reduction of surface oxide. At pH 5, a shoulder appears at the lower potential side of p3 and becomes a peak (peak p4) at pH 5.5. For the further increase of pH, p2 and p3 disappear at pH

> 5.5 and the remaining peaks, p1 and p4, shift to further negative potentials accompanied by the remarkable decrease in peak current.

It is well known that CO, a poisoning species, is formed on the electrode surface at low potentials and significantly affects the oxidation of $HCOOH/HCOO^-$ on the positive-going scan. The coverage of adsorbed CO depends on several experimental conditions, especially the initial potential and the time before the potential scan [9], which makes quantitative analysis of the oxidation current on the positive-going scan difficult. Therefore, we focus here on the oxidation peaks on the negative-going scan in which the effect of $CO_{ads}$ is negligible as will be shown later (5.3.2). As shown in Figure 4.2b, the peak current, $i_p$, is maximal around pH 4 and remarkably decreases at both lower and higher pHs. Inset to this figure shows the data in the pH range of 0-1 measured with $HClO_4$ as the supporting electrolyte. Since $ClO_4^-$ is adsorbed on Pt less strongly than phosphate anions (or not adsorbed at all), $i_p$ is larger in the $HClO_4$ solutions [23, 36]. Since HCOOH is a weak acid with a pKa of 3.75 [37], if the direct HCOOH pathway were the main reaction route, the oxidation current should decrease with increasing pH due to the decrease of HCOOH concentration. However, the oxidation current increases with pH as shown in Figure 4.2 and as have been reported in earlier studies as described in Figure 4.1. The peak current of the oxidation peak, $j_p$, monotonically increases with increasing pH from 0 to ~4 and the remarkably decreases at higher pHs (Figure 4.2b). Note that $j_p$ is maximal at pH close to the pKa of HCOOH.

The increase of $j_p$ with increasing pH in acidic and neutral media apparently cannot be explained by the direct HCOOH mechanism. Rather, the result suggests that $HCOO^-$ is more reactive than HCOOH and that most of the current corresponds to its oxidation. However, if it is so, why does the oxidation decrease at pH > 5 despite the further increase of $HCOO^-$ concentration (red dotted curve in Figure 4.2b)? John et al. [27] investigated the oxidation of $HCOO^-$ in alkaline meida and proposed that $HCOO^-$ is adsorbed on the Pt electrode so

strongly that its oxidation is very slow. The pH dependence of $E_p$ and $i_p$ suggests that the reaction mechanism or some reaction conditions are different at pH above and below ~5.

### 4.3.2 SEIRAS studies

To obtain further insights into the reaction, ATR-SEIRAS coupled to cyclic voltammetry was employed. Figure 4.3a shows a series of SEIRA spectra of the surface of a Pt thin film electrode deposited on a Si ATR prism collected in buffer solution with pH 1.5 during a potential scan from 0 to 1.2 and back to 0 V at 20 mV $s^{-1}$. In this experiment, a lower HCOONa concentration of 20 mM was used because CV measurements in 50 mM HCOONa solutions were seriously affected by ohmic drop and it was not successfully corrected especially in neutral solutions due to a large oxidation current arising from a large surface area of the thin film electrode (real surface area was estimated to be of ~10 $cm^2$ from the charge for under potential deposition of hydrogen, $H_{upd}$). A single beam spectrum collected at 0 V in the HCOONa-free solution was used as the reference in calculating the spectra. At the beginning of the potential scan (i.e., at 0 V), the spectrum is dominated by a strong peak at 2050~2070 and a medium strong peak at ~1850 $cm^{-1}$ assigned to linear CO ($CO_L$) and bridge-bonded CO ($CO_B$), respectively. The dip at 1610 $cm^{-1}$ is the bending mode of water that was removed from the interface by the adsorption of CO [35, 38]. The CO bands disappear at around 0.6 V due to the oxidative removal of adsorbed CO, while a new band emerges at 1325 $cm^{-1}$ at around 0.5 V. This band has been assigned to the symmetric O–C–O stretching mode of bridge-bonded formate [6]. The asymmetric O-C-O stretching mode of the bridge-bonded formate, expected around 1590 $cm^{-1}$, is missing in the spectra due to the surface selection rule in SEIRAS [39]. The broad band at ~1050 $cm^{-1}$ that emerges after $CO_{ads}$ being oxidized completely are a P-O stretching vibration of phosphate adsorbed on the electrode surface ($H_2PO_4^-$ and/or $HPO_4^-$ [40]). The spectral changes are reversed on the

reverse negative-going scan. Since the IR absorption enhancement is limited mostly to adsorbed species [7, 29], the adsorption bands of HCOOH, the dominant species in the bulk solution, are absent in the spectra (for example, ν(C=O) expected around 1700 $cm^{-1}$). The spectral range below 950 $cm^{-1}$ was not accessible due to the strong absorption of the Si prism.

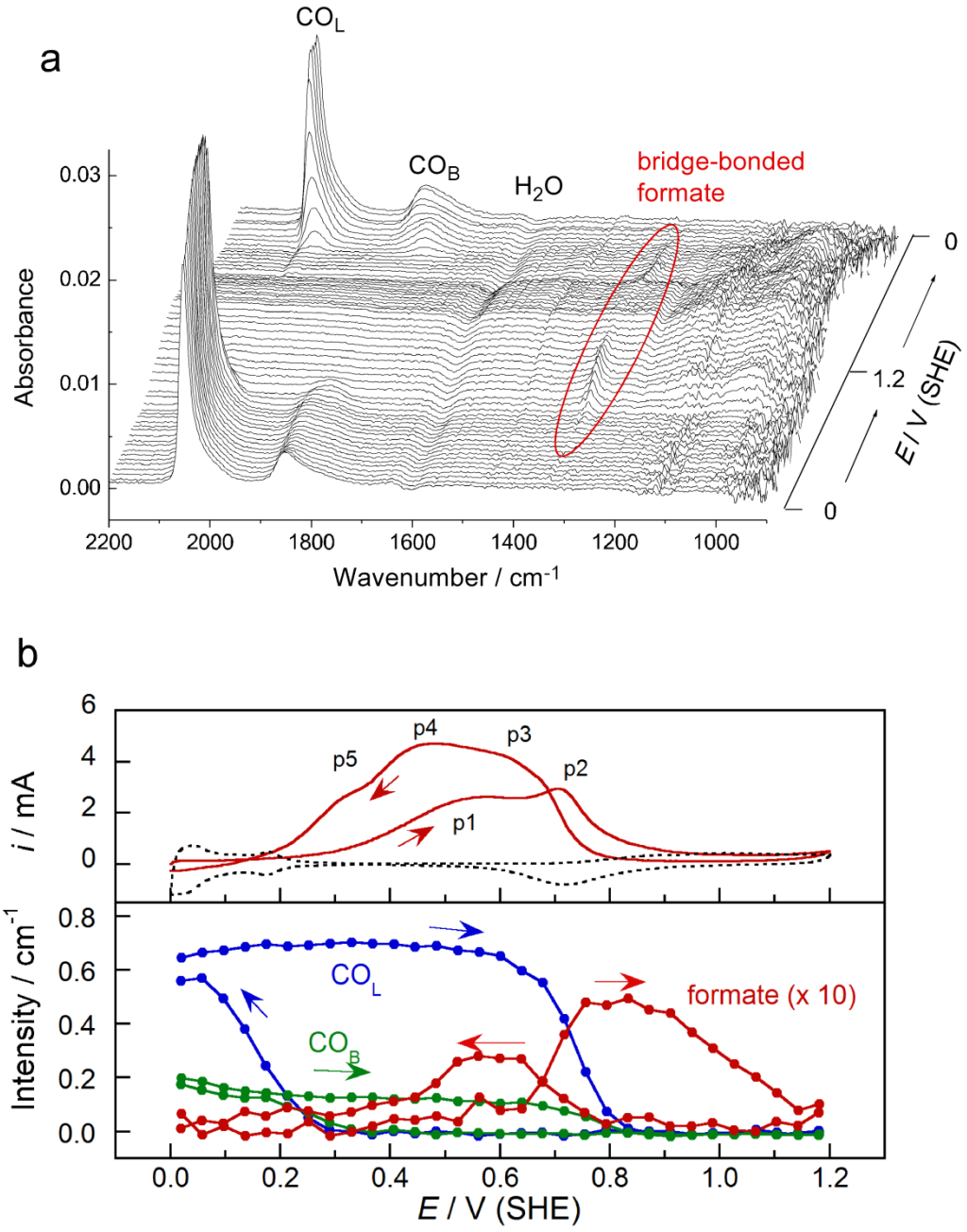


***Figure 4.3.*** (a) SEIRA spectra of the surface of a Pt thin film electrode sequentially collected during a potential sweep from 0 to 1.2 and back to 0 V at 20 mV $s^{-1}$ in buffer solution with pH 1.5

containing 20 mM HCOONa. (b) CV recorded simultaneously with the SEIRA spectra (upper) and the potential dependence of the integrated intensities of $CO_{L,}$ $CO_B$, and bridge-bonded formate bands (lower) taken from (a). The dashed trace is the CV in the same electrolyte without HCOONa.

The CV collected simultaneously with the SEIRA spectra is shown in Figure 4.3(b) (upper panel). The CV is slightly different from that recorded with the rotating disk electrode in the same electrolyte (second CV from the bottom in Figure 4.2a). Three oxidation peaks (or shoulders) are observed on the negative-going scan. The shoulder at 0.3 V corresponds to peak p5 in taking into account of the pH dependence of the peak potential, while the shoulder at about 0.6 V (denoted by p3) is slightly more positive and the peak at 0.45 V (denoted by p4) is slightly more negative compared to peak p3 (0.55 V) observed with the rotating disk electrode (Refer to Figure 4.2a). Since peak p4 and peak p5 were larger than peak 3 at lower $HCOOH/HCOO^-$ total concentrations (data not shown), the difference in $HCOOH/HCOO^-$ concentration is one of the reasons for the different voltammetric features. It is noted that similar features have been reported also in $H_2SO_4$ [41] and $HClO_4$ [42]. The origins of the multiple oxidation peaks will be discussed later.

To find correlations between the CV and SEIRA spectra, the integrated intensities of the $CO_L$, $CO_B$, and bridge-bonded formate bands were plotted as a function of applied potential in the same figure (lower panel). The results are essentially identical to those obtained in $H_2SO_4$ [10, 11], but it is worthwhile to review the same for the sake of comparing them to $HCOO^-$ oxidation in neutral and alkaline media. The electrode surface is almost fully covered by CO at the beginning of the potential scan as evidenced by the complete missing of the hydrogen desorption peaks on the CV. In the potential range where peak p1 appears, the band intensities of the $CO_L$ and $CO_B$ are almost constant, but a previous study has revealed that 10-20% of adsorbed CO is oxidized in this potential range (the so-called peroxidation) [43]. At higher potentials, both $CO_L$ and $CO_B$ bands sharply decreases their intensities due to

the oxidative removal of adsorbed CO ($CO_{ads}$) and peak p2 appears due to the increase of active sites. The oxidative removal of $CO_{ads}$ also facilitates the adsorption of bridge-bonded formate. The band intensity of the bridge-bonded formate continues to increase up to ~0.9 V and then decreases to nearly zero at 1.2 V. This band reappears on the reverse negative-going scan after the reduction of the surface oxide. These observations indicate that pre-adsorbed bridge-bonded formate suppresses the oxidation of the Pt surface on the positive-going scan and that it is not adsorbed on fully oxidized surface.

It is apparent from the figure that the oxidation current is not proportional to the intensity of the bridge-bonded formate at all. Such an experimental result was a basis of the claim that bridge-bonded formate is not the intermediate and rather a site-blocking spectator in HCOOH oxidation [15, 16]. However, it should be noted that bridge-bonded formate is much more stable in the Pt surface oxidation region than in the double layer region, as has been demonstrated by an experiment using isotope labeled HCOOH (Figure 5 in ref. [11]). Since the coverage of an intermediate species should be small when the reaction is very fast, oxidation current is not always proportional to the coverage of the intermediate.

We carried out the same experiments in buffer solutions with different pHs and observed that the bridge-bonded formate band completely disappears at pH > 6 as shown in Figure 4.4a, in which the spectra collected at pH = 6.8 are shown. The disappearance of the bridge-bonded formate is well correlated with the decrease in HCOOH concentration (see blue dashed trace in Figure 4.2b) and indicates that bridge-bonded formate is formed only from HCOOH. If bridge-bonded adsorbed formate were quickly decomposed to $CO_2$, its coverage could be smaller. However, a similar result was obtained for acetic/acetate (pKa=4.75) that is not oxidized at all in this potential range, i.e., the symmetric O-C-O strecting vibration of adsorbed acetate was observed only at pH < 5 (See Figure 4.5). Therefore, the absence of bridge-bonded adsorbed formate in neutral solution is not due to its rapid oxidation. The strong band around 1130 $cm^{-1}$ in the spectra that appears after the

oxidative removal of $CO_{ads}$ is assigned to a P-O stretching mode of a phosphate anion (most likely $H_2PO_4^-$ [40]) adsorbed on the electrode surface because this band was also observed in the same electrolyte solution without HCOONa. In the negative-going scan, a very weak band assigned to either carbonate [44] or bicarbonate [45] derived from $CO_2$ is observed around 1450 $cm^{-1}$. No singnals corresponding to the proposed strongly adsorbed $HCOO^-$ or other related species were dected.

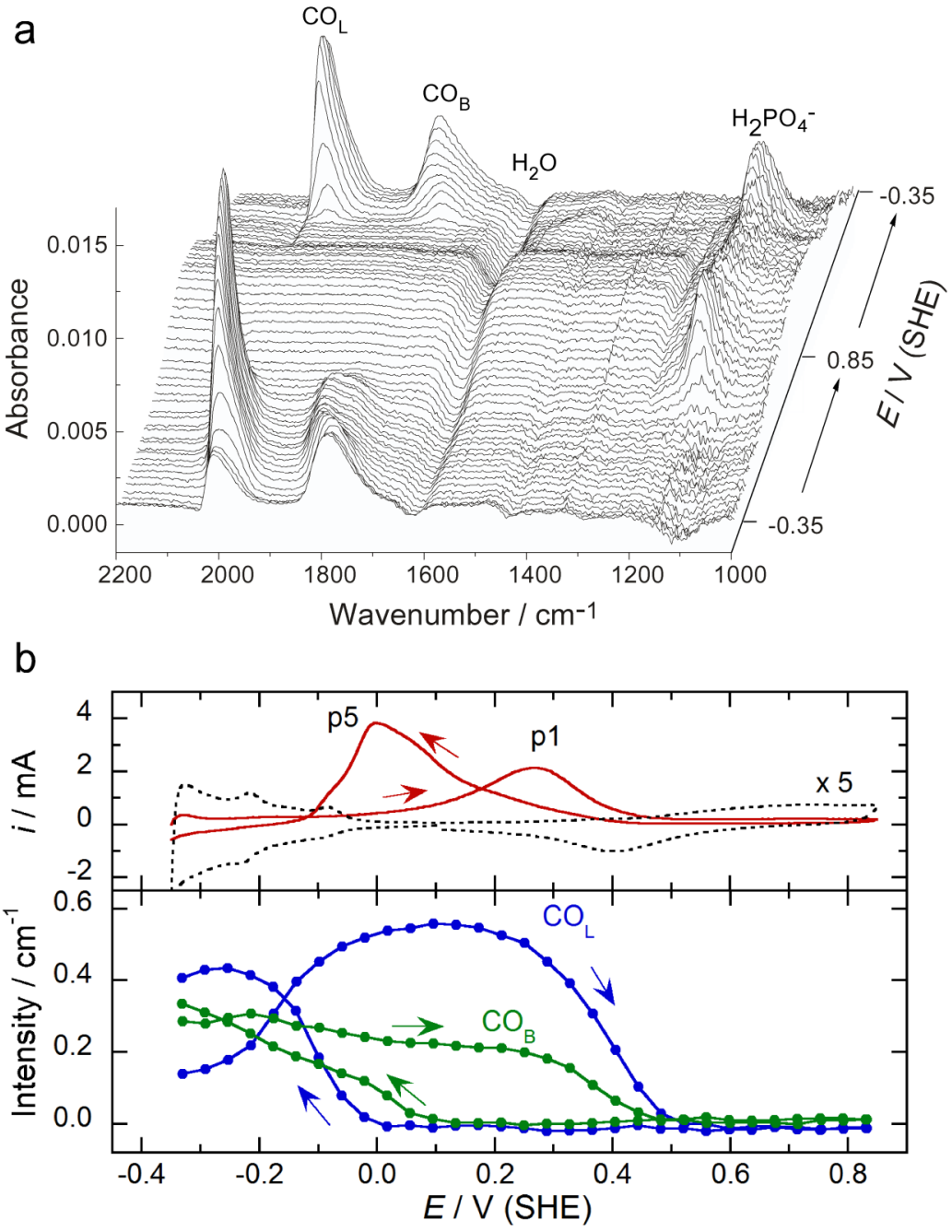

***Figure 4.4.*** (a) SEIRA spectra of the surface of a Pt thin film electrode sequentially collected during a potential sweep from −0.35 to 0.85 and back to −0.35 V at 20 mV $s^{-1}$ in buffer solution with pH 6.8 containing 20 mM HCOONa. (b) CV recorded simultaneously with the SEIRA spectra (upper panel) and the integrated intensities of the $CO_L$ and $CO_B$ bands in (a) plotted as a function applied potential. The dashed trace in the upper panel is the CV in the same electrolyte without HCOONa.

The CV recorded simultaneously with the SEIRA spectra is shown in Figure 4.4b (upper panel) together with the potential dependence of the integrated band intensities of $CO_L$ and $CO_B$ taken from the spectra in Figure 4.4a (lower panel). The CV is simpler than that at pH 1.5 and oly one anodic peak is observed in the both positive- and negative- going scans at different potentials. If the CV is plotted against the reversible hydrogen electrode (RHE), the peaks in the positive- and negative-going scans correspond to peak p1 and peak p5 in the CV at pH 1.5 (Figure 4.3b, upper panel), respectively. On the other hand, anodic peaks corresponding to peak p2, p3, and peak p4 are absent on the CV at this pH, indicating that bridge-bonded formate is responsible for the appearance of these anodic peaks. One more notable feature different from that at pH 1.5 is the lower coverage of $CO_{ads}$. The intensity of the $CO_B$ band is almost identical to that observed at pH 1.5 (Figure 4.3b), but the $CO_L$ band is much smaller at the beginning of the potential scan. The $CO_L$ band grows in the potential range between -0.3 and 0 V. In the negative-going scan, $CO_{ads}$ starts to be formed at 0V and saturates at ~ -0.3 V, idicating that $CO_{ads}$ is formed in a limited potential range.

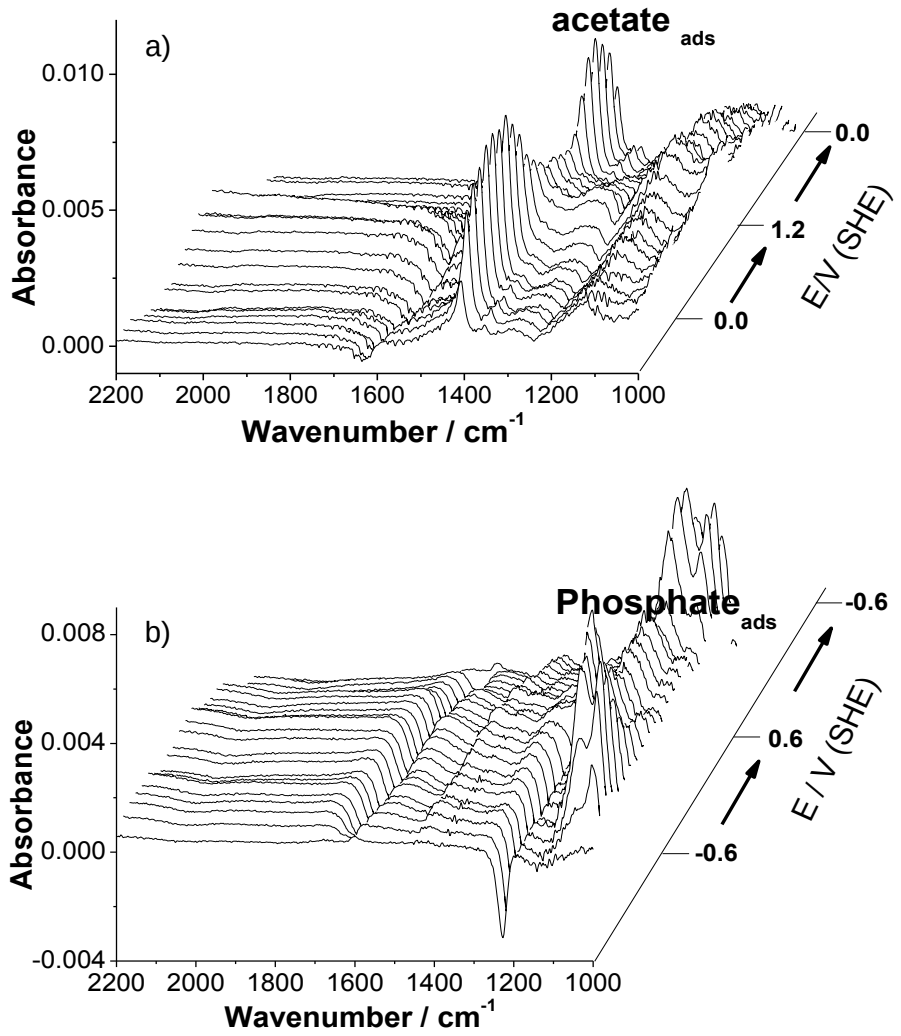


***Figure 4.5.*** SEIRA spectra of the surface of a Pt thin film electrode sequentially collected at 20 mV $s^{-1}$ in buffer solution with (a) pH 1.5 and (b) 11.6 containing 100 mM $CH_3COOH$.

Oxidation of $HCOO^-$ in alkaline media is significantly slower than $HCOOH/HCOO^-$ oxidation in acidic and neutral media (Figure 4.2). The voltammetric features of $HCOO^-$ oxidation in alkaline media are slightly different from those in acidic and neutral solutions. A representative CV at pH 11.7 for the Pt thin film electrode is presented in Figure 4.6a (upper panel). Two peaks are observed on the positive-going scan and one peak on the negative-going scan. Taking into account the pH dependence of oxidation peaks, the second

peak at −0.05 V on the positive-going scan and the peak at −0.33 V on the negative-going scan correspond to peak p1 and peak 5 in Figures 4.3 and 4.4 (on the RHE scale). On the other hand, the first anodic peak at -0.35 V in the positive-going scan, labeled as p0, has not its counterpart at pH 1.4 and 6.8. Peak p0 and peak p5 occurs at almost the same potentials and their peak current are almost the same, indicating that the same reaction takes place at both peak p0 and peak p5. Since the peak currents of peak p0 and peak p5 were propotional to the concentration of $HCOO^-$, these peaks are ascribed to $HCOO^-$ oxidation. From the comparison of CV with the potential dependence of the integrated band intensities of $CO_L$ and $CO_B$ in the same figure (lower panel), the appearance of the new oxidation peak on the positive-going scan is apparently due to the much lower coverage of $CO_{ads}$, which is confirmed by the weak integrated band intensities of $CO_L$ and $CO_B$ shown in the same figure (lower panel): The maximum intensiy of $CO_L$ is only 20% of that observed in acidic solutions (full CO coverage) and that of $CO_B$ is comparable to that in acidic and neutral media.

Stripping voltammetry by John et al. [27] reveled that two strongly adsorbed species are formed from $HCOO^-$ at low potentials and exhibit two oxidative stripping peaks at peak p0 and peak p1. The authors ascribed the stripping peaks to the oxidation of an intermediate of $HCOO^-$ oxidation (termed as X1) and of $CO_{ads}$ (termed as X2), respectively. However, the infrared data shown above indicates that $CO_L$ and $CO_B$ are oxidized selectively at peak p0 and at peak p1, respectively. Other adsorbates detected by SEIRAS were (bi)carbonate and phosphate anion, and no infrared absorption bands that could be ascribed to the intermediate of $HCOO^-$ oxidation were detected (the spectra are not shown because the spectral features were similar to those in Figure 4.4a). Accordingly, we assign X1 and X2 to $CO_L$ and $CO_B$, respectively. The peak current of peak p1 was independent of concentration of $HCOO^-$, indicating that p1 arises only from the oxidation of $CO_B$.

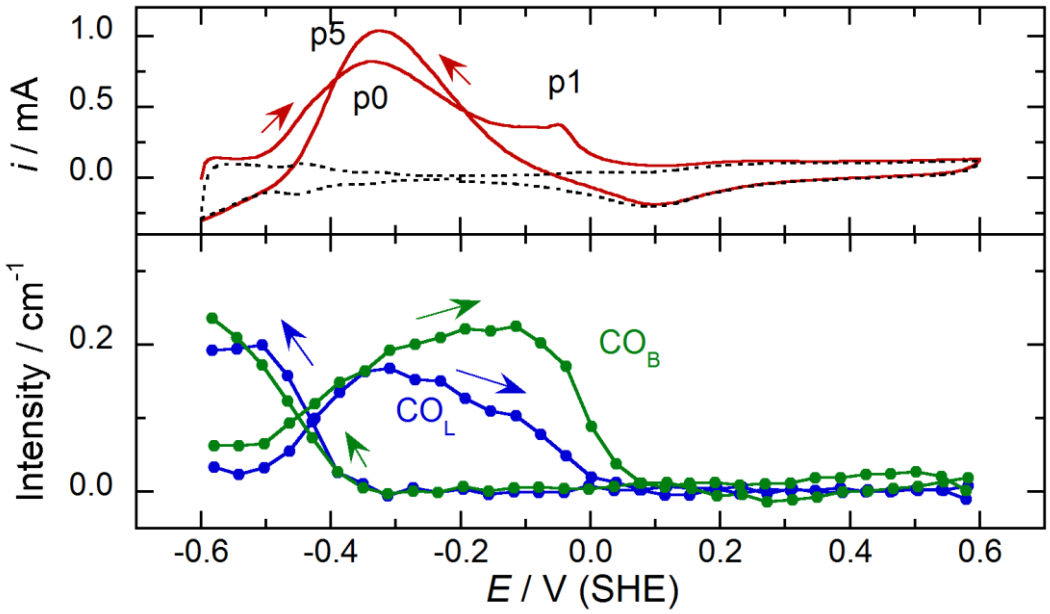


***Figure 4.6.*** CV for 20 mM $HCOO^-$ in buffer solution with pH 11.7 at 20 mV $s^{-1}$ (upper panel) and recorded simultaneously with the SEIRA spectra (upper panel) and the potential dependence of the integrated intensities of the $CO_L$ and $CO_B$ bands taken from SEIRA spectra collected simultaneously with the CV (lower panel). The dashed trace in the upper panel is the CV in the same electrolyte without HCOONa.

### 4.3.3 Summary of spectroelectrochemical measurements: Pourbaix diagram

All the results of the electrochemical and spectroelectrochemical measurements are summarized in a Pourbaix diagram (*E* vs. pH diagram) in Figure 4.7. Blue symbols represent the peak potentials of peak p3, peak p4, and peak p5 at pH 1.5, and peak 5 at pH>6. The results in the pH range between 3 and 5, where the oxidation current is large (Figure 4.2b), were omitted in the diagram because the voltammetric features in the negative-going scan were seriously distorted by the ohmic drop, which arose from the large real surface area of the thin film electrode (~10 $cm^2$ determined from the charge under the hydrogen desorption peaks) and a relatively large cell constant of ~10Ω (mostly due to the resistance of the thin film electrode). Instead, the peak potentials of the anodic peak, $E_p$, observed with a rotating Pt

disc electrode (5 mm in diameter) in the same buffered solutions containing 50 mM HCOOH/$HCOO^-$ (Figure 4.2b) recorded in the negative-going scan are shown by black symbols. In this case, only a single oxidation peak was observed at pH < 5. The peak shifted to lower potentials with increasing pH at a rate of 60 mV per pH and a shoulder appeared at around pH 5.5. At higher pHs, the higher potential component of the anodic peak disappeared and the lower potential component shifted to the lower potentials accompanying by the decrease in peak current. The peak potentials in the two independent measurements are in good agreement at pH > 6. Red symbols represent the potential at which the IR band of $CO_{ads}$ appeared in the negative-going scan. The onset potential of $CO_{ads}$ formation is independent of pH at pH < ~5 and negatively shifted at pH > ~5 at a rate of 60 mV per pH. Additionally shown are the surface oxidation and upd hydrogen adsorption ($H_{upd}$) regions, which were determined in the positive- and negative-going scans, respectively, in the supporting electrolyte solutions free of HCOOH/$HCOO^-$ (experimental data points were omitted to avoid complexity). The white area is the double-layer region, but it is noted that some amount of surface oxide or $OH_{ads}$ remains in this region in the negative-going scan during which the IR and electrochemical data were collected due to the relatively slow kinetics of the reduction of surface oxide (see dotted CVs in figures. 4.3, 4.4, and 4.6 recorded in HCOONa-free electrolyte solutions). Finally, green symbols represent the potentials at which the band of adsorbed phosphate appeared in the positive-going scan in the HCOOH/$HCOO^-$ free solutions. This data could be a rough measure of the onset potential of the adsorption of anionic species, including $HCOO^-$ and $OH^-$. In fact, the onset of $OH^-$ adsorption is reported to be located in the $H_{upd}$ region [46].

The Pourbaix diagram highlights two interesting features of HCOOH/$HCOO^-$ oxidation and $CO_{ads}$ formation. One is that $E_p$ is located in the double layer region at pH < 5.5 and jumps to the onset potential of $H_{upd}$ at pH > 5.5. The other is that the onset of $CO_{ads}$ formation is independent of pH at pH < 5.5, while it depends on pH at pH > 5.5 and is located

at the onset potential of $H_{upd}$. Remembering that bridge-bonded formate is adsorbed on the electrode surface at pH < 6, the different pH dependences of $E_p$ and $CO_{ads}$ formation at pH < 5.5 and > 5.5 will be related to the presence and absence of bridge-bonded adsorbed formate rather than the acid-base equilibrium of HCOOH in the solution ($pK_a$ = 3.75). In fact, Cuesta et al. [13, 14] showed that $CO_{ads}$ is formed in acidic media by the reduction of bridge-bonded adsorbed formate ($HCOO_{ads} + H^+ + e^- \rightarrow CO_{ads} + H_2O$). The rate of the reaction depends on potential [13, 14, 47], but the onset potential is not necessary to be pH dependent. The pH-independence could also be explained by the pure chemical dehydration of HCOOH ($HCOOH \rightarrow CO_{ads} + H_2O$), but this mechanism is not suitable since $\theta_{CO}$ increases as the potential is made more negative (Figure 4.3), i.e., $CO_{ads}$ formation is an electrochemical reduction process.

On the other hand, the source of $CO_{ads}$ is $HCOO^-$ in alkaline media. And bridge-bonded formate is absent. As shown in Figures 4.4 and 4.6, $CO_{ads}$ accumulation occurs in a limited potential range locating in between the red and green lines in Figure 4.7, i.e., in the potential range where both $HCOO^-$ and $H_{upd}$ can be coadsorbed. Further detailed examination of $CO_{ads}$ accumulation is shown in Figure 4.8. To find the relationship between $CO_{ads}$ formation and potential, voltammetric measurements varying lower potential limit are performed. Figure 4.8 shows cyclic voltammograms measured as a function of the lower potential limit. We observe that peak current are decreased with increasing lower potential limit. Peak current is favored at the lower potential limits relative to the adsorption/desorption of weakly adsorbed hydrogen. This is in agreement with literature results suggesting that $H_{ads}$ is involved in $CO_{ads}$ formation [48]. Therefore, $CO_{ads}$ is likely to be formed by a reaction of adsorbed $HCOO^-$ with $H_{upd}$ although we did not observe the adsorbed $HCOO^-$ by SEIRAS. Since $HCOO^-$ competes with $OH_{ads}$ for free sites, $CO_{ads}$ accumulation is slow in alkaline media compared with that in acid [27], which has been observed in the present experiments.

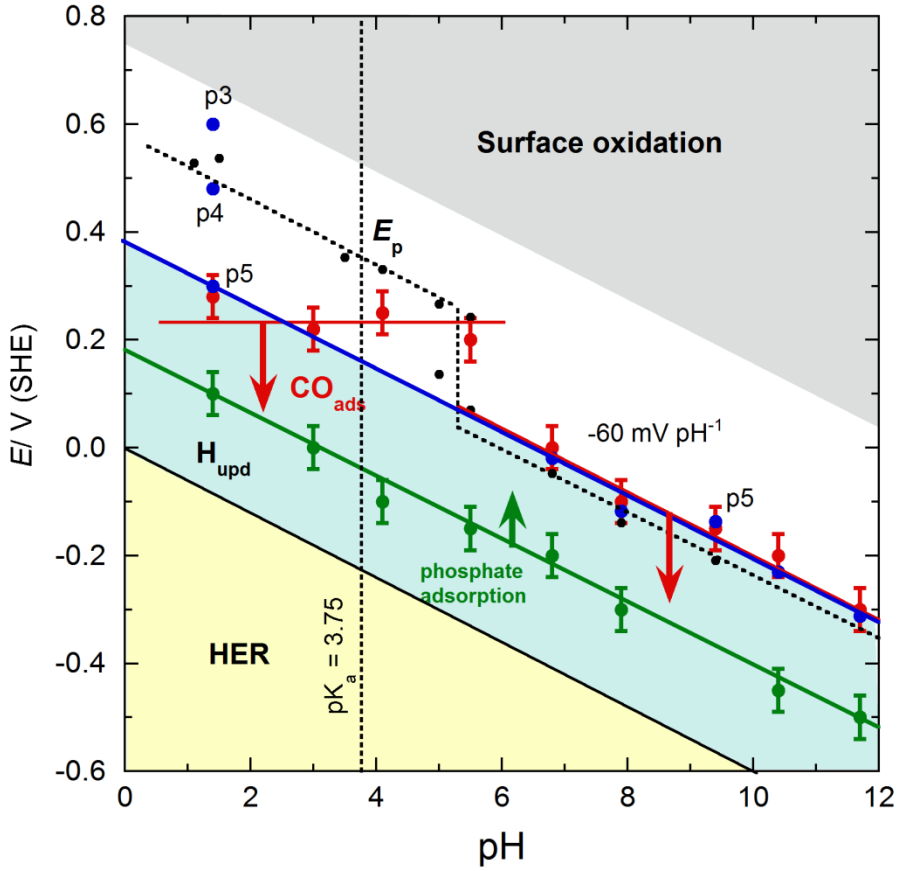


***Figure 4.7.*** Pourbaix diagram of the HCOOH/HCOO$^-$ oxidation on Pt. Black symbols: peak potential of the anodic peak, $E_p$, taken from Ref. [49] ; blue symbols: peak potentials of the anodic peaks or shoulders in the negative-going scan; red symbos: onset potential of $CO_{ads}$ formation in the negative-going sweep; green symbols: onset potential of the adsorption of phosphate anions in the positive-going scan. See further details in the text.

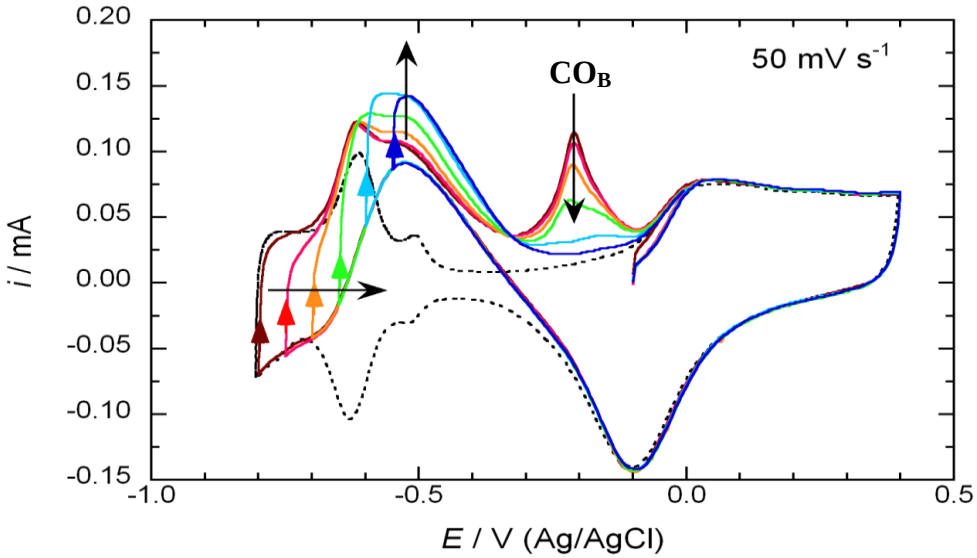


***Figure 4.8.*** Variance of CV measured at 50 mV $s^{-1}$ on Pt in 0.1 M NaOH and 10 mM HCOONa as a function of lower potential limit. Initial potential is -0.1V and then potential is scanned in the forward direction and back to lower potential limit.

## 4.4 The origin of the pH dependence of HCOOH/$HCOO^-$ oxidation

### 4.4.1 Phenomenological explantion

The experimental result shown in Figure 4.2 clearly shows that $HCOO^-$ is more reactive than HCOOH in acidic and neutral media, but the oxidation current is very small in alkaline media. Earlier electrochemical studies suggested that $HCOO^-$ is oxidized *via* a strongly adsorbed intermediate other than CO [36, 50]. John et al. [27] observed that two strongly adsorbed species exist on the Pt surface that are oxidized at different potentials. They ascribed the species that is oxidized at a higher potential (corresponds to peak p1 in Figure 4.6) to adsorbed CO and the other that is oxidized at a lower potential (in the potential range of peak 0) to an oxygen-rich species with a strong Pt-C bond such as Pt-COOH. However, we

have shown in Figure 4.6 that adsorbed $CO_L$ is oxidized at a lower potential than $CO_B$. Therefore, the strongly adsorbed species John et al. observed electrochemically is very likely to be $CO_L$. On the basis of this observation, they proposed the latter species being the intermediate of $HCOO^-$ oxidation and explained the slow kinetics of $HCOO^-$ oxidation in strong alkaline media by the high stability of the intermediate and also by the suppression of its adsorption by adsorbed hydroxyl species, $OH_{ads}$. Even if the explanation were correct, their explanation cannot explain the extremely high activity of $HCOO^-$ at around pH 4. Furthermore, if the intermediate were so stable as assumed, it is expected to be detected by SEIRAS. However, no possible intermediates were detected in alkaline solutions in the present study despite the very high sensitivity of SEIRAS. Rather it is more reasonable to assume that $HCOO^-$ is directly oxidized to $CO_2$ very quickly so that adsorbed $HCOO^-$ precursor cannot be detected by SEIEAS.

Here we term this mechanism as ***direct $HCOO^-$ pathway*** for distinguishing it from bridge-bonded formate and direct HCOOH pathways. No information is available about the nature of the adsorbed $HCOO^-$ precursor, but a possible precursor is formate bonded to the surface *via* single oxygen atom (monodentate formate); monodentate formate is known to be easily oxidized to $CO_2$ on NiO(111) in UHV [51].

### 4.4.2 Kinetic model

As shown in Figure 4.2b, peak current ($j_p$) of the HCOOH/$HCOO^-$ oxidation in the negative-going scan shows a volcano-shaped pH dependence peaked at pH ~ 4. Since the HCOOH concentration decreases with pH, the increase of $j_p$ at pH < 4 apparently cannot be explained by the direct HCOOH mechanism which assumes HCOOH oxidation *via* a weakly adsorbed HCOOH precursor. Bridge-bonded adsorbed formate mechanism also is not compatible with the result because the coverage of bridge-bonded adsorbed formate was almost constant at pH < 4. Rather, the result strongly suggests that $HCOO^-$ is more reactive than HCOOH and its oxidation mostly contributes to the anodic current. However, if it is so, why does the anodic current decrease at pH > 5 despite the further increase of $HCOO^-$ concentration? Grozovski et al. [18] explained the small anodic current in alkaline media to the absence of adsorbed formate on the electrode surface. On the other hand, John et al. [27] proposed that $HCOO^-$ is adsorbed on the electrode so strongly that its oxidation is very slow. However, both proposals do not account for the very high activity of $HCOO^-$ in weakly acidic and neutral media. Given that HCOOH/$HCOO^-$ oxidation is kinetically controlled [12, 49], we propose a simple kinetic model that reasonably explains the significant pH dependence of HCOOH/$HCOO^-$ oxidation. The essence of the model is schematically depicted in Figure 4.9. Following the Butler-Volmer rate law, the rate constant of $HCOO^-$ oxidation ($k_{ox}$) should increase exponentially as the potential is made more positive (the blue curve in Figure 4.9a). On the other hand, free surface sites available for $HCOO^-$ oxidation are reduced as the potential is made more positive due to the oxidation of the electrode surface. The potential dependence of the coverage of surface oxide ($\theta_{ox}$) may be represented as the black trace. Since the oxidation current is proportional to $k_{ox}(1-\theta_{ox})$, a peak should appear in the voltammogram at a potential where $\theta_{ox} \sim 0.5$, as shown by the red curve in the figure. The onset of the surface oxidation shifts negatively as the pH of the solution is increased at a rate

of 60 mV per pH, while $k_{ox}$ is independent of pH. Accordingly, the anodic peak shifts negatively and becomes smaller with increasing pH. The peak current also should be proportional to the concentration of $HCOO^-$ ($[HCOO^-]$), which increases as the pH is increased. As a result, the peak current, $j_p = 2Fk_1(1-\theta_{ox})\ [HCOO^-]$, is expected to yield a volcano-type pH dependence peaked at pH ~ $pK_a$ of HCOOH, as shown by the red trace in Figure 4.9b. The validity of this idea is substantiated in the following by mathematical modeling of the steady-state voltammogram.

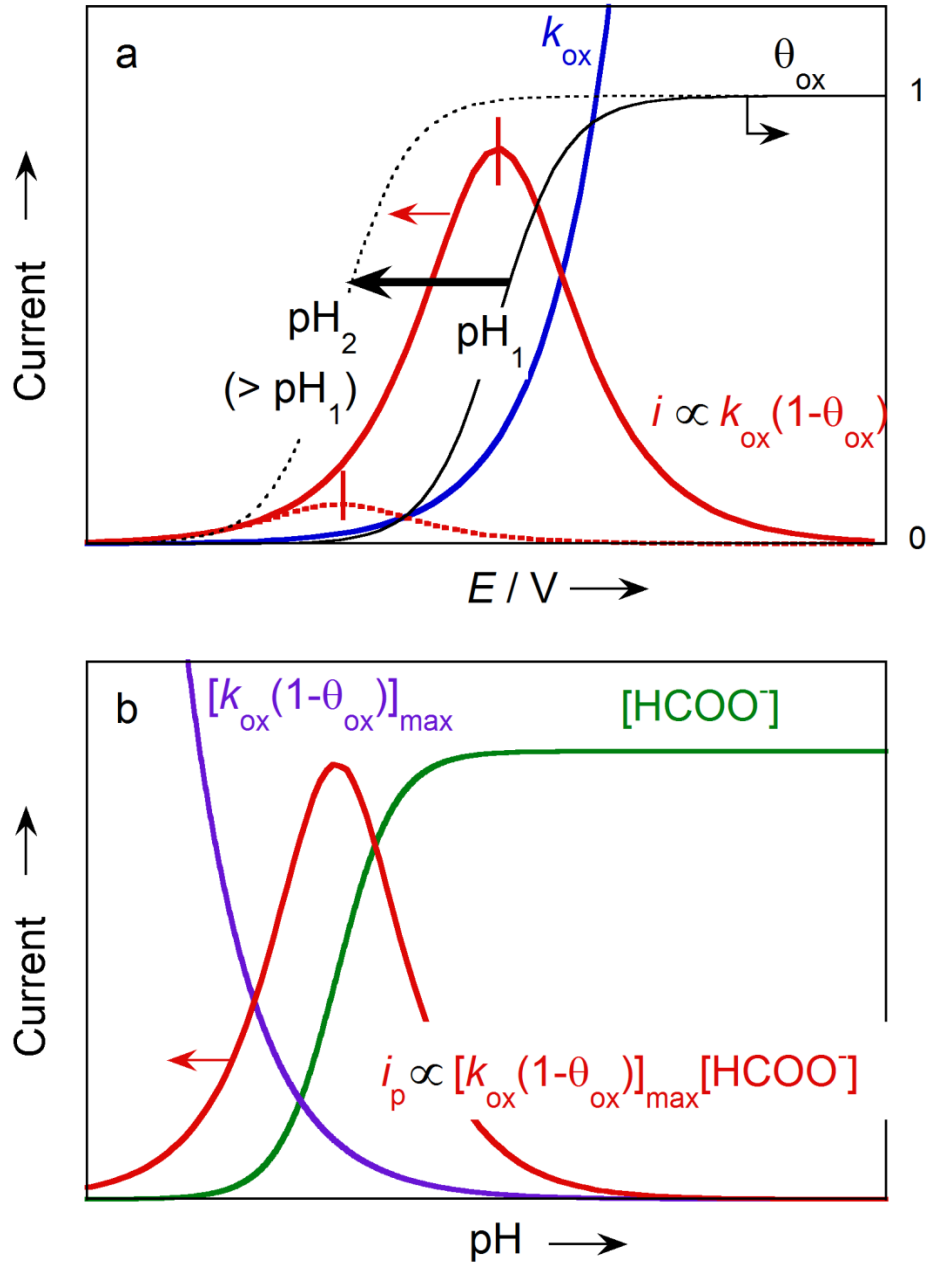


***Figure. 4.9.*** Schematic explanations (a) for the negative shift and the decrease of the $HCOO^-$ oxidation peak associated with an increase of pH from $pH_1$ to $pH_2$, and (b) for the pH dependence of the peak current. $k_{ox}$ is the rate constant and $\theta_{ox}$ represents the coverage of Pt oxide or adsorbed OH. See further details in the text.

### 4.4.3 The kinetic modeling

The validity of model (Figure 4.9) is substantiated in the following by mathematical modeling of steady-state voltammograms. It has been established experimentally that HCOOH is adsorbed on Pt as bridge-bonded formate in acidic media: [6, 10, 15]

$$HCOOH + 2Pt \leftrightarrows b\text{-}HCOO_{ads} + H^+ + e^- \quad (4.1)$$

The decrease of its coverage at high pHs is well correlated with the decrease of HCOOH concentration in the bulk, implying that bridge-bonded formate is formed only from HCOOH. Following Samjeské et al. [10], bridge-bonded adsorbed formate is assumed to be irreversibly oxidized to $CO_2$:

$$b\text{-}HCOO_{ads} \rightarrow CO_2 + H^+ + e^- + 2Pt \quad (4.2)$$

Since the oxidation of $HCOO^-$ *via* a weakly adsorbed $HCOO^-$ precursor (direct $HCOO^-$ pathway) is believed to be very fast, it is simply represented as

$$HCOO^- \rightarrow CO_2 + H^+ + 2e^- \quad (4.3)$$

We will model the surface oxidation by a simple reversible reaction represented by

$$H_2O + Pt \leftrightarrows Pt\text{-}OH_{ads} + H^+ + e^- \quad (4.4)$$

On a real polycrystalline surface, $OH_{ads}$ is oxidized further to yield surface oxide [52]. However, to model the inhibition of $HCOOH/HCOO^-$ oxidation by Pt surface oxidation, the introduction of OH is sufficient in alkaline media [27], and reaction 4.4 serves that purpose well. We do not consider the formation of CO because $HCOOH/HCOO^-$ is oxidized on a clean Pt surface not significantly poisoned by $CO_{ads}$ on the negative-going scan. Adsorption of phosphate anions is also neglected for the sake of simplicity because the pH dependence of $HCOOH/HCOO^-$ oxidation similar to that observed in phosphate buffered solutions (Figure 4.2) has also been observed in $ClO_4^-$ and $HSO_4^-/SO_4^{2-}$ solutions [22, 25, 26, 36].

Under these conditions, and assuming that the adsorption of bridge-bonded formate and OH can be described by the Langmuir isotherm, the coverage of bridge-bonded formate ($\theta_{b\text{-}f}$) and adsorbed $OH_{ads}$ ($\theta_{OH}$) satisfy the following differential equations:

$$\frac{d\theta_{b\text{-}f}}{dt} = k_1[HCOOH](1-\theta_{b\text{-}f}-\theta_{OH}) - k_{-1}[H^+]\theta_{b\text{-}f} - k_2\theta_{b\text{-}f} \qquad (4.5)$$

$$\frac{d\theta_{OH}}{dt} = k_4(1-\theta_{b\text{-}f}-\theta_{OH}) - k_{-4}[H^+]\theta_{OH} \qquad (4.6)$$

where $k_{\pm i}$ (i = 1, 2, 3, and 4) is the rate constant of each reaction step at a potential $E$ and is assumed to follow the Butler-Volmer rate law with a transfer coefficient $\alpha$:

$$k_i = k_i^{eq}\exp\left[\frac{\alpha nF(E-E_i^{eq})}{RT}\right] \quad , \quad k_{-i} = k_{-i}^{eq}\exp\left[\frac{-(1-\alpha)nF(E-E_i^{eq})}{RT}\right] \qquad (4.7)$$

with plus for forward reaction (oxidation or adsorption) and minus for backward reaction (reduction or desorption). $k_i^{eq}$ is the rate constant at the equilibrium potential $E_i^{eq}$ , and $F$, $R$, and $T$ have the usual meanings. Although first order [18], second order [14, 53], and parabolic [9-11] rate equations with respect to $\theta_{b\text{-}f}$ have been proposed for reaction (4.2), the first order rate law is assumed for the sake of simplicity. By applying the steady-state approximation

$$\frac{d\theta_{b\text{-}f}}{dt} = \frac{d\theta_{OH}}{dt} = 0 \tag{4.8}$$

the total current density $j_{total}$ is given by adding up all contributions from the oxidation of HCOOH *via* bridge-bonded formate (reactions (4.1) and (4.2)), $j_{b\text{-}formate}$, and the direct $HCOO^-$ oxidation (4.3), $j_{HCOO\text{-}}$:

$$\begin{aligned} j_{total} &= j_{b-formate} + j_{HCOO^-} \\ &= 2Fk_2\theta_{b\text{-}f} + 2Fk_3(1-\theta_{b\text{-}f}-\theta_{OH})[HCOO^-] \end{aligned} \tag{4.9}$$

Where

$$\theta_{b\text{-}f} = \left[1 + \frac{k_{-1}[H^+] + k_2}{k_1[HCOOH]}\left(1 + \frac{1}{K_4}\right)\right]^{-1} \tag{4.10}$$

$$\theta_{ox} = (1-\theta_{b\text{-}f})/(1+K_4) \tag{4.11}$$

and

$$K_4 = \frac{k_{-4}}{k_4}[H^+] = K_4^{eq}[H^+]\exp\left[\frac{-F(E-E_4^{eq})}{RT}\right] \quad (4.12)$$

In Figure 4.10, steady-state voltammograms for [HCOOH/$HCOO^-$] = 0.1 M calculated by using the parameter set shown in the caption are presented. The parameters were chosen to give the maximum of the peak current, $j_p$, of ~ 5 mA $cm^{-2}$ around pH 4 for [HCOOH/$HCOO^-$] = 50 mM (Figure 4.2) and $\theta_{b\text{-f}}$ ~ 0.8 for [HCOOH/$HCOO^-$] = 10 mM [18]. Among the parameters, the most important is $k_2^{eq}$, which must be non-zero, i.e., bridge-bonded adsorbed formate must be decomposed to $CO_2$. Otherwise, the electrode surface is fully covered by bridge-bonded adsorbed formate over a wide potential and pH range and $HCOO^-$ oxidation is seriously suppressed. As shown in Figure 4.10a, the simulated steady-state voltammogram is strongly depends on pH. In accordance with the experiment, the peak current for $HCOO^-$ oxidation, $j_{p,HCOO-}$, increases monotonically with increasing pH up to 4.5 and decreases at higher pHs as shown in Figure 4.10b (red trace), while the current carried by the bridge-bonded adsorbed formate pathway ($j_{p,b\text{-formate}}$) is very small over the wide pH range. The observed pH dependence of the adsorption of bridge-bonded formate at pH < 6 also is well reproduced as shown in the colored contour plot in Figure 4.10c. (Note that in reality its adsorption is limited in the low potential region due to the accumulation of $CO_{ads}$).

The model also simulates the negative shift of peak potential $E_p$ with pH but does not reproduce the experiment perfectly. In the simulation, $E_p$ shifts to lower potentials with increasing pH with a slope of −60 mV per pH except in the pH range between 4 and 6 where the shift is larger, whereas the peak splits into two at pHs around 5 in the experiment (Figure 4.7). The discrepancy may be due to the island formation of bridge-bonded adsorbed formate in the real system, which cannot be simulated by the Langmuir adsorption isotherm used in

the simulation (equation 4.5). Island formation of bridge-bonded adsorbed formate has been suggested in both UHV [54] and electrochemical environment [55].

The dotted straight line in Figure 4.10b represents the pH dependence of $E_p$ when bridge-bonded formate is assumed not to be adsorbed as on Pd. A comparison of the $E_p$ curves with and without bridge-bonded adsorbed formate reveals that $E_p$ is positively shifted by bridge-bonded adsorbed formate. The shift ($\Delta E_p$) becomes larger as $\theta_{b\text{-}f}$ increases. Following the Buttler-Volmer rate law, the calculated positive shift of $\Delta E_p \sim 0.1$ V increases $j_{p,HCOO^-}$ by a factor of 7. The shift amounts to 0.2 V in the experiment, which increases $j_{p,HCOO^-}$ by a factor of 49. Due to this effect, the suppression of the direct $HCOO^-$ pathway by bridge-bonded adsorbed formate is not fatal despite the its large coverage (> 0.95). The positive shift of $E_p$ is due to the suppression of surface oxidation by bridge-bonded adsorbed formate, as can be seen from the pH dependence of $\theta_{OH}$ (light blue contour plot) in Figure 4.10c. In fact, the suppression of surface oxidation by bridge-bonded adsorbed formate has been confirmed experimentally [11]. The $E_p$-pH curve shown by the pink thick dashed trace is located at the boundary of the bridge-bonded formate and OH adsorption regions (at $\theta_{OH} \approx \theta_{b\text{-}f}$). Since $\theta_{b\text{-}f}$ is less than 1 (i.e., $k_2^{eq} \neq 0$), $HCOO^-$ oxidation in the surface oxidation region of Pt (in the blank solution) becomes possible. Adsorbed bridge-bonded formate is a site-blocking spectator for the direct $HCOO^-$ oxidation, but it should be noted adsorbed bridge-bonded formate suppresses the adsorption of OH and surface oxidation of Pt and facilities the direct $HCOO^-$ oxidation. Due to this effect, the experimental $j_p$-$E_p$ curve broadens into the low pH region, as can be seen from a comparison of Figure 4.2b and 4.10b.

A remaining issue is whether HCOOH is directly oxidized. Theoretical studies compared the energetics of the bridge-bonded adsorbed pathway and the direct HCOOH pathway [19-21], but the direct $HCOO^-$ pathway was not considered in the theoretical studies. Regarding this issue, it is worth noting that the direct $HCOO^-$ oxidation gives a

considerable current even in acidic media (Figures. 4.10 and 4.13) despite its negligibly small concentration (0.018% at pH 0). This means that HCOOH is oxidized after being converted to $HCOO^-$. The direct HCOOH pathway never exceeds the direct $HCOO^-$ pathway, if any: If oxidation current due to direct HCOOH pathway were comparable to or larger than that due to the direct $HCOO^-$ pathway, the monotonic increase of the oxidation current with pH in acidic media (Figure. 4.2) cannot be explained. Furthermore, as has been discussed above, the oxidation of HCOOH through $HCOO^-$ is very favorable. Therefore, the direct HCOOH mechanism is not likely to work.

Both the experiment and simulation show that an optimal performance is obtained at pH close to $pK_a$ of HCOOH. This is ascribed to the increase of $HCOO^-$ concentration and the decrease of the reaction rate with pH. The same trend has been observed also for oxidation of some alcohols and aldehydes [23]. If bridge-bonded formate are assumed not to be adsorbed on the electrode, as in the case of HCOOH oxidation on Pd [56], the simulation showed that the maximum of $i_p$ appears exactly at pH = $pK_a$. A theoretical thermodynamic argument has shown that this is a generic nature for decoupled proton-electron transfer reactions ($AH \leftrightarrows A^- + H^+$, $A^- \rightarrow A + e^-$) [32]. The same conclusion can be obtained also by using the simple kinetic model proposed in the present study (See section 5.5). Therefore, the pKa of the molecule of interest is an important factor for predicting the optimal pH. In fact, electrocatalytic oxidation of alcohols that have large $pK_a$ values is more facile in alkaline media than in acidic media [20, 21, 33].

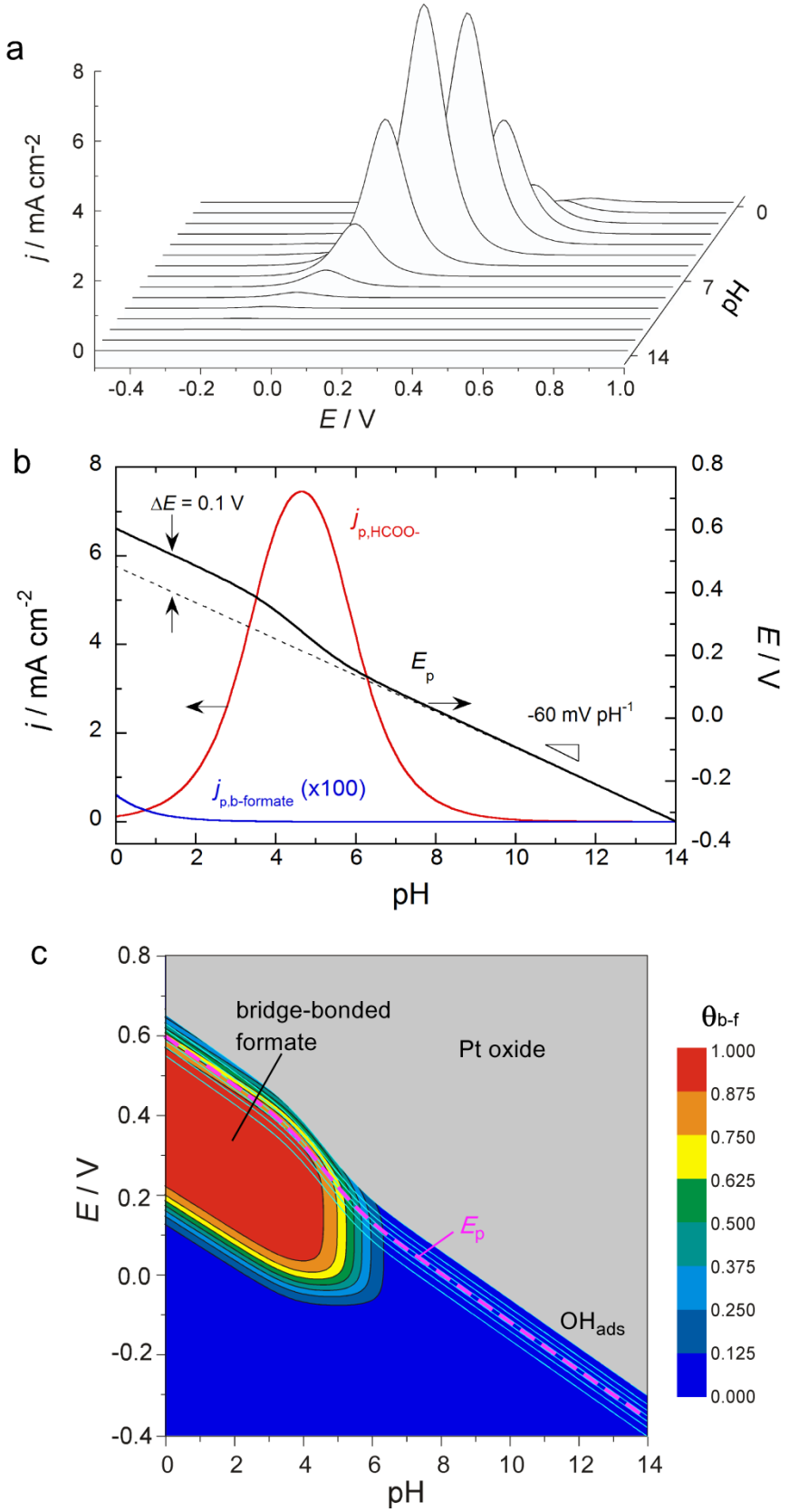


***Figure 4.10.*** (a) Simulated pH dependence of the steady-state voltammogram for $HCOOH/HCOO^-$ oxidation. The parameters used were $pK_a$=3.75, [$HCOOH/HCOO^-$] = 0.1 M, $\alpha$ =

0.5, $k_1^{eq} = 8\times10^{-8}$ s$^{-1}$, $k_3^{eq} = 10^{-10}$ mol$^{-1}$ s$^{-1}$ , $k_{-3}^{eq} = 10^{-14}$ mol$^{-1}$ s$^{-1}$, $k_4^{eq} = 5\times10^{-16}$ s$^{-1}$, $K_2^{eq} = 1$ mol$^{-1}$ s$^{-1}$, $E_1^{eq} = 0$ V, $E_2^{eq} = 0.5$ V, $E_3^{eq} = 0.3$ V, and $E_4^{eq} = 0$ V. (b) Simulated pH dependence of peak currents via the direct $HCOO^-$ pathway ($j_{p,HCOO-}$, red trace) and via the bridge-bonded formate pathway ($j_{p,HCOOH}$, blue trace), and of the peak potential $E_p$ (black solid trace). The dotted straight line is the pH dependence of $E_p$ when bridge-bonded adsorbed formate is absent from the electrode surface. (c) Potential and pH dependece of the coverage of bridge-bonded formate (colored contor plot) and adsorbed OH (light blue contor plot). The dashed pink line is the pH dependece of $E_p$ (same as that in (b)).

### 4.4.4 Validity of the perameters

As shown above, the simple model reasonably explains the potential and pH dependence of HCOOH/$HCOO^-$ oxidation. To confirm the validity of the simulation, it is necessary to mention about some important parameters used. The most important parameter is $k_2^{eq}$, the reaction rate constant of the oxidation of bridge-bonded formate. Note that $k_2^{eq}$ is not zero. Since oxidation of bridge-bonded formate yield active sites, $HCOO^-$ also can be oxidized despite the high bridge-bonded formate coverage. On the other hand, if $k_2^{eq} = 0$ (i.e., if bridge-bonded formate were a site-blocking spectator as Chen et al. argued [15, 16]), the electrode surface is fully covered by bridge-bonded formate in wide $E$ and pH ranges and only $HCOO^-$ can be oxidized in a high pH range as shown in Figure 4.11.

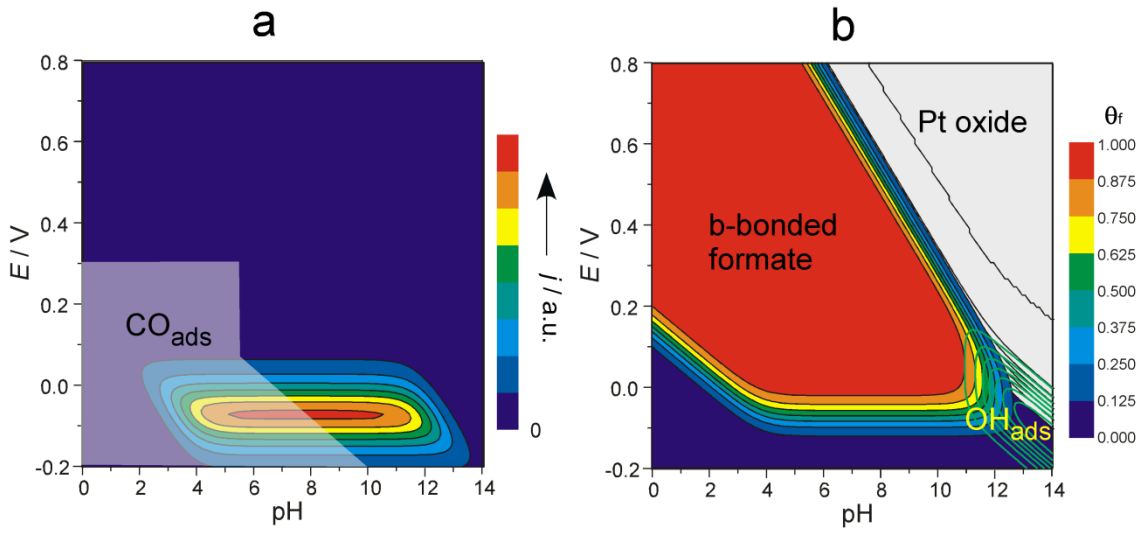


***Figure 4.11.*** Simulation when bridge-bonded formate is assumed to be site-blocking spectator (i.e., $k_2^{eq} = 0$). (a) Both oxidation current and (b) bridge bonded formate coverage are simulated.

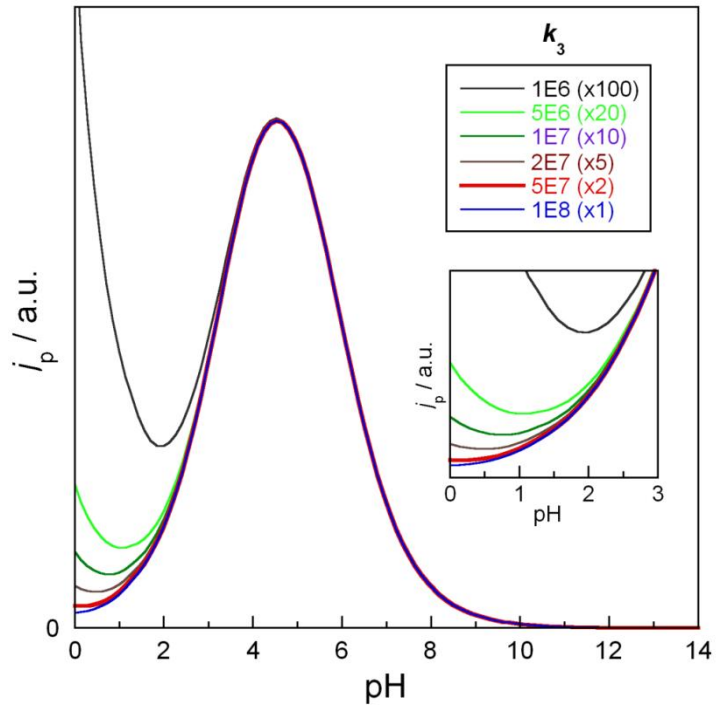


***Figure 4.12.*** Simulation for contribution of $HCOO^-$ oxidation to the total current varying the $k_3^{eq}$.

Next important parameter is $k_3^{eq}$, which determines the contribution of *direct* $HCOO^-$ oxidation to the total current. As shown in Figure 4.10(b), $j_{\text{b-formate}}$ decreases and

$j_{HCOO^-}$ increases for the increase of pH. Accordingly, the total current should have a local minimum in the pH range between 0 and 2 when $k_3^{eq}$ is smaller than $5\times10^7$ (Figure 4.12), which conflicts with the observed monotonic increase of current in the acidic media (Figure 4.2b).

### 4.4.5 The role of bridge-bonded adsorbed formate in HCOOH/HCOO$^-$ oxidation

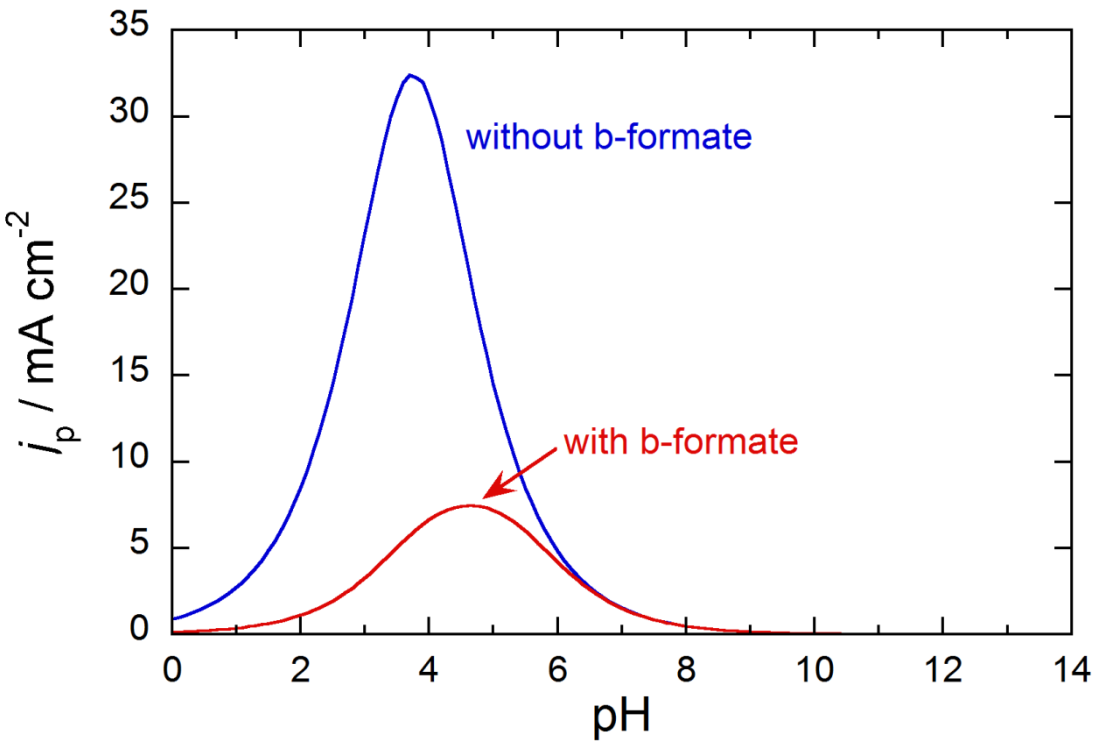


***Figure 4.13.*** Simulated pH dependence of peak currents in the presence (red curve) and absence (blue curve) bridge-bonded adsorbed formate. The parameters used were the same as in fig. 5.10, but the coverage of bridge-bonded adsorbed formate, $\theta_{b\text{-}f}$, was set zero in the latter.

As shown above, the decomposition of bridge-bonded adsorbed formate is very slow. Therefore bridge-bonded adsorbed formate blocks active sites and inhibits the direct $HCOO^-$ pathway as shown in Figure 4.13, where the simulated pH dependence of peak current with

(red curve) and without (blue curve) bridge-bonded adsorbed formate are compared. It shows that the suppression of the direct $HCOO^-$ pathways is not very significant despite the high $\theta_{b\text{-}f}$ due to the positive shift of $E_p$. The simulation gives an answer to a question why Pd on which bridge-bonded adsorbed formate does not exist has a higher catalytic activity than Pt for HCOOH oxidation in acidic media [56]. Nevertheless, it should be noted that bridge-bonded adsorbed formate enhances $HCOO^-$ oxidation.

## 4.5 Effect of pH dependence on electrocatalytic proton-coupled electron transfer reactions: General consideration

Using the kinetic model presented in this manuscript, peak current $j_p$ and peak potential $E_p$ are calculated for a generic decoupled proton-electron transfer reaction:

$$AH \leftrightarrows A^- + H^+ \tag{4.13}$$

$$A^- \rightarrow B + e^- \tag{4.14}$$

$$Pt + H_2O \leftrightarrows Pt\text{–}OH + H^+ + e^- \tag{4.15}$$

Molecule AH is in an acid-base equilibrium with base $A^-$. $A^-$ is assumed to be adsorbed on the electrode surface only weakly and oxidized very quickly, so that its coverage is neglected. Oxidation of the electrode surface is modeled by the adsorption of OH species, the precursor of surface oxidation. This species is enough to represent the inhibition of weakly adsorbed species. The Buttler-Volmer rate law and the Nernst equation are used to represent the rate of oxidation reaction (4.14) and OH adsorption (4.15), respectively. For given pH, current density $j$ is given as

$$j = 2Fk_2(1-\theta_{OH})[A^-] \tag{4.16}$$

where

$$k_2 = k_2^{\mathrm{eq}} \exp\left\{\frac{\alpha F\left(E - E_2^{\mathrm{eq}}\right)}{RT}\right\} \tag{4.17}$$

$$[\mathrm{A}^-] = \frac{[\mathrm{AH} + \mathrm{A}^-]}{1 + 10^{\mathrm{pK_a} - \mathrm{pH}}} \tag{4.18}$$

$$\theta_{\mathrm{OH}} = 1/\left(1 + K_3\right) \tag{4.19}$$

$$K_3 = \frac{k_{-3}}{k_3}[\mathrm{H}^+] = K_3^{\mathrm{eq}}[\mathrm{H}^+]\exp\left\{\frac{-F(E - E_3^{\mathrm{eq}})}{RT}\right\} \tag{4.20}$$

From Eqs. (4.17), (4.19), and (4.20), we have

$$j = 2F\left[\mathrm{A}^-\right]k_2^{\mathrm{eq}} \exp\left\{\frac{\alpha F}{RT}\left(E - E_2^{\mathrm{eq}}\right)\right\}\frac{\exp\left\{\frac{-F}{RT}(E - E_3^{\mathrm{eq}})\right\}}{1 + \exp\left\{\frac{-F}{RT}(E - E_3^{\mathrm{eq}})\right\}} \tag{4.21}$$

By differentiating $j$ with $E$ and setting it to zero

$$\frac{\mathrm{d}\,j}{\mathrm{d}\,E} = 2F\left[\mathrm{A}^-\right]k_2^{\mathrm{eq}}\frac{\frac{\alpha F}{RT}\exp\left\{\frac{-\alpha F}{RT}(E - E_2^{\mathrm{eq}})\right\}\exp\left\{\frac{-F}{RT}(E - E_3^{\mathrm{eq}})\right\}}{\left[1 + \exp\left\{\frac{-F}{RT}(E - E_3^{\mathrm{eq}})\right\}\right]^2} \times \left[K_3^{\mathrm{eq}}[\mathrm{H}^+]\exp\left\{\frac{-F}{RT}(E - E_3^{\mathrm{eq}})\right\} - 1\right] = 0 \tag{4.22}$$

the potential at which the oxidation current is maximal, peak potential $E_\mathrm{p}$, is obtained as

$$E_p = E_3^{\mathrm{eq}} + \frac{RT}{F}\left[\ln\left(K_3^{\mathrm{eq}}\left[H^+\right]\right)\right] \tag{4.23}$$

Note that $\theta_{\mathrm{OH}}$ is 0.5 at $E_\mathrm{p}$.

Current at $E = E_\mathrm{p}$, $j_\mathrm{p}$, is given as

$$j_p = Fk_2^{\mathrm{eq}} \frac{[\mathrm{AH}+\mathrm{A}^-]}{1+10^{\mathrm{pK_a}-\mathrm{pH}}} \exp\left\{\frac{\alpha F}{RT}\left(E_3^{\mathrm{eq}}-E_2^{\mathrm{eq}}\right)\right\} \exp\left[\alpha \ln\left(K_3^{\mathrm{eq}}\left[H^+\right]\right)\right]$$
$$= F[\mathrm{AH}+\mathrm{A}^-]k_2^{\mathrm{eq}} \exp\left\{\frac{\alpha F}{RT}\left(E_3^{\mathrm{eq}}-E_2^{\mathrm{eq}}\right)\right\} \frac{\exp\left[\alpha \ln\left(K_3^{\mathrm{eq}}10^{-\mathrm{pH}}\right)\right]}{1+10^{\mathrm{pK_a}-\mathrm{pH}}} \quad (4.24)$$

where $\exp\left[\alpha \ln\left(K_3^{\mathrm{eq}}10^{-\mathrm{pH}}\right)\right]$ and $1/\left(1+10^{\mathrm{pK_a}-\mathrm{pH}}\right)$ represent the pH dependence of the reaction rate and $HCOO^-$ concentration, respectively. From the derivative of $j_p$ with pH

$$\frac{\mathrm{d}\, j_p}{\mathrm{d\,pH}} = F[\mathrm{AH}+\mathrm{A}^-]k_2^{\mathrm{eq}} \exp\left\{\frac{\alpha F}{RT}\left(E_3^{\mathrm{eq}}-E_2^{\mathrm{eq}}\right)\right\} \frac{\ln 10 \cdot \exp(\alpha K_3^{\mathrm{eq}}10^{-\mathrm{pH}})\left[(1-\alpha)10^{\mathrm{pK_a}-\mathrm{pH}}-\alpha\right]}{\left(1+10^{\mathrm{pK_a}-\mathrm{pH}}\right)^2} \quad (4.25)$$

the optimal pH is given as pH = p$K_a$, if transfer coefficient $\alpha$ is 0.5. The conclusion is identical to the theoretical argument by Koper [31, 32]. When some other species is strongly adsorbed on the electrode surface such as bridge-bonded formate in HCOOH oxidation or $\alpha$ is not 0.5, the optimal pH is slightly shifted, but p$K_a$ is a good measure for predicting optimal pH.

Very recently, Koper [31] represents general theoretical analysis for multiple proton-electron transfer reactions, based on the microscopic theory of proton-coupled electron transfer reactions, recent developments in the thermodynamic theory of multi-step electron transfer reactions, and the experimental realization that many multiple proton-coupled electron transfer reactions feature decoupled proton-electron steps (equation 4.26) [30-32]. :

$$A + nH^+ + ne^- \leftrightarrows B \quad (4.26)$$

or equivalently : $A + nH_2O + ne^- \leftrightarrows B + nOH^-$ "alkaline media"

In case of single proton-coupled electron transfer, the *redox* reaction of interest is written as:

$$A + H^+ + e^- \leftrightarrows AH \quad (4.27)$$

According to equation 4.27, a typical potential energy surface spanned by the collective solvent coordinate coupled to electron transfer (ET) and the collective solvent coordinate coupled to proton transfer (PT) is described by Figure 4.14 [31].

If we consider the formic acid oxidation reaction, it will be written in two-proton two-electron transfer reaction (See equation 4.28).

$$A + 2H^{+} + 2e^{-} \leftrightarrows AH_2 \tag{4.28}$$

Analogous to single proton-coupled electron transfer, three alternative pathways to the fully concerted pathway, two of which bypass the formation of the AH intermediate are illustrated in Figure 4.15.

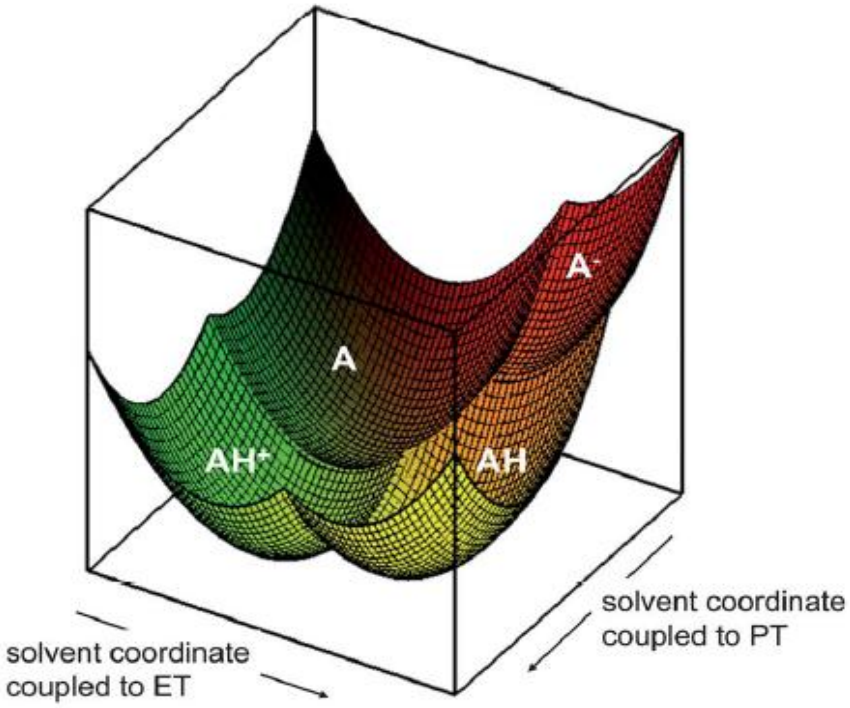


***Figure 4.14.*** Typical two-dimensional potential energy surface for reaction. ET and PT correspond to electron transfer and proton transfer, respectively. Adopted from [31].

One pathway goes through the $AH^+$ and the $AH_2^+$ intermediates, which may be termed the "protonation pathway (when considered as a reduction reaction, indicated by the red arrows); the other pathway goes through the $A^-$ and the $AH^-$ intermediates, which may be termed the "electronation" pathway (when considered as a reduction, indicated by the blue arrows). The third pathway forms the AH intermediate in a sequential PCET reaction rather than a CPET reaction (indicated by the green arrows shortcutting from the red and blue pathways to the black pathway) [31].

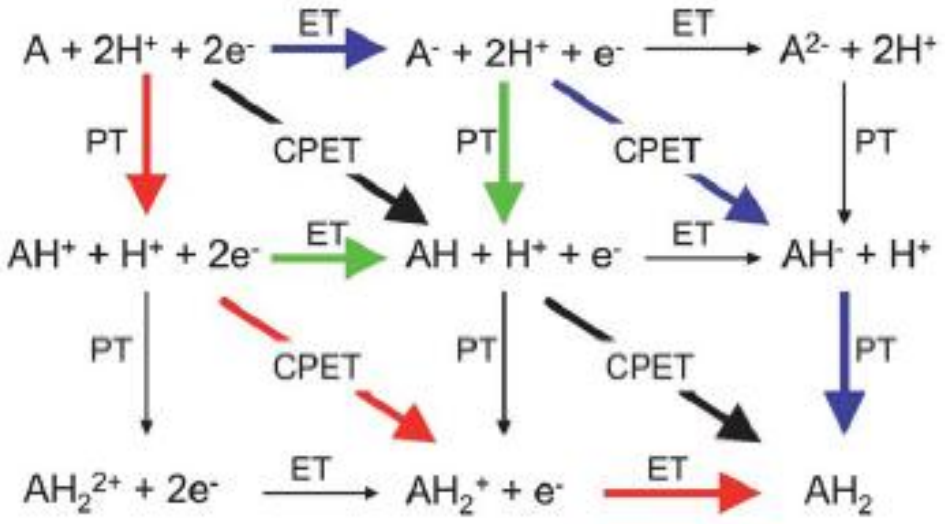


***Figure 4.15.*** Square scheme for a two-proton two-electron transfer reaction, equation (4.28). Blak pathway is the fully concerted pathway. Red pathway is the "protonation" pathaway. Blue pathway is the "electronation" pathway. In a pathway following one of the green lines, the first PCET is sequential, the second PCET is concerted. Adopted from [32].

The protonation pathway consists of the following three reaction steps: (4.29-4.31)

$$A + H^+ \leftrightarrows AH^+ \tag{4.29}$$

$$AH^+ + H^+ + e^- \leftrightarrows AH_2^+ \tag{4.30}$$

$$AH_2^+ + e^- \leftrightarrows AH_2 \quad (4.31)$$

Since equation 4.29 step in this sequence does not involve electron transfer, we will not write the equilibrium potentials but instead the Gibbs free energies for the reactions [31]:

$$\Delta G_{A/AH+} = G(AH^+) - G(A) - G(H^+) = PA(A) - G(H^+) \quad (4.32)$$

$$= -2.303\ RT \times\ [pK_a(A) - pH]$$

Equation 4.32 obviously illustrates that only if pKa=pH, an optimal catalyst with zero theromodynamic overpotential can be found [31]. An extremely useful principle from heterogenous catalysis, the so-called *Sabatier principle*, state that *the best catalyst binds the key intermediates(s) neither too weakly nor too strongly.* Theoretically, such a catalyst has zero overpotential, and would therefore be optimal. It means equation 4.32 is thermodynamically most favorable reaction. The analysis clearly predicts that the best catalyst operates with a pH close to the pKa of the intermediate [31].

To demonstate that the above conclusion is not an artifact of the thermodynamic analysis, a kinetic treatment of the model equation (4.29-4.31) is established, which yields the same result.

We write the following rate equations for the separate steps:

$$v_1 = k_1(C^o{}_A - C_{AH^+})C_{H^+} - k_{-1}C_{AH+} \quad (4.33)$$

$$v_2 = k_2 C_{AH^+} C_{H^+} \exp\left(\frac{-\alpha_2 F(E - E_2^{\,o})}{RT}\right) - k_{-2} C_{AH_2^+} \exp\left(\frac{(1-\alpha_2) F(E - E_2^{\,o})}{RT}\right) \tag{4.34}$$

$$v_3 = k_3 C_{AH_2^+} \exp\left(\frac{-\alpha_3 F(E - E_3^{\,o})}{RT}\right) - k_{-3} C_{AH_2} \exp\left(\frac{(1-\alpha_3) F(E - E_2^{\,o})}{RT}\right) \tag{4.35}$$

At the equilibrium potential, the rate of generation of $AH_2$ from reaction (4.31) is gained by calculating the equilibrium concentration of $AH_2^+$ from equation (4.34) and the equilibrium concentration of $AH^+$ from equation (4.33). Remembering that it is the measurable rate if reaction 5.31 is the rate-determining step. If we set the activity of $AH_2$ equal to 1, $C_A$ is the $C_A^o$ for simplicity, and define corresponding equilibrium constant equation 4.29 and 4.30, equation 4.36 can be obtained [31]:

$$\vec{v}_3 = k_3 \frac{(C^o{}_A)^{\frac{1}{2}-\frac{\alpha_3}{2}} C_{H^+}{}^{1-\alpha 3}}{C_{H^+} + K_1^{-1}} K_2 \exp\left(\frac{-F\left[(1+\alpha_3) E^o{}_{A,\frac{2H^+}{AH_2}} - E^o{}_2 - \alpha_3 E^o{}_3\right]}{RT}\right) \tag{4.36}$$

The E$^o$'' and *K*'s in this equation are all constants, independent of pH. Figure 4.16 explains this rate as a function of pH, with all constants equal to unity and $\alpha_3 = 0.5$ and confirms that this plot is a volcano with a maximum at $pH = \exp\left[-2.303 \big/ K_1\right] = pKa$ [31].

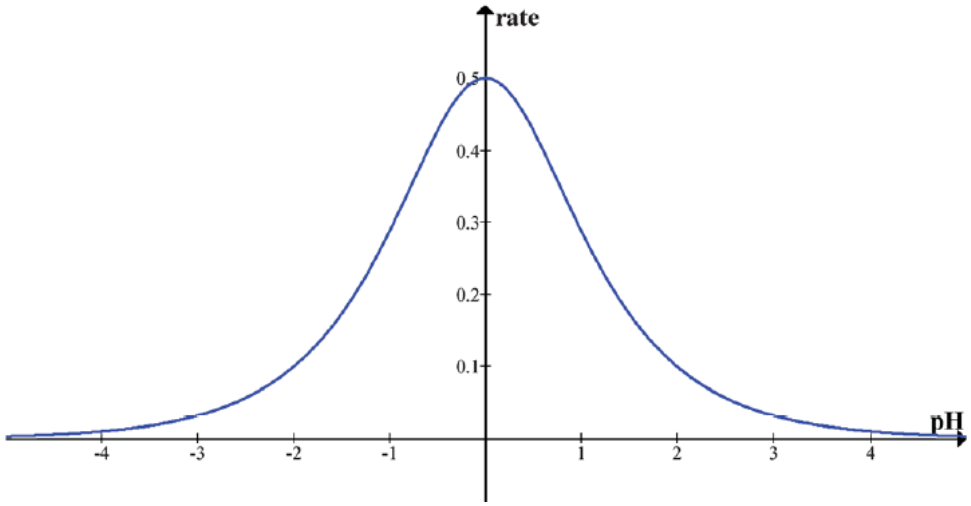


***Figure 4.16.*** A plot of equation 4.36 for all constant equal unity and $\alpha_3 = 0.5$. Adopted from [31].

Theory of multiple proton-coupled electron transfer reactions certainly describes that the electrochemical oxidation of alcohols on metal electrodes is very sensitive to pH, and is much more active toward alkaline solution. From a comparison of a series of similar poly-ols on a gold electrode, it is confirmed that the onset potential for oxidation scaled linearly with the pKa of the corresponding alcohol [33]. Alcohols have a high pKa. That is reason why alkaline media are preferred. Eelectrooxidation of methanol and formaldehyde will be discussed in chapter 5 later.

## 4.6 Interpretation of multiple oxidation peaks in cyclic voltammograms

As shown in Figure 4.3, HCOOH oxidation in acidic media exhibits two anodic peaks in the positive-going scan (peak p1 and peak p2), while a single oxidation peak is observed with shoulders at both positive and negative side in the negative-going scan (a single peak

with a shoulder at the low potential side is observed at higher HCOOH concentrations) [3, 9, 11, 41, 57]. The interpretation of the complex voltammetric features has been the subject of discussion, because the origins of the two anodic peaks in the positive-going scan are the key issues for understanding electrochemical oscillations observed during HCOOH oxidation [57-60].

The two oxidation peaks in the positive-going scan are often interpreted in terms of two different reactions at different potentials [3, 61]. However, such an explanation will not be reasonable because HCOOH oxidation after being converted to $HCOO^-$ is the major reaction route in acidic media and the contribution of CO pathway to the total current is negligible [9, 15, 16]. Breiter [62] postulated that the first anodic peak is due to oxidation of HCOOH to $CO_2$ on the small fraction of the surface which was not blocked by adsorbed intermediates. Oxidation of these intermediates at more positive potentials uncovers a large number of active sites on which further oxidation of HCOOH can take place, thus causing the rise in current leading to the second anodic peak. A similar explanation was made also by Strasser et al.[57]. On the other hand, Okamoto and Tanaka [63] proposed that $H_2O$ adsorbed at free sites suppresses $CO_{ads}$ oxidation to yield the negative differential resistance at the positive side of peak p1 and the replacement of adsorbed $H_2O$ by $OH_{ads}$ facilitates $CO_{ads}$ oxidation at higher potentials leading to the second peak. The role of $CO_{ads}$ is well supported by SEIRAS (Figure. 4.3). However, these earlier explanations are insufficient because the adsorption of bridge-bonded formate on the electrode surface was not included (which was not known before the SEIRAS study by Miki et al. in 2002 [6]). Samjeské et al. [9, 10] explained the NDR and the second anodic peak by assuming that bridge-bonded adsorbed formate is decomposed to $CO_2$ and that its reaction rate is a strong function of the coverage of free sites. However, this explanation conflicts with the conclusion in the present study that the decomposition of bridge-bonded adsorbed formate is very slow and HCOOH oxidation *via* $HCOO^-$ is the major reaction pathway.

Here we will provide a new interpretation on the basis on the following experimental results: (i) when neither $CO_{ads}$ nor bridge-bonded adsorbed formate exist on the surface (or when $\theta_{CO}$ is small), $HCOO^-$ oxidation yields a single anodic peak appears at a same low potential in both the positive- and negative-going scan (Figure 4.6), (ii) in the presence of $CO_{ads}$, the anodic peak in the positive-going scan is shifted positively to a potential at which $CO_{ads}$ is oxidized (Figure 4.4), and (iii) the second anodic peak appears only when bridge-bonded formate is coadsorbed with CO (Figure 4.3). In the last case, $CO_{ads}$ is not essential because a similar CV is observed also on Au, where bridge-bonded formate is adsorbed but $CO_{ads}$ is absent [53]. The results clearly indicate that bridge-bonded adsorbed formate is responsible for the second peak. Since bridge-bonded adsorbed formate enables $HCOO^-$ oxidation at high potentials by suppressing the oxidation of the electrode surface as mentioned before, the second peak appears in the surface oxidation region.

The multiple anodic peaks in the negative-going scan also can be ascribed to bridge-bonded adsorbed formate as has been suggested before. Since bridge-bonded adsorbed formate is likely to form islands, $HCOO^-$ oxidation in the island occurs at higher potential than in the regions free of bridge-bonded adsorbed formate to yield multiple anodic peaks in the voltammogram.

## 4.7 Conclusion and remarks

The examination of the pH dependence of HCOOH/$HCOO^-$ oxidation on a Pt electrode over the wide range of pH (0-12) revealed that oxidation current for the same HCOOH/$HCOO^-$ total concentration shows a volcano-shaped pH dependence peaked at pH 4-5, which is close to the pKa of HCOOH (pKa = 3.75). A simple mathematical modeling of the reaction revealed that the main reaction route is the oxidation of $HCOO^-$ over the whole

pH range and that HCOOH is oxidized after being converted to $HCOO^-$ *via* the acid-base equilibrium ($HCOOH \leftrightarrows HCOO^- + H^+$). The ascending part at pH < $pK_a$ is ascribed mainly to the increase of the molar ratio of $HCOO^-$, while the descending part at pH > $pK_a$ is ascribed to the suppression of $HCOO^-$ oxidation by adsorbed OH and/or surface oxidation. The SEIRAS revealed that HCOOH is adsorbed on Pt as bridge-bonded adsorbed formate at pH < ~5. The bridge-bonded adsorbed formate blocks active sites for $HCOO^-$ oxidation but enhances $HCOO^-$ oxidation at high potentials by preventing the adsorption of OH and oxidation of the electrode surface. $CO_{ads}$ is formed by the reduction of bridge-bonded adsorbed formate at pH < ~ 5 and presumably by a reaction of transiently adsorbed $HCOO^-$ and $H_{ads}$ at pH > ~5. The mechanistic model presented in this work also well explains the complex CVs of HCOOH oxidation in acidic media.

In earlier studies, the reaction mechanism of HCOOH oxidation (bridge-bonded formate and direct HCOOH pathways) has been discussed on the basis of the relation between oxidation current ($j$) and the coverage of bridge-bonded adsorbed formate ($\theta_{b\text{-}f}$) [10, 14, 16, 18, 53]. Note that it is assumed an *a priori* in the arguments that the reactant is only HCOOH. However, as has been shown here, the major reactant is $HCOO^-$ even in acidic media. The main reaction route is the direct $HCOO^-$ pathway that was not considered in previous studies. Since the relationship between $\theta_{b\text{-}f}$ and $HCOO^-$ oxidation is complex as has been discussed above and the weak adsorption of $HCOO^-$ will be greatly affected by the co-adsorption of supporting anions, such an approach to identify the reaction mechanism will not be fruitful, and could even be misleading. The situation is the same in previous theoretical studies, where no attention was paid to direct $HCOO^-$ oxidation [19-21].

The most important finding in the present study is that the best performance can be achieved at pH ≈ $pK_a$. This is a general property in catalytic proton-coupled electron transfer reactions. In this point of view, it can be inferred that most DFAFCs using cation- and anion-exchange membranes are not operated under the optimal conditions. If pH in the membranes

could be less than −6, however, higher performance is expected from the mathematical simulation shown in the present work. The results reported in this dissertation forces the revision of interpretations made in earlier experimental and theoretical studies. The scheme of the new pathway for electrooxidation of formic acid is shown in Figure 4.17.

....

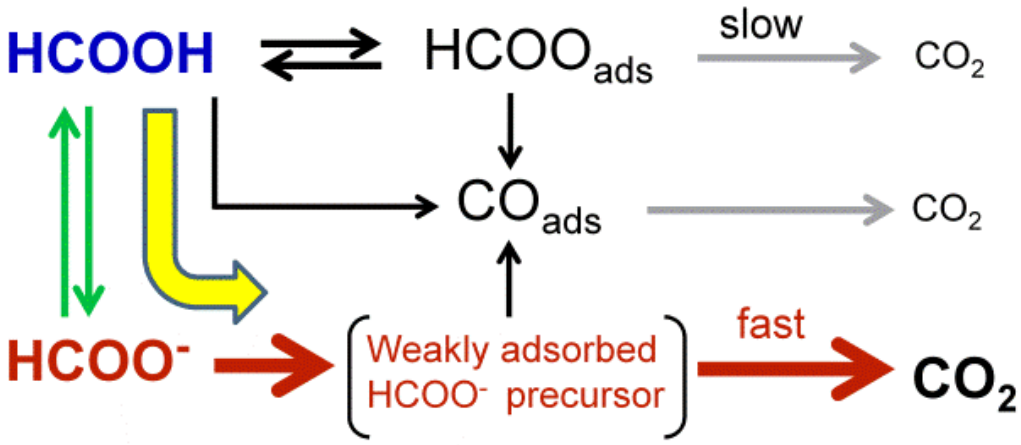


***Figure 4.17.*** The schematic of the new pathway for electrooxidation of formic acid.

# References

[1] A. Capon, R. Parsons, J. Electroanal. Chem., 44 (1973) 1-7.
[2] A. Capon, R. Parsons, J. Electroanal. Chem., 45 (1973) 205-231.
[3] A. Capon, R. Parsons, J. Electroanal. Chem., 44 (1973) 239-254.
[4] K. Kunimatsu, J. Electroanal. Chem., 213 (1986) 149-157.
[5] K. Kunimatsu, H. Kita, J. Electroanal. Chem., 218 (1987) 155-172.
[6] A. Miki, S. Ye, M. Osawa, Chem. commun., (2002) 1500-1501.
[7] M. Osawa, Bull. Chem Soc. Jpn., 70 (1997) 2861-2880.
[8] M. Osawa, Surface-Enhanced Infrared Absorption Spectroscopy, in: Handbook of Vibrational Spectroscopy, John Wiley & Sons, Ltd, (2006).
[9] G. Samjeske, A. Miki, S. Ye, A. Yamakata, Y. Mukouyama, H. Okamoto, M. Osawa, J. Phys. Chem. B, 109 (2005) 23509-23516.
[10] G. Samjeske, M. Osawa, Angew. Chem. Int. Ed., 44 (2005) 5694-5698.
[11] G. Samjeske, A. Miki, S. Ye, M. Osawa, J. Phys. Chem. B, 110 (2006) 16559-16566.
[12] M. Osawa, K. Komatsu, G. Samjeske, T. Uchida, T. Ikeshoji, A. Cuesta, C. Gutierrez, Angew. Chem. Int. Ed., 50 (2011) 1159-1163.
[13] A. Cuesta, G. Cabello, C. Gutierrez, M. Osawa, Phys. Chem. Chem. Phys., 13 (2011) 20091-20095.
[14] A. Cuesta, G. Cabello, M. Osawa, C. Gutierrez, ACS Catal., 2 (2012) 728-738.
[15] Y.X. Chen, M. Heinen, Z. Jusys, R.J. Behm, Langmuir 22 (2006) 10399-10408.
[16] Y.X. Chen, M. Heinen, Z. Jusys, R.J. Behm, Angew. Chem. Int. Ed., 45 (2006) 981-985.
[17] Y.X. Chen, M. Heinen, Z. Jusys, R.J. Behm, ChemPhysChem, 8 (2007) 380-385.
[18] V. Grozovski, F.J. Vidal-Iglesias, E. Herrero, J.M. Feliu, ChemPhyschem, 12 (2011) 1641-1644.
[19] M. Neurock, M. Janik, A. Wieckowski, Faraday Discuss., 140 (2008) 363-378.
[20] H.F. Wang, Z.P. Liu, J. Phys. Chem. C, 113 (2009) 17502-17508.
[21] W. Gao, J.A. Keith, J. Anton, T. Jacob, J. Am. Chem. Soc., 132 (2010) 18377-18385.
[22] R.P. Buck, L.R. Griffith, J. Electrochem. Soc., 109 (1962) 1005-1013.
[23] V.S. Bagotzky, Y.B. Vasilieyev, Electrochim. Acta, 9 (1964) 869-882.
[24] B. Beden, C. Lamy, J.M. Leger, J. Electroanal. Chem, 101 (1979) 127-131.
[25] H. Kita, T. Katagiri, K. Kunimatsu, J. Electroanal. Chem., 220 (1987) 125-138.
[26] J.L. Haan, R.I. Masel, Electrochim. Acta, 54 (2009) 4073-4078.
[27] J. John, H.S. Wang, E.D. Rus, H.D. Abruna, J. Phys. Chem. C, 116 (2012) 5810-5820.

[28] P.A. Christensen, A. Hamnett, D. Linares-Moya, Phys. Chem. Chem. Phys, 13 (2011) 11739-11747.
[29] M. Osawa, In-situ surface-enhanced infrared spectrscopy of the electrode/solution interface, in: R.C. Alkire, D.M. Kolb, J. Lipkowski, P.H. Ross (Eds.) Diffraction and Spectroscopic Methods in Electrochemistry (Advances in Electrochemical Science and Enginnering, Vol. 9), Wiley-VCH, Weinheim, (2006), pp. 269-314 (Chapter 8).
[30] M.T.M. Koper, J. Electroanal. Chem., 660 (2011) 254-260.
[31] M.T.M. Koper, Chem. Sci., (2013).
[32] M.T.M. Koper, Phys. Chem. Chem. Phys., 15 (2013) 1399-1407.
[33] Y. Kwon, S.C.S. Lai, P. Rodriguez, M.T.M. Koper, J. Am. Chem. Soc., 133 (2011) 6914-6917.
[34] M. Osawa, K. Ataka, K. Yoshii, T. Yotsuyanagi, J. Electron Spectrosc. Relat. Phenom., 64-65 (1993) 371-379.
[35] K. Ataka, T. Yotsuyanagi, M. Osawa, J. Phys. Chem., 100 (1996) 10664-10672.
[36] R.R. Adzic, M.I. Hofman, D.M. Drazic, J. Electroanal. Chem., 110 (1980) 361-368.
[37] W.M. Haynes, CRC Handbook of Chemistry and Physics. 92nd Edition, CRC Press: Cleveland, 2011-2012.
[38] M. Osawa, M. Tsushima, H. Mogami, G. Samjeske, A. Yamakata, J. Phys. Chem. C, 112 (2008) 4248-4256.
[39] M. Osawa, K. Ataka, K. Yoshii, Y. Nishikawa, Appl. Spectrosc., 47 (1993) 1497.
[40] R. Gisbert, G. Garcia, M.T.M. Koper, Electrochim. Acta, 55 (2010) 7961-7968.
[41] H. Okamoto, W. Kon, Y. Mukouyama, J. Phys. Chem. B, 109 (2005) 15659-15666.
[42] G.-Q. Lu, A. Crown, A. Wieckowski, J. Chem. Phys. B, 103 (1999) 9700-9711.
[43] G. Samjeske, K. Komatsu, M. Osawa, J. Phys. Chem. C, 113 (2009) 10222-10228.
[44] T. Iwasita, A. Rodes, E. Pastor, J. Electroanal. Chem., 383 (1995) 181-189.
[45] A. Berna, A. Rodes, J.M. Feliu, F. Illas, A. Gil, A. Clotet, J.M. Ricart, J. Phys. Chem. B, 108 (2004) 17928-17939.
[46] N.M. Markovic, H.A. Gasteiger, N. Philip, J. Phys. Chem., 100 (1996) 6715-6721.
[47] V. Grozovski, V. Climent, E. Herrero, J.M. Feliu, ChemPhysChem, 10 (2009) 1922-1926.
[48] J. Jiang, J. Scott, A. Wieckowski, Electrochim. Acta, 104 (2013) 124-133.
[49] J. Joo, T. Uchida, A. Cuesta, M.T. Koper, M. Osawa, J. Am. Chem. Soc., (2013).
[50] Y.Y. Gao, C.H. Tan, Y.P. Li, J. Guo, S.Y. Zhang, Int. J. Hydrogen Energy, 37 (2012) 3433-3437.
[51] A. Bandara, J. Kubota, K. Onda, A. Wada, S.S. Kano, K. Domen, C. Hirose, J. Phys. Chem. B, 102 (1998) 5951-5954.
[52] H. Angerstein-Kozlowska, B.E. Conway, W.B.A. Sharp, J. Electroanal. Chem., 43 (1973) 9-36.

[53] A. Cuesta, G. Cabello, F.W. Hartl, M. Escudero-Escribano, C. Vaz-Domínguez, L.A. Kibler, M. Osawa, C. Gutiérrez, Catal. Today, 202 (2013) 79-86.
[54] R.G. Sharpe, M. Bowker, J. Phys.: Condens. Matter, 7 (1995) 6379-6392.
[55] J. Wojtowic, N. Marincic, B.E. Conway, J. Chem. Phys., 48 (1968) 4333-4345.
[56] H. Miyake, T. Okada, G. Samjeske, M. Osawa, Phys. Chem. Chem. Phys, 10 (2008) 3662-3669.
[57] P. Strasser, M. Lubke, F. Raspel, M. Eiswirth, G. Ertl, J. Chem. Phys., 107 (1997) 979-990.
[58] P. Strasser, M. Eiswirth, G. Ertl, J. Chem. Phys., 107 (1997) 991-1003.
[59] M.T.M. Koper, Oscillations and Complex Dynamical Bifurcations in Electrochemical Systems, in: Advances in Chemical Physics, John Wiley & Sons, Inc., 2007, pp. 161-298.
[60] H. Okamoto, Electrochim. Acta, 37 (1992) 37-42.
[61] W. Gao, J.E. Mueller, Q. Jiang, T. Jacob, Angew. Chem. Int. Ed., 51 (2012) 9448-9452.
[62] M.W.Breiter, Electrochemical processes in fuel cells, Springer-Verlag, New York, (1969).
[63] H. Okamoto, N. Tanaka, Electrochim. Acta, 38 (1993) 503-509.

# Chapter 5. Electrooxidation of methanol on Pt

## 5.1 Introduction

Direct methanol fuel cells (DMFCs) that use methanol as fuel is anticipated to be as power sources for electric devices, such as cellular phone, laptop computer, scooter, etc [1-4] due to the higher volumetric energy density (5 kWh/L) of methanol, which is larger than that of formic acid (2 kWh/L). Furthermore, liquid at room temperature can be easily stored and transported by using the present fuel infrastructure with only slight modifications. Owing to this technological importance, the electrooxiadtion of methanol has been studied extensively as reviewed by Cohen et al. [5]

It is widely believed that methanol is oxidized to $CO_2$ in acidic media successively through formaldehyde and formic acid suggested by Bagotzky et al. [6] (Figure 5.1).

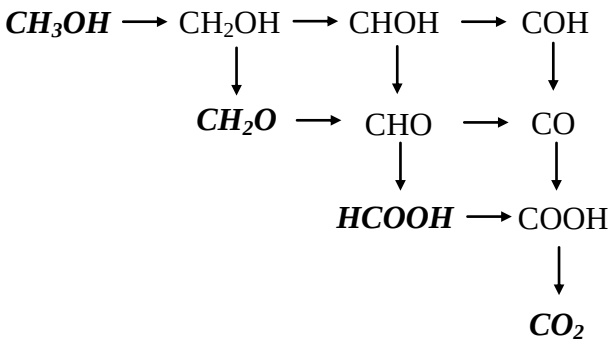


***Figure 5.1.*** The Bagotzky model for electrooxidation of methanol in acidic media. Adopted from [6].

However, several other factors make our full understanding difficult. One is that methanol is oxidized via dual-pathway mechanism as in formic acid case; direct pathway via adsorbed active intermediate and indirect pathway via adsorbed CO. Homogeneous reaction of

methanol with formic acid and formaldehyde yielding methyl formate ($HCOOCH_3$) and dimethoxymethane ($H_2C(OCH_3)_2$), respectively, [7] also makes the situation more complex.

$$HCOOH + CH_3OH \leftrightarrows HCOOCH_3 + H_2O \quad (6.1)$$

$$H_2CO + 2CH_3OH \leftrightarrows CH_2(OCH_3)_2 + H_2O \quad (6.2)$$

Abd et al. [8] recently found that methylformate originates also from the direct oxidation reaction of methanol at the surface and the reaction (5.1) in solution is too slow as to affect the kinetic of methanol oxidation. Hydration of formaldehyde, a possible reaction intermediate, to methylene glycol ($CH_2(OH)_2$) (Keq = 2280) [Guthrie, J. P. *Can. J. Chem.* **1975**, *53*, 898]

$$H_2CO + H_2O \rightarrow CH_2(OH)_2$$

may also affect the methanol oxidation.

So far, much mechanistic insights have been obtained by studies on poly- and single-crystal electrodes [9, 10] by applying various *in situ* spectroscopic techniques such as *in situ* infrared spectroscopy (IR) [11], product analysis by on-line differential electrochemical mass spectrometry (DEMS) [9], high performance liquid chromatography (HPLC) [12], and NMR [13]. An important finding was made by Chen et al. [14], who reported for the first time that bridge-bonded formate is adsorbed on Pt electrode during methanol oxidation and proposed that bridge-bonded adsorbed formate is an reactive intermediate in the non-CO pathway. However, there is no consensus on the real reaction mechanism yet. Furthermore, our understanding about the mechanism of CO poison formation on the catalyst is still poor.

In recent years, the study of methanol oxidation in alkaline media has been a growing interest since the advent of anion exchange membrane. Following to the criterion described in Chapter 5 that the performance of electrocatalytic oxidation is optimal at pH close to the pKa

of the molecule, the oxidation of mechanol (pKa = 15.5) is expected be faster in alkaline media than in acidic media. In fact, Sobkowski et al. [15] found that the rate of methanol oxidation on Pt is higher in alkaline media than in acidic media. Kwon et al. [16] also reported high oxidation activity of methanol on gold in alkaline media. However, the study in alkaline media [3, 17-19] is very limited compared to that in acid media [4, 14, 20, 21]. No systematic studies of pH dependence have been reported in the literature. Thus, the mechanistic study of electrooxidation of methanol at the molecular level in both acidic and alkaline media is highly required and will provide useful information for designing effective catalysts for alkaline DMFCs.

This chapter is devoted to reveal the mechanism by using SEIRAS combined with electrochemistry in a wide range of pH. The oxidation of formaldehyde, a possible partially oxidized molecule, was also examined for more understanding of methanol oxidation. Special attention is focused whether the Bagotzky model is applicable to alkaline media as well, although some molecules involved must be replaced by their negative ions (for example, formic acid/formate).

## 5.2 Experiments

### 5.2.1 Spectroelectrochemical measurements

The flow cell described in Chapter 2 was used in the experiments because accumulation of partially oxidized molecules (HCOH and HCOOH) and their reaction with methanol could make difficult the analysis and could mislead. [22] By continuously flushing the solution, such a problem is expected to be reduced.

The working electrode was prepared by chemical deposition of Pt on a Si prism (Chapter 2). The flow rate was controlled to roughly 30 μL/s. Since the cell volume was 200

μL, the solution in the cell was totally replaced within about 7s. The counter electrode inserted into flow cell was a Pt gauze and reference electrode used was an Ag/AgCl (saturated KCl) that was connected to the cell by a glass tube.

SEIRAS spectra were recorded on a Bio-Rad FTS-60A/896 FT-IR spectrometer equipped with an MCT detector and a homemade single-reflection accessory. The spectrometer was operated in the rapid-scan kinetic mode (40 kHz) with a spectral resolution of 4 $cm^{-1}$ and the time resolution is 1s. A reference spectrum of the clean electrode surface ($R_o$) was collected in advance in the supporting electrolyte without methanol or formaldehyde, and the sample spectra (R) were collected after exchanging the blank solution to the sample solution containing molecules at a desired concentration (20 mM - 0.2 M for methanol or 10-20 mM for formaldehyde). All spectra are shown in absorbance units defined as $A = -\log(R/R_o)$.

The electrolyte solution used was a 0.2 M phosphate buffer solution with pHs between 1.5 to 12. Methanol was analytical grade purchased by Sigma Aldrich. All solutions were prepared from water purified with a Milli-Q TOP system (TOC 3ppb) and deaerated with Ar prior to each experiment. Since commercially available formaldehyde contains methanol as a stabilizer, formaldehyde solution was prepared by dissolving paraformaldehyde (Merck) in the supporting electrolyte solution at 70$^oC$ [7].

## 5.3 Results and discussion

### 5.3.1 Cyclic voltammetry with a rotating Pt disc electrode (RDE)

Representative cyclic voltammograms (CVs) for 0.2 M methanol at various pHs are shown in Figure 5.2a. Consistent with the prediction that the oxidation rate becomes maximal at pH close to the pKa of the molecule (Chapter 4), the peak current ($i_p$) in the positive-going scan increases with increasing pH. The pH dependence of $i_p$ is shown in Figure 5.2b. Interestingly, however, the peak current in the negative-going scan is almost independent of pH. In acidic media, $i_p$s in the both scans are almost the same. Peak potential is found to shift negatively with increasing at a rate of about 60 mV per pH, and hence it is constant on the reversible hydrogen electrode (RHE) scale. It was also found that peak current slightly decreases as the rotating speed of the electrode is increased (data not shown). Since no such effect was found in formic acid/formate oxidation, the result for methanol oxidation suggests that some partially oxidized species is formed and its further oxidation was suppressed by its removal from the electrode surface under rotating conditions.

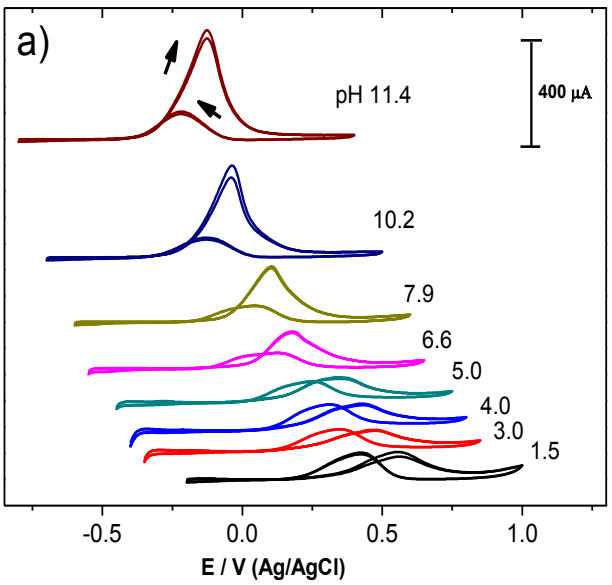

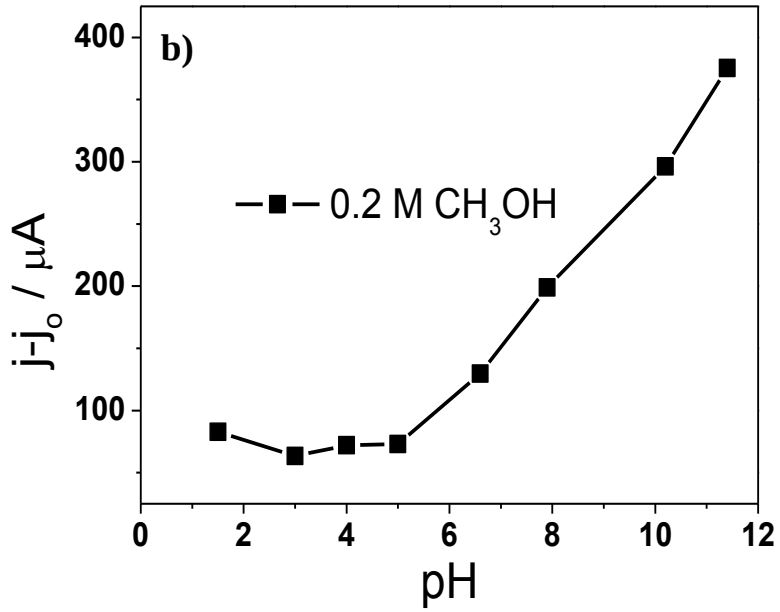


***Figure 5.2.*** (a) Cyclic voltammograms of a rotating Pt disk electrode (1000 rpm) in 0.2 M phosphate buffer solutions containing 0.2 M $CH_3OH$ recorded at 50 mV $s^{-1}$. The pH values of the solutions are shown in the figure. (b) Peak current in the positive-going scan.

Since formaldehyde is a candidate for the partially oxidized species formed during methanol oxidation, its oxidation was also examined for comparison. Representative CVs for 20 mM formaldehyde are shown in figure 5.3a. Oxidation current for formaldehyde also increases with increasing pH. A slight different from methanol oxidation is that oxidation peak currents in both the positive- and negative-going scans increases with increasing pH. Close inspection of the CVs reveals that the oxidation peak in the negative-going scan is a single in acidic solutions and splits into two in neutral and alkaline solutions. It is also worth noting that the peak current is much larger than observed for methanol oxidation despite much smaller concentration (20 mM for formaldehyde and 0.2 M for methanol), indicating formaldehyde is much more reactive than methanol. The pH dependence of the peak current in the negative-going scan is plotted in figure 5.3b.

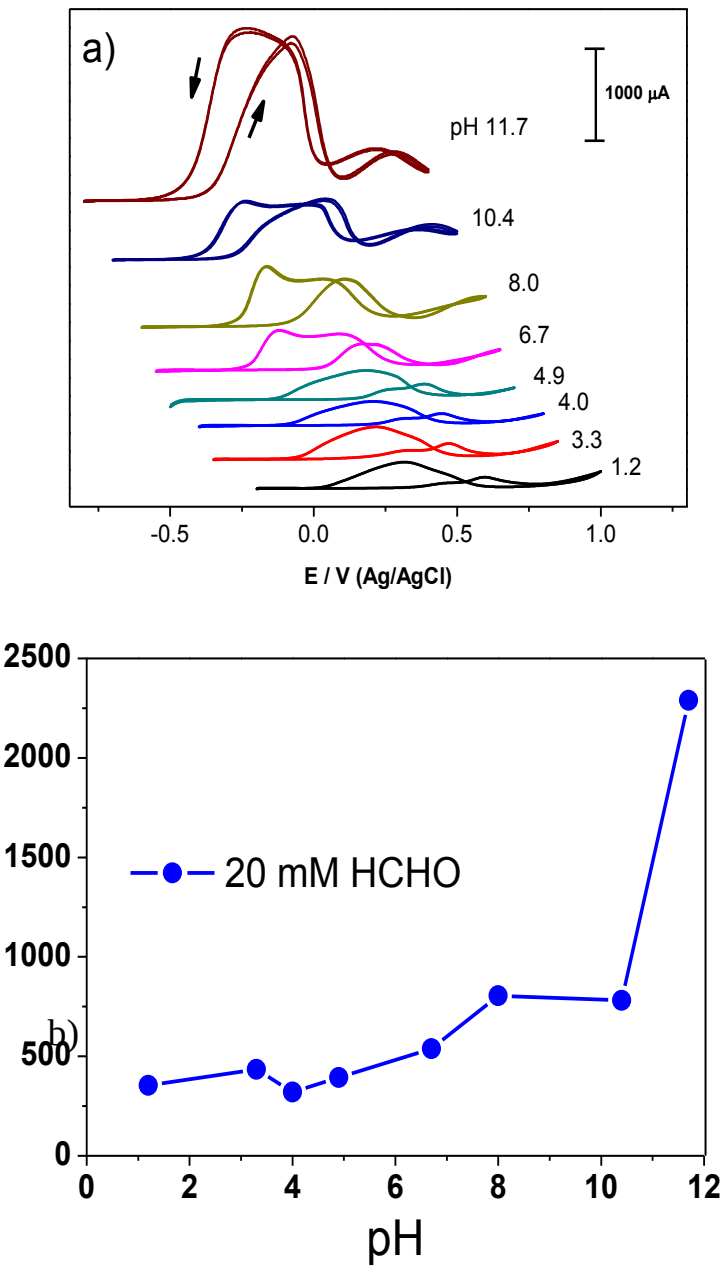


***Figure 5.3.*** (a) Cyclic voltammograms of a rotating Pt disk electrode (1000 rpm) in 0.2 M phosphate buffer solutions containing 20 mM HCHO recorded at 50 mV $s^{-1}$. The pH values of the solutions are shown in the figure. (b) The pH dependence of peak current in the negative-going scan.

### 5.3.2 Partially oxidized soluble byproducts

In order to investigate the intermediate species formed during methanol oxidation, on-line HPLC coupled with linear sweep voltammetry was used. The results obtained in buffer solutions at pH 3, 7 and 13 are shown in Figure 5.4 (bottom panels) together with the positive-going linear sweep voltammograms (LSVs) recorded simultaneous (upper panels). Formic acid and formaldehyde were detected by on-line HPLC. Note that, formate is detected as formic acid since 0.5 mM $H_2SO_4$ was used as the eluent. At pH 3 and pH 7, almost the same amount of formic acid (red dot) and formaldehyde (bleu square) are formed at the oxidation peak at ~ 0.8 V vs. RHE (which corresponds to 0.45 V at pH 3 and 0.2 V at pH 7 vs. Ag/AgCl). Formaldehyde appears to be produced slightly earlier than formic acid, which may imply that formaldehyde is produced first and further oxidized to formic acid as Bagotzky *et* al. [6] suggested, i.e., the oxidation proceeds in the order of methanol → formaldehyde → formic acid, although a possibility that formaldehyde and formic acid are formed independently cannot be ruled out completely. In marked contrast, formate is the major product at pH 13 (formic acid exist as formate in alkaline media) and the production of formaldehyde is very small, which is in good agreement with the result conducted in 0.5 M KOH solution [12]. Remembering that formaldehyde is very reactive and formate is hardly oxidized in alkaline media (Chapter 4), the high yield of formic acid may be due to the oxidation of formaldehyde to formic acid.

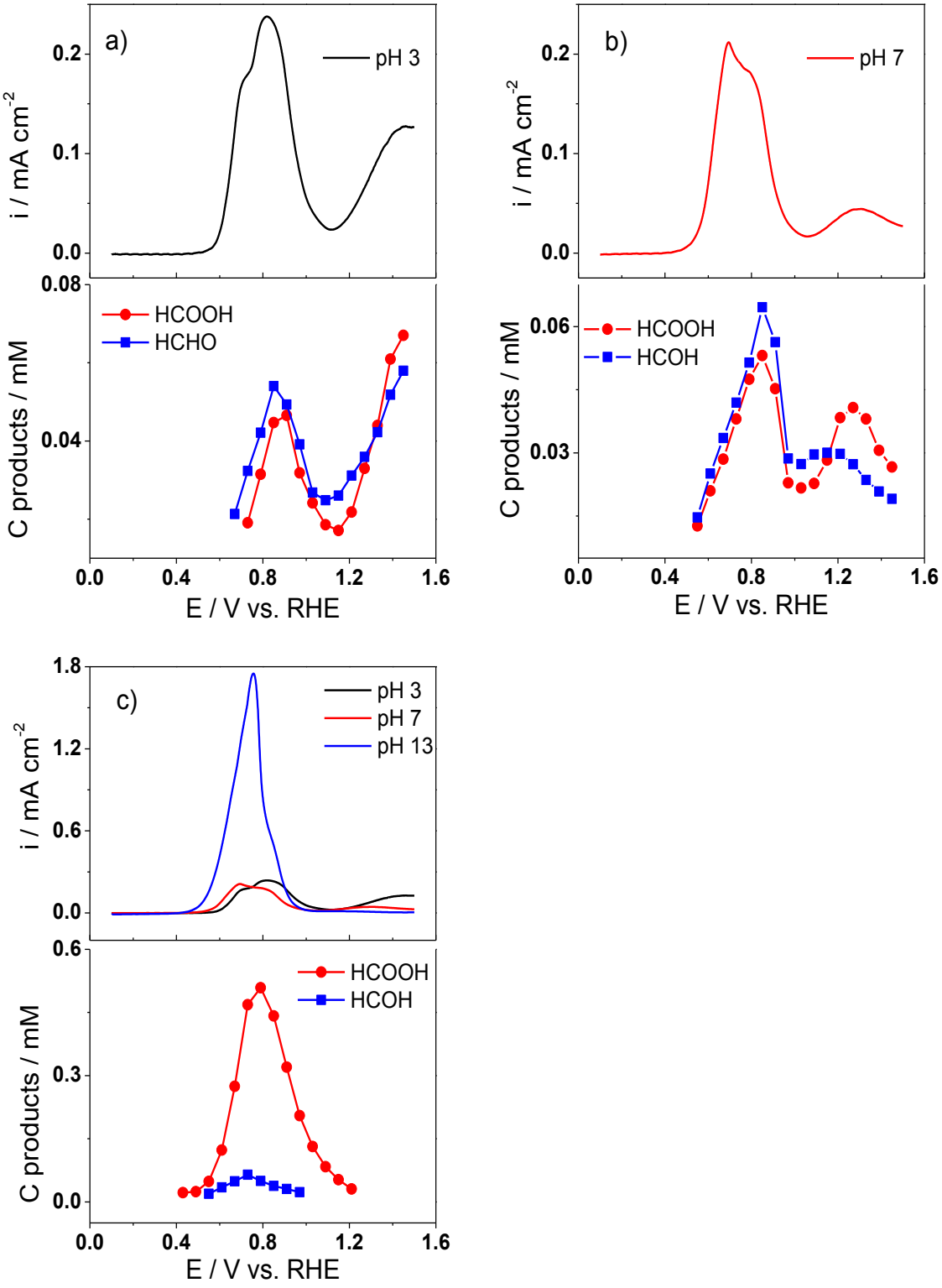


***Figure 5.4.*** Potential dependence of the concentrations of byproducts formed during 0.2 M methanol oxidation in 0.2 M phosphate buffer solution of (a) pH 3, (b) pH 7, and (c) pH 13 measured with on-line HPLC. Top panels are the LSVs simultaneously recorded with the HPLC analysis. Note that, since 0.5 mM $H_2SO_4$ was used as the eluent, the real product is formate in the neutral and

alkaline media.

### 5.3.3 SEIRAS study

Figure 5.5a shows the SEIRA spectra of a Pt thin film electrode in 0.2 M $H_3PO_4$ (pH 1.5) containing 0.2 M methanol recorded during a potential scan from -0.2 to 1.0 to and back to -0.2 V at 20 mV $s^{-1}$. The strong peak at 2050~2070 $cm^{-1}$ and the weak band at ~1850 $cm^{-1}$ are assigned to the C-O stretching modes of linear CO ($CO_L$) and bridge-bonded CO ($CO_B$), respectively. The negative peak at 1610 $cm^{-1}$ is the bending mode of water that was removed from the surface by the adsorption of CO. The band that emerges at 1323 $cm^{-1}$ at high potentials after disappearance of the CO bands is assigned to the symmetric O-C-O stretching mode of bridge bonded formate. The spectral changes are reversed on the reverse backward scan. This result is essentially identical to that report by Chen et al. [14]

In Figure 5.5b, the CV collected simultaneously with the spectra and the potential dependence of the integrated intensities of $CO_L$, $CO_B$, and bridge-bonded adsorbed formate are compared. At the beginning of the potential scan (i.e., at -0.2 V vs. Ag/AgCl), the CO bands are negligible and grow with increasing potential up to 0.3 V in the positive-going scan. Subsequently, these CO bands start to decrease their intensities and completely disappear at around 0.6 V due to the oxidative stripping of adsorbed CO. In the negative-going scan, the CO bands reappear at around 0.6 V and continues to increase its intensity to saturation. Since oxidation of adsorbed CO does not occur at low potentials, the band intensity does not go back to the initial value (i.e., zero).

Associated with the oxidative removal of adsorbed CO in the positive-going scan, the symmetric O-C-O stretching mode of bridge-bonded adsorbed formate emerges. It will be reasonable to assume that bridge-bonded adsorbed formate is caused by the adsorption of formic acid that is formed by partial oxidation of methanol. The intensity of this band reaches

a maximum at 0.6 V and then decreases at higher potentials. In the negative-going scan, this band increases in intensity again due to the reduction of surface oxide on the Pt electrode. The potential at which the intensity of bridge-bonded adsorbed formate becomes maximal coincide with the oxidation peak in both the positive- and negative-going scans, from which Chen et al. [14] proposed that bridge-bonded adsorbed formate is a reaction intermediate. However, as discussed in Chapter 4, it is stable and more likely to be a site-blocking spectator rather than reaction intermediate. Kunimatsu et al. [J. Electroanal. Chem.. 632 (2009) 109] assigned the oxidation peak to the oxidation of adsorbed CO, i.e., non-direct pathway through adsorbed CO. However, a DEMS experiment carried out in 10mM methanol and 0.5 M $H_2SO_4$ yield values of 50, 34, and 16% for formaldehyde, formic acid, and $CO_2$ formation, respectively, at 0.65 V vs. RHE (about 0.45 V vs. Ag/AgCl). [H. Wang, T. Loffler and H. Baltruschat, J. Appl. Electrochem., 2001, 31, 759–765.] Therefore, the oxidation peaks are ascribed mostly to the oxidation of methanol to formaldehyde and formic acid.

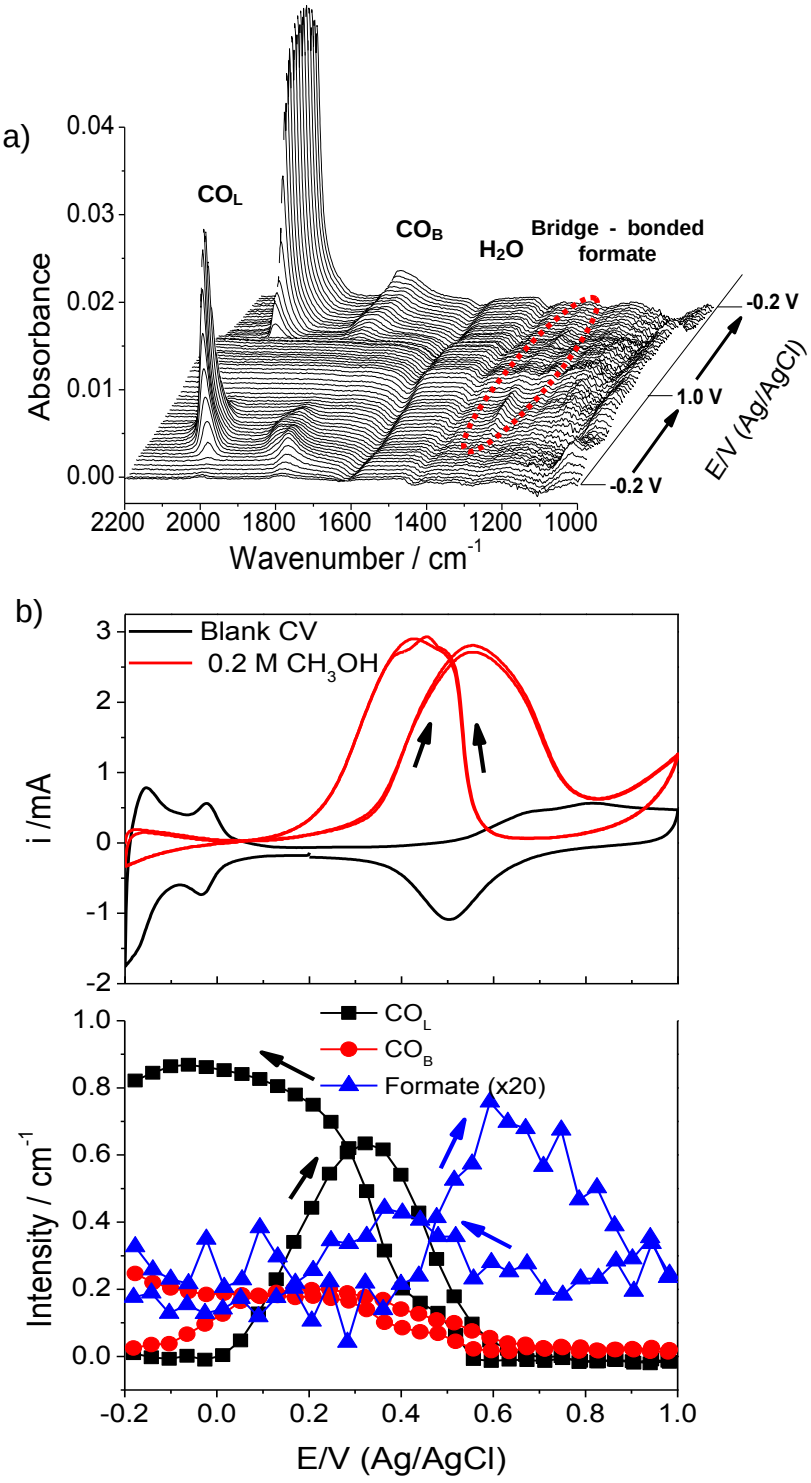


***Figure 5.5.*** (a) SEIRA spectra of the surface of a Pt thin film electrode sequentially collected during a potential sweep from -0.2 to 1.0 and back to -0.2 V at 20 mV $s^{-1}$ in buffer solution with pH 1.5 containing 0.2 M $CH_3OH$. (b) CV recorded simultaneously with the SEIRA spectra (upper) and

the potential dependence of the integrated intensities of $CO_{L,}$ $CO_B$, and bridge-bonded formate bands (lower) taken from (a). The black line is the CV in the same electrolyte without $CH_3OH$.

So as to fruitfully extend understanding of reaction mechanism, the same experiments were performed at different pHs. The results at pH 7.6 are shown in Figure 5.6. Two differences from pH 1.5 are found in the SEIRA spectra. One is the absence of bridge-bonded adsorbed formate. This result is due to the conversion of formic acid to formate in the neutral solution, as has been shown in Chapter 4. The other is the presence of band around 1100 $cm^{-1}$ assigned to a P-O stretching mode of phosphate anion adsorbed on the surface. This is also the case of formic acid oxidation and due to the absence of bridge-bonded adsorbed formate. The results at pH 11.6 are essentially identical to those at pH 7.6, as shown in Figure 5.7. In both neutral and alkaline solutions, the oxidation peak starts to flow associated with the oxidation of adsorbed CO and decreases associated with the surface oxidation. In the negative-going scan, on the other hand, the oxidation current starts to flow associated with the reduction of surface oxide and decreases associated with the accumulation of adsorbed CO. That is, the oxidation current is a function of the number of free sites. Regarding this issue, it is worth noting that CO accumulation in the negative-going scan occurs in a narrower potential range in the alkaline solution than in acidic solution, i.e., CO accumulation becomes faster with increasing pH. The pH dependence of CO accumulation can explain why the difference of the oxidation peakss in the positive- and negative-going scans becomes remarkable with increasing pH.

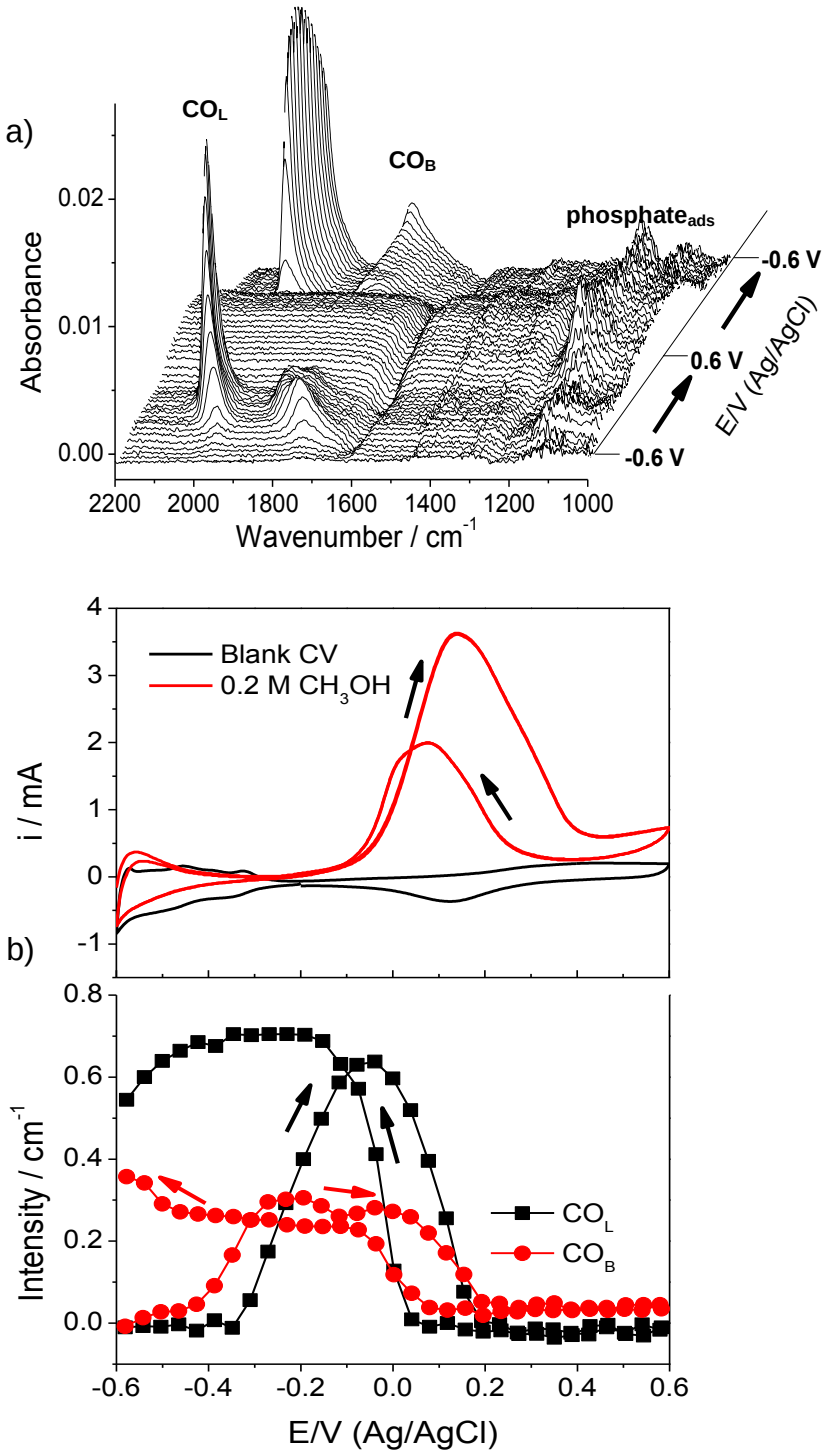


***Figure 5.6.*** (a) SEIRA spectra of the surface of a Pt thin film electrode sequentially collected during a potential sweep from -0.6 to 0.6 and back to -0.6 V at 20 mV $s^{-1}$ in buffer solution with pH 7.6 containing 0.2 M $CH_3OH$. (b) CV recorded simultaneously with the SEIRA spectra (upper) and the potential dependence of the integrated intensities of $CO_L$ and $CO_B$ taken from (a). The solid line is

the CV in the same electrolyte without $CH_3OH$.

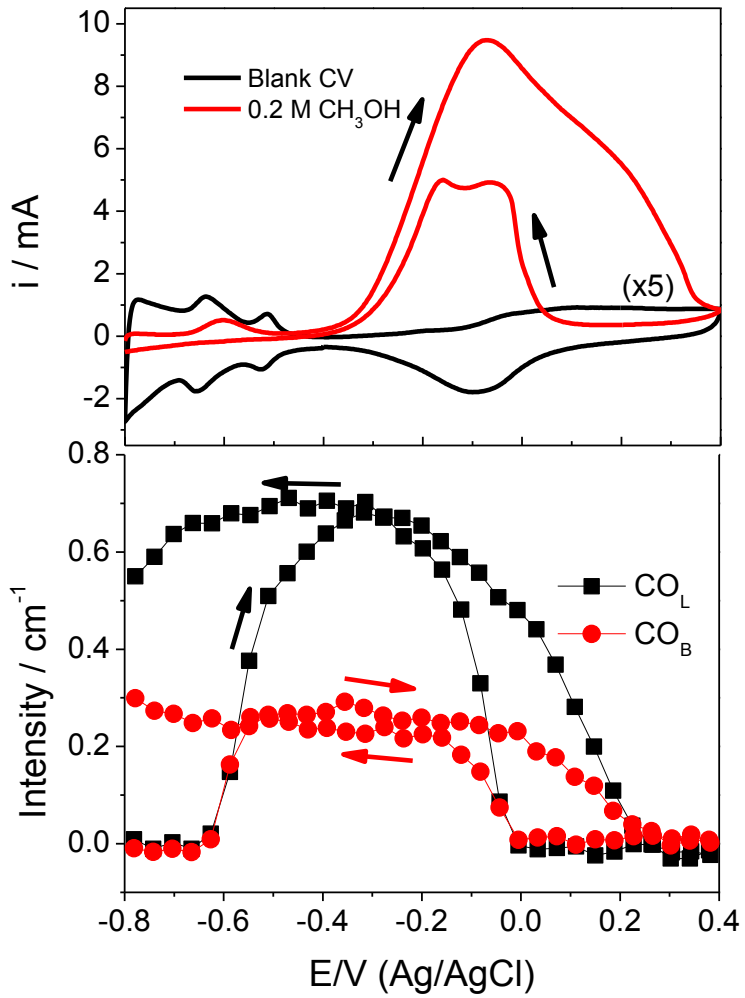


***Figure 5.7.*** CV recorded simultaneously with the SEIRA spectra (upper) and the potential dependence of the integrated intensities of $CO_L$ and $CO_B$ at 20 mV $s^{-1}$ in buffer solution with pH 11.6 containing 0.2 M $CH_3OH$. The solid line is the CV in the same electrolyte without $CH_3OH$.

A remaining most important question is why the oxidation current increases with increasing pH. As has been discussed earlier, methanol is oxidized to formaldehyde and formaic acid (formate in neutral and alkaline media). Formaldehyde is easily oxidized to formic acid/formate, while formic acid/formate is hardly oxidized in alkaline media.

Therefore, the oxidation current should be affected by the ratio of formaldehyde to formic acid/formate. In order to explain the significant increase of the oxidation with increasing pH, we propose that the ratio becomes larger with increasing pH, although formic acid detected by on-line KPLC was major species. As have already been mentioned, the preferential detection of formic acid can be ascribed to the oxidation of formaldehyde to formate. Otherwise, the large oxidation current in alkaline media cannot be explained. Further experiments to confirm this assumption are going on.

## 5.4 Conclusion

The electrooxidation of methanol on Pt was performed by SEIRAS coupled with cyclic voltammetry in a wide range of pH. The oxidation peak current in the positive-going scan increased with increasing pH, while that in the negative-going scan was independent of pH. The dependence of the scan direction was ascribed to the pH dependence of poisoning rate by adsorbed CO. On-line HPLC analysis of the solutions during potential scan revealed that formaldehyde and formic acid (formate in neutral and alkaline media) are formed in this order (methanol → formaldehyde → formic acid/formate). The oxidation of formaldehyde is very fast over the entire pH range, while that of formic acid/formate is very slow in alkaline media. Due to this reason, the final product of methanol oxidation is formic acid/formate in alkaline media.

# References

[1] R.P. Buck, L.R. Griffith, J. Electrochem. Soc., 109 (1962) 1005-1013.

[2] S. Wasmus, A. Kuver, J. Electroanal. Chem., 461 (1999) 14-31.

[3] V.S. Bagotzky, Vassilye.Yb, Electrochim. Acta, 12 (1967) 1323-1343.

[4] T. Iwasita, Electrochim. Acta, 47 (2002) 3663-3674.

[5] J.L. Cohen, D.J. Volpe, H.D. Abruna, Phys. Chem. Chem. Phys., 9 (2007) 49-77.

[6] V.S. Bagotzky, Y.B. Vassiliev, O.A. Khazova, J. Electroanal. Chem., 81 (1977) 2 29-238.

[7] A. Miki, S. Ye, T. Senzaki, M. Osawa, J. Electroanal. Chem., 563 (2004) 23-31.

[8] A.A. Abd-El-Latif, H. Baltruschat, J. Electroanal. Chem., 662 (2011) 204-212.

[9] T.H.M. Housmans, A.H. Wonders, M.T.M. Koper, J. Phys. Chem. B, 110 (2006) 10021-10031.

[10] M. Nakamura, K. Shibutani, N. Hoshi, Chemphyschem, 8 (2007) 1846-1849.

[11] E.A. Batista, G.R.P. Malpass, A.J. Motheo, T. Iwasita, J. Electroanal. Chem., 571 (2004) 273-282.

[12] A. Santasalo-Aarnio, Y. Kwon, E. Ahlberg, K. Kontturi, T. Kallio, M.T.M. Kope r, Electrochem. Commun., 13 (2011) 466-469.

[13] O.H. Han, K.S. Han, C.W. Shin, J. Lee, S.S. Kim, M.S. Um, H.I. Joh, S.K. Ki m, H.Y. Ha, Angew. Chem. Int. Ed., 51 (2012) 3842-3845.

[14] Y.X. Chen, A. Miki, S. Ye, H. Sakai, M. Osawa, J. Am. Chem. Soc., 125 (2003) 3680-3681.

[15] J. Sobkowski, K. Franaszczuk, K. Dobrowolska, J. Electroanal. Chem., 330 (199 2) 529-540.

[16] Y. Kwon, S.C.S. Lai, P. Rodriguez, M.T.M. Koper, J. Am. Chem. Soc., 133 (20 11) 6914-6917.

[17] J.S. Spendelow, J.D. Goodpaster, P.J.A. Kenis, A. Wieckowski, Langmuir, 22 (20 06) 10457-10464.

[18] Z.Y. Zhou, N. Tian, Y.J. Chen, S.P. Chen, S.G. Sun, J. Electroanal. Chem., 573 (2004) 111-119.

[19] K. Matsuoka, Y. Iriyama, T. Abe, M. Matsuoka, Z. Ogumi, J. Power Sources, 1 50 (2005) 27-31.

[20] L.W. Liao, S.X. Liu, Q.A. Tao, B. Geng, P. Zhang, C.M. Wang, Y.X. Chen, S. Ye, J. Electroanal. Chem., 650 (2011) 233-240.

[21] S. Park, Y. Xie, M.J. Weaver, Langmuir, 18 (2002) 5792-5798.

[22] S.X. Liu, L.W. Liao, Q. Tao, Y.X. Chen, S. Ye, Phys. Chem. Chem. Phys., 13 (2011) 9725-9735.

[23] Y. Kwon, M.T.M. Koper, Analytical chemistry, 82 (2010) 5420-5424.

# Chapter 6. Summary and prospect

Electrooxidation of small organic molecules such as $C_1$ fuels has gained long interests owing to use of electrochemical energy conversion devices. Furthermore, it is the most fundamental reaction model to understand the more complicated molecules ($C_n$ >= 2) oxidation. To date, it is well known that small organic molecules are oxidized to $CO_2$ through dual path mechanism. One path is self poisoning of reactive surface by $CO_{ads}$, the other path is fast reaction *via* reactive intermediate species. Although the studies for electrooxidation mechanism of small organic molecules have been studied intensively and extensively combined with *in situ* spectroscopy technology, it still remains strong debates for what is the real reactive intermediate. If we accurately diagnose the reaction mechanism, it is helpful to design the effective and efficient catalysts for fuel cells technologies.

In Chapter 3, to aid in understanding the phenomena of poising species on the catalyst, CO oxidation on poly-crystalline Pt electrode is scrutinized in alkaline media. From the results, the origin of the prepeak preceding a main peak is the partial oxidation of linear CO ($CO_L$) triggered by site conversion of bridged bonded CO ($CO_B$) into linear CO ($CO_L$). And then, surface diffusion concurrently take places by which the highly compressed metastable CO adlayer is relaxed to a more open structures. Shortly, CO at near step are oxidized faster than CO at terraces. After all, CO is fully oxidized by a Langmuir-Hinshelwood mechanism with fast surface diffusion at the main oxidation peak. The fast CO diffusion towards active defect sites and subsequent oxidation was manifested itself by broadening and red shift of the terrace CO band. And the mobility of $CO_{ads}$ plays a significant role in $CO_{ads}$ electrooxidation kinetics proved by chronopotentiometry for galvanostatic oxidation. A remaining critical issue why mobility of $CO_{ads}$ on surface in alkaline media is

low could be mainly explained by *"electronic effect"* owing to a lowering absolute potential regardless of carbonate adsorption, if any.

Chapter 4 highlights effect of pH on electrocatalytic oxidation of formic acid and formate ion on platinum. Electro-oxidation of formic acid on Pt in acid is one of the most fundamental model reactions in electrocatalysis research. However, its reaction mechanism is still a matter of strong debate. Two different mechanisms, bridge-bonded adsorbed formate mechanism and direct oxidation mechanism, have been proposed by assuming *a priori* that formic acid is the major reactant. Through systematic examination of the reaction over a wide pH range (0-12) by cyclic voltammetry and surface-enhanced infrared spectroscopy (SEIRAS), it is found that formate ion is the major reactant over the whole pH rage examined, even in strong acid. The experimental results are reasonably explained by a new mechanism in which formate ion is directly oxidized *via* a weakly adsorbed formate precursor. The reaction serves as a generic example illustrating the importance of pH variation in ***catalytic proton-coupled electron transfer reactions***. In summary, we have shown that $HCOO^-$ is efficiently oxidized on Pt most probably *via* a weakly adsorbed $HCOO^-$ precursor. Due to the low concentration of $HCOO^-$ in acidic media and to the decrease of reaction rate in alkaline media, the oxidation current reaches a maximum at a pH close to the p*K*a of HCOOH as described in figure 4.2b. Oxidation of HCOOH takes place after it has been converted to $HCOO^-$ through the acid-base equilibrium in the bulk near the electrode surface, as this pathway is more facile than its oxidation *via* bridge-bonded adsorbed formate and *via* a weakly adsorbed HCOOH precursor.

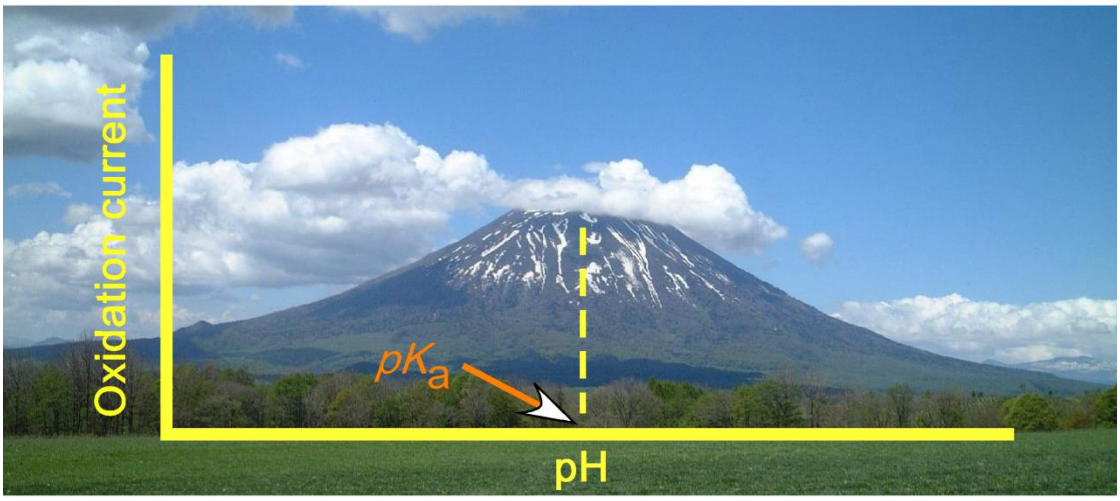


***Figure 6.1*** (a) Graphical representation of pH dependence of the peak current for organic molecules oxidation on Pt electrode. Best performance can be achieved at pH≈pKa.

Chapter 5 dealt with the electrooxidation of methanol on Pt electrode in alkaline media. On-line HPLC analysis of the solutions during potential scan revealed that formaldehyde and formic acid (formate in neutral and alkaline media) are formed in this over (methanol → formaldehyde → formic acid/formate). The oxidation of formaldehyde is found as a reactive intermediate for non CO path over the entire pH range. However, formate is not reactive intermediate compared to formaldehyde in alkaline media. Due to this reason, the final product of methanol oxidation is formic acid/formate in alkaline media. Very recently, electrochemical reaction is complying with the theory of *multiple proton-electron transfer reactions* proposed by koper *et al.* [1]. This theory is well correlated with alcohol oxidation as well. Therefore, electrooxidation of methanol is facilitated toward to alkaline media as described previously. Interestingly, CO path largely contribute the oxidation current in sufficiently alkaline media due to its enhanced oxidation rate *via Langmuir-Hinshelwood mechanism* rather than acid media.

The topic dealt with in dissertation has been of longstanding interest to many areas of

science and technology, including ***surface science***, ***catalysis***, ***fuel cells***, ***energy conversion***, and ***green chemistry***. Therefore, we believe that the findings in the present work have potential of broad interest. The results reported in this dissertation force to revise the interpretations made in earlier experimental and theoretical studies.

# Prospect

The usefulness of SEIRAS technique was adapted for several electrochemical systems. The real time monitoring of the potential-dependent reactions on the interface is one of the greatest advantages. In the following, electrocatalytic reaction for applying to energy conversion and promising diagnostic probes for analytical characterization of the interface using SEIRAS are introduced.

## Energy conversion (Direct Liquid Fuel Cells)

To distinguish the real reaction mechanism is very important issue in electrocatalysis fields owing to designing an effective catalysts for polymer electrolyte membrane fuel cells (PEMFCs). Among small organic molecules used as fuel, such as formic acid and methanol, common bridge-bonded formate ($HCOO_{ads}$) appears in the electrooxidation reaction as an intermediate. And bridge-bonded formate has been strong debates whether it is a reactive intermediate or not. If bridge bonded formate is not reactive intermediate, it should be suppressed to be adsorbed on the surface or it can be used as a current carrier as much as possible. On the basis of our SEIRAS result, surprisingly, $HCOO^-$ is found as a reactive intermediate for formic acid oxidation, even in strong acid media. And bridge-bonded formate ($HCOO_{ads}$) is not considered as site-blocking spectator. However, its oxidation contribution for current carrier is much smaller than that of $HCOO^-$. Next, when it comes to

methanol oxidation, formaldehyde plays a crucial role as a reactive intermediate. However, formate is determined as a non-reactive species. ***Both the experiment and simulation show that an optimal performance is obtained at pH close to pKa of organic molecules as shown in figure 6.1.*** Therefore, the pKa of the molecules of interest is an important factor for predicting the optimal pH. In fact, electrocatalytic oxidation of alcohols that have large pKa values is more facile in alkaline media than in acidic media. However, formate is not oxidized further in alkaline media.

As summary, it can be inferred that most DFAFCs using cation-and anion exchange membranes are not operated under the optimal conditions. On the other hand, **anion exchange membrane** is recommended to apply to DMFCs when considering its pKa. We must also consider how to oxidize $HCOO^-$ in alkaline media.

## Analytical characterization of interface using SEIRAS

ATR-SEIRAS is superior to IRAS in interfacial selectivity and surface sensitivity, and is free from the mass transport limitation. These merits of ATR-SEIRAS enable time-resolved monitoring of electrochemical reactions and have shifted the targets of *in-situ* simple systems to more complicated reaction systems including bio-electrochemical reactions [2]. Further faster time-resolved measurements in the *ps* range are possible by the laser-induced temperature jump method. In addition to the expansion of time resolution, the expansion of spectral range to far IR is also required with use of a synchrotron far-IR facility and a helium-cooled bolometer since metal-adsorbate vibrations modes take place in this range [2].

## AFM-IR developed for nanometer scale chemical identification

The technique of infrared (IR) spectroscopy has been applied for chemical identification of organic materials, but its use has been limited by shortages to resolve chemistry on the nanometer scale. Conversely, atomic force microscopy (AFM) has superior spatial resolution in the nanometer range, but has been unable to provide chemical information. Atomic force microscope infrared spectroscopy (AFM-IR) can probe IR absorption spectra with results that agree closely with bulk IR measurement, and this high resolution IR spectroscopic imaging is combined with the nanometer-scale spatial resolution of AFM (See figure 6.2) [3]. Although this technique has recently become popular, it would be a still promising for advanced analytical measurements. Such as *electrocatalysis*, *semiconductors*, *medical diagnostics* and *biochemistry* [3].

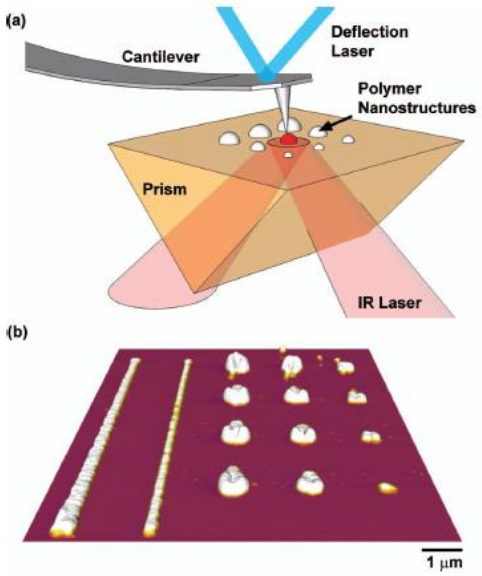


***Figure 6.2*** (a) Graphical representation of AFM-IR on polymer nanostructures of differing size. The thermomechanical expansion of the absorbing polymer nanostructure shocks the AFM cantilever into oscillation. The deflection laser measures the cantilever response to the shock from the

polymer structure. (b) An AFM image of polyethylene nanostructures fabricated using a heated AFM probe with heights ranging from 10 nm to 100 nm. Tip temperature, speed, and dwell time controlled the sizes of the fabricated structures. Adapted from [3].

## Combination of ATR-SEIRAS and IRAS measurements

Electrochemical infrared spectroscopy is usually carried out in two reflection modes such as external reflection with a thin-layer between prism and working electrode (denoted as IRAS) and internal reflection defined as ATR-SEIRAS. ATR-SEIRAS is more sensitive in detecting surface species than IRAS whereas IRAS is more sensitive in observing solution species trapped in the thin layer [4, 5]. Although surface enhancement was also observed in IRAS in some cases, the limited mass transport and the serious interference of solution signals are often problems when it is applied to characterize surface species during reaction processes. Therefore, combination of ATR-SEIRAS and IRAS measurements is expected to clarify the electrocatalytic reaction mechanism and thus may be considered as a helpful development in electrochemical surface infrared spectroscopy [5].

# References

[1] M.T.M. Koper, Chem. Sci., (2013).

[2] M. Osawa, In-situ Surface-Enhanced Infrared Spectroscopy of the Electrode/Solution Interface, in: Advances in Electrochemical Science and Engineering, Wiley-VCH Verlag GmbH, 2008, pp. 269-314.

[3] J.R. Felts, H.N. Cho, M.F. Yu, L.A. Bergman, A.F. Vakakis, W.P. King, Review of Scientific Instruments, 84 (2013).

[4] M. Osawa, Surface-Enhanced Infrared Absorption, in: S. Kawata (Ed.) Near-Field Optics and Surface Plasmon Polaritons, Springer Berlin Heidelberg, 2001, pp. 163-187.

[5] Y.-Y. Yang, J. Ren, H.-X. Zhang, Z.-Y. Zhou, S.-G. Sun, W.-B. Cai, Langmuir, 29 (2013) 1709-1716.

# List of Publications

Refs. 1-2 contains part of the present thesis


[1] Jiyong Joo, Taro Uchida, Angel Cuesta, Marc T. M. Koper, and Masatoshi Osawa*, The effect of pH on the electrocatalytic oxidation of formic acid/formate on platinum: A mechanistic study by surface-enhanced infrared spectroscopy coupled with cyclic voltammetry, *Electrochim. Acta, (2014) accepted*

[2] Jiyong Joo, Taro Uchida, Angel Cuesta, Marc T. M. Koper, and Masatoshi Osawa*, Importance of Acid-Base Equilibrium in Electrocatalytic Oxidation of Formic Acid on Platinum, *J. Am. Chem. Soc.,* **135** *(2013) 9991*

[3] Jiyong Joo, Jae Kwang Lee, Youngkook Kwon, C.R. Jung, E.S. Lee, J.H. Jang, H.ye Jin Lee, Sunghyun Uhm, Jaeyoung Lee*, Enhancement of CO Tolerance on Electrodeposited Pt Anode for micro PEM Fuel Cells, *Fuel Cells*, **10** (2010) 926

[4] Jae-Young Lee, Jiyong Joo, Jae Kwang Lee, Sunghyun Uhm, Eon Soo Lee, Jae Hyuk Jang, Nam-Ki Kim, Yong-Chul Lee, Jaeyoung Lee*, Effect of hydrogen partial pressure on a PEFC performance, *Korean J. Chem. Eng.,* **27** *(2010) 843*

[5] Hongrae Jeon, Jiyong Joo, Youngkook Kwon, Tae-Geun Noh, Jaeyoung Lee*, Morphology effects of electrodeposited Pt nanoparticles and its application as anode catalysts in polymer electrolyte formic acid fuel cells, *J. Power Sources,* **195** *(2010) 5929*

[6] Sunghyun Uhm, Jiyong Joo, Sungyool Bong, Hasuck Kim, Role of graphene as a catalyst support in SOM oxidation, *ECS Trans.,* **33** *(2010) 1725*

# Acknowledgements

I am extremely grateful to all those who helped me to concentrate on the study the Catalyst Research Center at Hokkaido University as a doctoral student.

First of all, I am extremely appreciative of my supervisor Professor Masatoshi Osawa. He gives me not only fundamental background of SEIRAS techniques but also serves as a paragon, demonstrating the attitude of a true scientist. I would like to acknowledge the opportunity to study in Japan as a PhD student. It was a great privilege to be one of the members of the interfacial spectrochemistry laboratory. I would also like to express my gratitude to the advisory committee members, Professor Toyoji Kakuchi, Professor Wataru Ueda, and Professor Kei Murakoshi, for their invaluable suggestions and advice.

I am much indebted to Professor Jaeyoung Lee who was my supervisor during my master's program at the GIST. He is my mentor and gives me inspiration to continue researching ceaselessly. I would also like to thank Professor Marc T. M. Koper of the University of Leiden for providing valuable comments and learning motivation.

In addition, I would like to express my deep appreciation to Professor Shen Ye, Dr. Taro Uchida and Dr. Kenta Motobayashi for their help with initial experimental introduction and taking care of huge obstacles that I faced in my daily life.

I will never forget the good memories and friendships with Interfacial Spectrochemistry Laboratory members that were formed. I am really happy to have met Takaya Ishino, Ryota Tomioka, Momo Yaguchi, Seigo Miyoshi and Tomoko Nomura. Moreover, I also thank Youngpil Chun who now studies in Australia as a doctoral student. My gratitude extends to Lee Sunjin, Lee Soungpil, Seo Hyoknam and Lee Juwon. They have always answered my calls warmly to help to mitigate my homesickness. I am proud of them as they are my precious friends.

Last, but not least, I would like to give special thanks to my beloved family. They always gave me their full emotional support. My mother and three sisters, Sumi, Youngmi, and Jinmi are the main roots of my energy to keep moving forward vigorously. I would like to dedicate my thesis to my family.

Boys, be ambitious.